IntechOpen

Advances In Hydrogen Generation Technologies

Edited by Murat Eyvaz

ADVANCES IN HYDROGEN GENERATION TECHNOLOGIES

Edited by **Murat Eyvaz**

Advances In Hydrogen Generation Technologies
http://dx.doi.org/10.5772/intechopen.71918
Edited by Murat Eyvaz

Contributors

Ahmed Ibrahim, Youssef Naimi, Amal Antar, Adriana Marinoiu, Raceanu Mircea, Carcadea Elena, Mihai Varlam, Flavio Colmati, Tatiana Duque Martins, Antonio Carlos Chaves Ribeiro, Roberto Lima, Leandro Lima Carvalho, Christian Gonçalves Alonso, José William Diniz Coutinho, André Mychell B. S. Sampaio, Geovany Albino De Souza, Lucas Aguiar, Diericon Sousa Cordeiro, Adão Marcos F. Costa, Thiago Soares Silva Ribeiro, Pedro Henrique Machado Godoy, Guilherme B. Meireles De Souza, Monah Magalhães, Nordin Sabli, Mohd Fadhzir Ahmad Kamaroddin, Tuan Amran Tuan Abdullah, Muhammad Burhan, Muhammad Wakil Shahzad, Kim Choon Ng

Notice

First published in London, United Kingdom, 2018 by IntechOpen
eBook (PDF) Published by IntechOpen, 2019
IntechOpen is the global imprint of INTECHOPEN LIMITED, registered in England and Wales, registration number: 11086078, The Shard, 25th floor, 32 London Bridge Street
London, SE19SG – United Kingdom
Printed in Croatia

British Library Cataloguing-in-Publication Data
A catalogue record for this book is available from the British Library

Additional hard and PDF copies can be obtained from orders@intechopen.com

Advances In Hydrogen Generation Technologies
Edited by Murat Eyvaz

p. cm.

Print ISBN 978-1-78923-534-0

Online ISBN 978-1-78923-535-7

eBook (PDF) ISBN 978-1-83881-629-2

Meet the editor

Dr. Murat Eyvaz is an assistant professor at the Environmental Engineering Department, Gebze Technical University (GTU). He received his BSc degree in Environmental Engineering from the Kocaeli University in Turkey in 2004 and completed his MSc and PhD degress in Environmental Engineering from the Gebze Institute of Technology (former name of GTU) in 2013. He completed his postdoctoral research in Membrane Technologies from the National Research Center in 2015. His research interests are water and wastewater treatment, electrochemical processes, filtration systems/membrane processes, and spectrophotometric and chromatographic analyses. He has coauthored numerous journal articles and conference papers and has taken part in many national projects. He serves as an editor of 30 journals and a reviewer of 100 journals indexed in SCI, SCI-E, and other indexes.

Contents

Preface

The ever-increasing global population makes an increasing demand on energy. Fossil fuels are at the forefront of energy sources that we still need. However, due to the limited resources of these fuels and global climate change, the availability of alternative sources and energy carriers has gained importance. For this reason, studies have been accelerated to obtain blue energy (water) and green energy (wind, solar, etc.) from new technologies to meet the increasing energy demand of human society. Among energy sources, hydrogen gas is clean and renewable and has the potential to solve the growing energy crisis in today's society because of its high-energy density and noncarbon fuel properties. It is also used for many potential applications in nonpolluting vehicles, fuel cells, home heating systems, and aircraft. In addition, using hydrogen as an energy carrier is a long-term option to reduce carbon dioxide emissions worldwide by obtaining high-value hydrocarbons through the hydrogenation of carbon dioxide. Water is considered as an ideal hydrogen source because it is clean, abundant, and renewable. Hydrogen production from water is achieved by water splitting using several methods such as thermal decomposition, electrolysis, photolysis, and photoelectrochemical methods.

This book presents the recent progresses and developments in water-splitting processes as well as other hydrogen generation technologies with challenges and future perspectives from the point of energy sustainability. In the first two chapters, the electrolysis of water, which attracts great attention due to its sustainability and renewability, is presented with the theoretical foundations of the operating principles of different types of electrolyzers. The most important technologies, such as alkaline electrolysis, proton exchange membrane electrolysis, and solid oxide high-temperature electrolysis, are addressed. In Chapter 3, the recent technological progress in light hydrocarbons regarding the sustainable hydrogen production is highligted, while the following two chapters evaluate the hydrogen production from ethanol by steam and use of hydrogen in a proton exchange membrane fuel cell. In the last chapter, a detailed performance model and optimization strategy is proposed for standalone operation of a concentrated photovoltaic system, with hydrogen production as an energy storage.

Asst. Prof. Murat Eyvaz
Co-Head of Department
Department of Environmental Engineering

Deputy Director
Science and Technology Application and Research Center

Gebze Technical University
Turkey

Chapter 1

Hydrogen Generation by Water Electrolysis

Youssef Naimi and Amal Antar

Additional information is available at the end of the chapter

http://dx.doi.org/10.5772/intechopen.76814

Abstract

Hydrogen is a promising energy vector for the future. Among the different methods of its production, the electrolysis of water has attracted great attention because it is a sustainable and renewable chemical technology. Thus, hydrogen represents a suitable energy vector for the storage of intermittent energies. This chapter is devoted to the hydrogen generation by water electrolysis as an important part of both existing and emerging industrial electrochemical processes. It aims to give an insight into the theoretical foundations of the operating principles of different types of electrolyzers. Also, it is developed in this chapter, the thermodynamic and kinetic aspects of the reactions taking place at the electrodes of water electrolysis. The evolution reaction of hydrogen has a rapid kinetics, and thus, the polarization of the cathode is not critical. On the other hand, the evolution reaction of oxygen is characterized by a very slow kinetics and is thus responsible for most of the overvoltage in the electrolysis of water. The most important technologies of water electrolysis are addressed: alkaline electrolysis, proton exchange membrane electrolysis, and solid oxide high-temperature electrolysis.

Keywords: hydrogen, oxygen, water electrolysis, catalyst, electrolyte, alkaline, polymer, solid oxide

1. Introduction

The United Nations (UN) published The Sustainable Development Program in 2015, which is an action plan for humanity, the planet, and prosperity. A total of 17 sustainable development goals and 169 targets are announced, which will stimulate action over the next 15 years in areas of critical importance for humanity and the planet (People, Planet, Prosperity, Peace, Partnership). The seventh goal is to ensure access to affordable, reliable, sustainable, and modern energy for all [1]. The hydrogen economy is seen as an instrument for the transformation of the energy system [2]. Hydrogen is the fuel most often used in fuel cells. It can have

several provenances (electrolysis of water, cracking or reforming of petroleum products), with obvious implications on its degree of purity and consequently on the choice of catalyst, electrolyte, and operating conditions. The production of hydrogen by the electrolysis technique is very interesting because it can use a non-greenhouse gas energy source (renewable or nuclear energy). In addition, it remains the basic technique for providing applications that require small volumes of high purity hydrogen, including the semiconductor and food industry.

Hydrogen is the lightest chemical element. Its molecules contain two hydrogen atoms. If this gas does not exist in its natural state, it is found in many molecules: water, sugar, proteins, hydrocarbons, and so on.

Hydrogen is a very light gas, colorless, odorless, and extremely flammable and reacts very easily in the presence of other chemicals. The properties of this gas are summarized in **Table 1** [3].

The advantages of using hydrogen as a fuel in fuel cells are:

- its high electrochemical reactivity,
- its high theoretical energy density,
- unlimited availability (as long as you can break down the water),
- its harmless combustion product (H_2O) for the environment.

Its low density under normal conditions, the difficulty of storage, and the risk of explosion can summarize the major drawbacks of the use of pure hydrogen in fuel cells.

Notwithstanding the increasing interest in hydrogen as an energy carrier, its main uses continue to be in petroleum refining, ammonia production, metal refining, and electronics fabrication, with an average worldwide consumption of about 40 million tons [4–8]. This large-scale hydrogen consumption consequently requires large-scale hydrogen production. Presently, the technologies that dominate hydrogen production include reforming of natural gas [9], gasification of coal and petroleum coke [10–12], as well as gasification and reforming of heavy oil [13, 14]. Although water electrolysis has been known for around 200 years [15, 16], it still contributes only a minor fraction of the total hydrogen production (4% of the worldwide hydrogen production) [17, 18]. When compared to other available methods, water electrolysis has the advantage of producing extremely pure hydrogen (>99.9%), ideal for some high value-added processes such as the manufacture of electronic components [4].

Molecular weight	**2016 g/mol**
Melting point	−259°C
Boiling point (1.013 bar)	−252.8°C
Evaporation heat (1.013 bar at boiling point)	454.3 kJ/mol
Density in the gas phase (1.013 and at 21°C)	0.0696 kg/m^3
Solubility in water (1.013 bar and 0°C)	0.0214 vol/vol

Table 1. Characteristics of hydrogen [3].

http://dx.doi.org/10.5772/intechopen.76814

2. Principle of water electrolysis

Water electrolysis is the process whereby water is split into hydrogen and oxygen through the application of electrical energy, as in Eq. (6). Typically, a water electrolysis unit consists of an anode, a cathode separated with an electrolyte, and a power supply. The electrolyte can be made of an aqueous solution containing ions, a proton exchange membrane (PEM) or an oxygen ion exchange ceramic membrane. A direct current (DC) is applied from the negative terminal of the DC source to the cathode (seat of the reduction reaction), where the hydrogen is produced. At the anode, the electrons produced by the electrochemical reaction return to the positive terminal of the DC source.

For the case of water electrolysis in an acid aqueous electrolyte, the processes that occur at the anode and the cathode are described, respectively, by Eqs. 1 and 2:

$$H_2O \rightarrow \frac{1}{2}O_2 + 2H^+ + 2e^- \qquad E^0_{H_2O/O_2} = 1.23V/ENH \tag{1}$$

$$2H^+ + 2e^- \rightarrow H_2 \qquad E^0_{H^+/H_2} = 0.00V/ENH \tag{2}$$

The half reactions occurring on the cathode and anode, respectively, can be written as:

$$2H_2O + 2e^- \rightarrow H_2 + 2OH^- \qquad E^0_{H_2O/H_2} = -0.83V/ENH \tag{3}$$

$$2OH^- \rightarrow \frac{1}{2}O_2 + H_2O + 2e^- \qquad E^0_{OH^-/O_2} = 0.4\ V/ENH \tag{4}$$

The global reaction for the two cases is:

$$H_2O \rightarrow H_2 + \frac{1}{2}O_2 \qquad \Delta E^0 = E^0_{H_2O/H_2} - E^0_{OH^-/O_2} = -1.23\ V \tag{5}$$

Electrolysis of water is not a spontaneous phenomenon because the standard global reaction potential is negative. Therefore, it needs an external intervention (power source) and the global reaction can be written as:

$$H_2O + electricity \rightarrow H_2 + \frac{1}{2}O_2 \tag{6}$$

3. Thermodynamic

The equation of the German chemist Walther Nernst can be obtained from thermodynamics. The variation of Gibbs free energy is a function of the concentrations of the species participating in a chemical reaction ($aA + bB + \ldots \rightarrow mM + nN + \ldots$):

$$\Delta G = \Delta G^0 + RT \cdot \ln\left(\frac{a_M^m \cdot a_N^n \cdot \ldots}{a_A^a \cdot a_B^b \cdot \ldots}\right) \tag{7}$$

where a_A^a, a_B^b, …, a_M^m, a_N^n, …, are the activities of the species.

Some species involved in the electrode reaction are solids or pure liquids. For these pure substances, the activity is constant and its value is considered unitary. The activity of the gases is usually taken to be the partial pressure of the gases expressed in the atmosphere, and the activity of the ions in dilute solution is generally considered to be their molar concentration. By substituting in Eq. (7) the reactions, and dividing each member of the equation by -nF, we obtain the Nernst equation. Nernst's equation expresses the relationship between the potential of an electrochemical cell and the concentrations of its constituents at equilibrium. In the specific case of an electrochemical cell, it is written:

$$\Delta \boldsymbol{E_{npile}} = \left(\boldsymbol{E^0_{Cathode}} - \boldsymbol{E^0_{Anode}}\right) - \frac{\boldsymbol{RT}}{\boldsymbol{nF}} \ln\left(\frac{\boldsymbol{a_M^m}.\boldsymbol{a_N^n}\ldots}{\boldsymbol{a_A^a}.\boldsymbol{a_B^b}\ldots}\right) \tag{8}$$

3.1. Faraday's law

In 1832, Michael Faraday stated his two laws of electrolysis:

1. The weights of substances formed at an electrode during electrolysis are directly proportional to the quantity of electricity that passes through the electrolyte.
2. The weights of different substances formed by the passage of the same quantity of electricity are proportional to the equivalent weight of each substance.

The quantity of material (m) produced is:

$$\mathrm{m} = \mathrm{k}\cdot \int_0^{\mathrm{t}} \mathrm{I}\cdot \mathrm{dt} \tag{9}$$

where k is a proportionality constant and I is the instantaneous current flowing through the cell. In a cell in which a continuous current circulates, the majority of this current is connected to chemical reactions (faradic current) and a small part, often negligible can be used for other purposes (non-Faradic current). Thus, the amount of material that forms or disappears at the electrodes is proportional to the intensity of the current and the duration of the electrolysis t. Knowing the number of moles is (m/M), which corresponds to a quantity of electricity $\left(Q = \frac{m}{M}\cdot N\cdot F = I\cdot t\right)$. Hence, Faraday's law:

$$m = \frac{I\cdot t\cdot M}{nF} \tag{10}$$

With: m is the mass of substances formed (g); M is the molar mass of substances formed (g/mol.); n is number of exchanged electrons, I is the current in amperes (A), $Q = I\cdot t$ is the quantity of electricity in coulomb (C), t is the time (s).

3.2. Cell voltage (difference of potential)

The potential difference for a cell of an electrolyzer, which is always $\Delta E = 1.8\tilde{}2.0\ V$ at the current density of $j = 1000 \sim 300\ Am^2$ in industry water electrolysis [17], is an addition of four terms:

$$\Delta E = \Delta \mathrm{E_{the}} + \eta_a + \eta_c + \mathrm{R{\cdot}I} \tag{11}$$

with: $\eta_a\ (V)$ is the anodic overvoltage; $\eta_c\ (V)$ is the cathodic overvoltage; R (Ω) is the global resistance and I (A) is the current.

Figure 1 shows the relationship between the electrolyzer cell potential and operating temperature [19–22]. The cell potential-temperature plane is divided into three zones by the so-called equilibrium voltage line and thermo-neutral voltage line. The equilibrium voltage is the theoretical minimum potential required to dissociate water by electrolysis, below which the electrolysis of water cannot proceed. The equilibrium voltage decreases with increasing temperature. The thermo-neutral voltage is the actual minimum voltage that has to be applied to the electrolysis cell, below which the electrolysis is endothermic and above which, exothermic. The thermo-neutral voltage naturally includes the overpotentials of the electrodes, which are only weakly dependent on temperature. Thus, the thermo-neutral voltage only exhibits a slight increase with temperature. If water electrolysis takes place in the shaded area in **Figure 4**, the reaction will be endothermic.

3.3. Electrodes polarizations

As these electrochemical reactions are heterogeneous surface processes, it is convenient to relate the reaction rate to the electrode area, A, as $\frac{dm}{A{\cdot}dt} = \frac{I}{A{\cdot}n{\cdot}F}$. Therefore, the expression for current density, $j = \frac{I}{A}$, may be rewritten as$j = \left(\frac{nF}{A} \cdot \frac{dm}{dt}\right)$.

For a general electrochemical reaction:

$$O + ne^- \rightleftarrows R \tag{12}$$

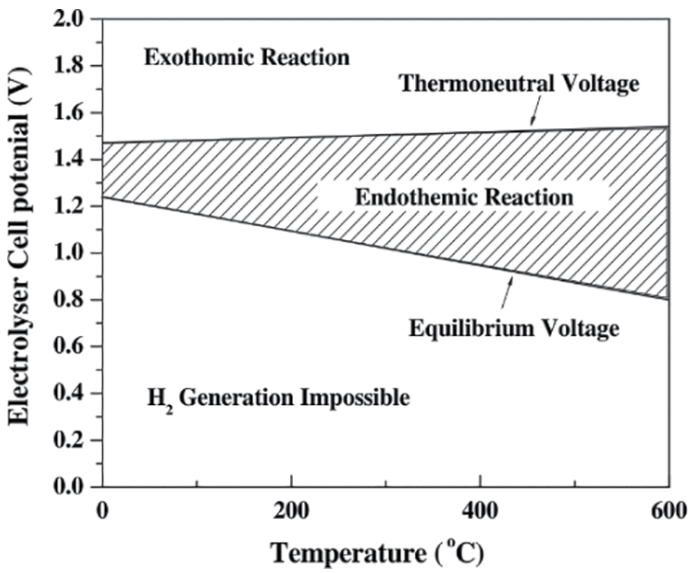

Figure 1. Cell potential for hydrogen production by water electrolysis as a function of temperature [19].

Under nonequilibrium potential conditions, the equation that best describes the current density versus potential is the Butler-Volmer expression:

$$j = \vec{j_a} + \overleftarrow{j_c} = nF\overleftarrow{k_0}C_R(0,t)e^{\left(\frac{\alpha_a nF(E-E^0)}{RT}\right)} - nF\vec{k_0}C_O(0,t)e^{\left(\frac{\alpha_c nF(E-E^0)}{RT}\right)} \tag{13}$$

where $\vec{j_a}$ and $\overleftarrow{j_c}$ are, respectively, the anodic and cathodic current density; $\overleftarrow{k_0}$ and $\vec{k_0}$ are, respectively, the rates constants of the anodic and cathodic reaction; α_a and α_c are, respectively, the anodic and cathodic exchanges coefficients; E^0 is the standard potential.

Under the control of electron transfer rate, (the concentration of the electrodes' surface is equal to the concentration in the bulk), this equation can be expressed as current density versus overpotential ($\eta = E - E_{eq}$):

$$j = j_0 j\left(e^{\left(\frac{\alpha_a nF\eta}{RT}\right)} - e^{\left(\frac{\alpha_c nF\eta}{RT}\right)}\right) \tag{14}$$

The anodic and cathodic exchanges coefficients (α_a, and α_c) are related ($\alpha_a + \alpha_c = 1$), and generally, $\alpha \approx \alpha_a \approx \alpha_c \approx \frac{1}{2}$. For a given single-step reaction at a constant temperature, the j versus η characteristics will depend on j_0, α_a, and α_c.

For large η values, the Butler-Volmer equations can be simplified to give the Tafel equation ($|\eta| = a \cdot \log|j| + b$):

$$\text{For } \eta \ll 0: \ \log(j) = -\log(j_0) - \frac{\alpha_c nF}{2.3RT}\cdot\eta \tag{15}$$

$$\text{For } \eta \gg 0: \ \log(j) = -\log(j_0) + \frac{\alpha_a nF}{2.3RT}\cdot\eta \tag{16}$$

For the hydrogen evolution reaction (HER), the Volmer-Tafel and Volmer-Heyrovský mechanisms are often proposed and well known [16, 23, 24]. The first step (Eq. 17) involves the formation of adsorbed hydrogen, which is then followed by either chemical desorption (Eq. 18) or electrochemical desorption (Eq. 19), where H_{ads} is an adsorbed hydrogen atom.

$$H_2O + e^- \rightleftarrows H_{ads} + OH^- \qquad \text{Volmer step} \tag{17}$$

$$2H_{ads} \rightleftarrows H_2 \qquad \text{Tafel step} \tag{18}$$

$$H_{ads} + H_2O + e^- \rightleftarrows H_2 + OH^- \qquad \text{Heyrovsḱy step} \tag{19}$$

For the hydrogen evolution reaction (HER), the overpotential, η_{H_2}, is generally calculated by the Tafel equation. Hydrogen formation is intrinsically determined by the strength of the bond between hydrogen and the electrode surface. Pd has the lowest heat of adsorption of hydrogen

($\Delta H_{ads,\,Pd,\,298}(H_2) = 83.kJ\ mol.^{-1}$); for Ni, the heat of adsorption is $\Delta H_{ads,\,Ni,\,298}(H_2) = 105\ kJ\ mol.^{-1}$ [25]. Electrode properties, type and concentration of the electrolyte, and temperature are parameters that also influence hydrogen formation. If hydrogen adsorption is the rate-determining step, electrode materials with more edges and cavities in their surface structure will favor electron transfer and create more centers for hydrogen adsorption. If hydrogen desorption is the rate-determining step, physical properties such as surface roughness or perforation will prevent bubbles from growing and increase electron transfer by adding reaction area, consequently increasing the rate of electrolysis [26]. When the overpotential is low, electron transfer is not as fast as desorption and hydrogen adsorption will be the rate-determining step. In contrast, when the potential is high enough, hydrogen desorption will be the rate-determining step.

The hydrogen adsorption energy is a good parameter to identify the most promising materials for the HER. If the activities for the HER of the coinage metals (I_B metals: Au, Cu, Ag), the platinum group (Pt, Ir, Ru) metals and the valve metal (Ti) in 0.1 M $HClO_4$, are plotted as a function of the $M–H_{ads}$ binding energy, a volcano relationship is established (**Figure 2**) with Ir and Pt at the apex of the volcano curve [27].

Further analysis of **Figure 2** reveals that the I_B group elements are positioned on the ascending slope of the volcano with the order activity increasing from Au < Cu < Ag. **Figure 1** also shows that the elements that interact strongly with H_{ads} (such as Ru and Ti) are positioned on the descending slope of the volcano, supporting previous suggestions that the $M–H_{ads}$ binding energy can be used as a descriptor for the HER. Not in passing, given that recent analysis has demonstrated that neither Ru nor Ti are bare metals in the HER region, it is suggested that, in fact, experimentally it is very difficult (impossible) to determine unambiguously solely based on the $M–H_{ads}$ energetics what would be the correct position of these two elements in the observed volcano relationship. This is most likely also true for the HER in alkaline solutions, when the rates of the reaction are much slower than in acidic environments [22].

The HER exchange current of Pt in acid media is at least two orders of magnitude higher than that in alkaline electrolytes, including KOH. This is due to the shorter $Pt - H_{ads}$ distance in alkaline media, as suggested by theoretical estimates. It has been claimed that $Ni(OH)_2$ nanoclusters on Pt surface enhance HER rates in 0.1 M KOH by one order of magnitude [26], although no theoretical explanation for this synergistic effect has been attempted. The long-term stability of $Ni(OH)_2$ in the strongly reducing environment occurring at the cathode is also not discussed.

The mechanism of the oxygen evolution reaction (OER) is more complex than that suggested for HER. The most generally accepted mechanism for the OER is that described by Cappadonia et al. [29]:

$$OH^- \rightleftarrows OH_{ads} + e^- \tag{20}$$

$$OH^- + OH_{ads} \rightleftarrows O_{ads} + H_2O + e^- \tag{21}$$

$$O_{ads} + O_{ads} \rightleftarrows O_2 \tag{22}$$

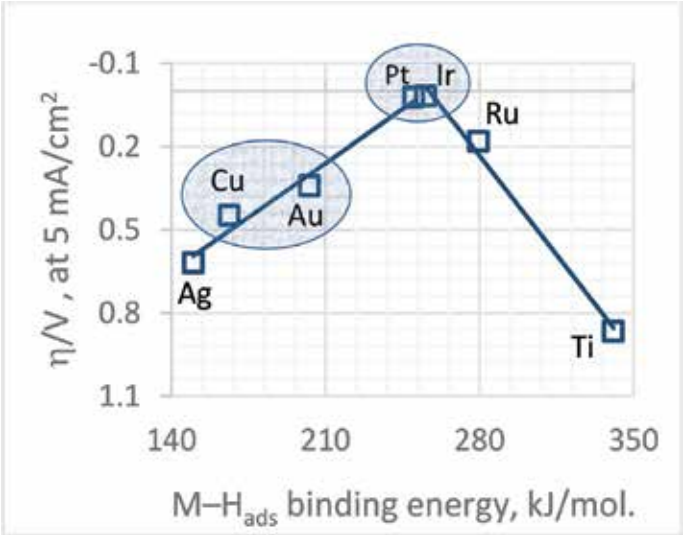

Figure 2. HER activity, overpotential (η) at 5 mA cm^{-2}, measured in 0.1 M $HClO_4$ (pH = 1) as a function of calculated M–H binding energy for several metals (volcano plot) [20].

The mechanism is controlled by the charge transfer (step 20 or 21) at low temperatures. On the other hand, at high temperatures, the recombination step (Eq. 22) controls the reaction on Ni electrode [22–30].

Generally, acid solutions or PEMs are used as electrolytes in water electrolyzers because acidic media show high ionic conductivity and are free from carbonate formation, as compared with alkaline electrolytes. Consequently, noble metals are used as electrocatalysts for OER in acidic media. Ruthenium and iridium have shown strong activity for OER, but they were passivated at very high anode potentials [31–36]. Bifunctional electrocatalysts, which can work for both oxygen evolution and oxygen reduction, have also been proposed for water electrolysis. A typical bifunctional electrocatalyst is composed of a noble metal oxide such as IrO2. For unsupported bifunctional electrocatalysts, Pt-MOx (M = Ru, Ir, Na), bimetallic (e.g., Pt-Ir), and trimetallic (e.g., $Pt_{4.5}Ru_4Ir_{0.5}$) materials have been developed [37–40].

At high current densities, are added to the polarization of the electrodes other resistances: ohmic losses in the electrolyte, resistances from bubbles, diaphragm, and ion transfer.

3.4. Electrical resistance

The electrical resistance in a water electrolysis system has three main components: (1) the resistance in the system circuits; (2) the mass transport phenomena including ions transfer in the electrolyte; (3) the gas bubbles covering the electrode surfaces and the diaphragm [15].

The nature and the dimensions of the materials used in the electrodes and the connections and the electric circuit, the methods of their preparations are responsible for the electrical resistance of the system. It can be expressed as follows:

$$R = \sum_i \frac{l_i}{A_i \cdot \chi_i} \tag{23}$$

where $\chi_i \left(\Omega^{-1} m^{-1}\right)$ is the electrical conductivity for each component of the circuit, including wires, connectors, and electrodes. This part of the resistance can be reduced by reducing the length of the wire, increasing the cross-section area and adopting more conductive wire material.

The ionic solution conductivity χ is a function of concentration and temperature. For an ionic solution containing ions (i), charged $+z_i$ or $-z_i$ and at the concentration C_i in $mol.\cdot m^{-3}$, the conductivity of the solution, noted $\chi \left(\Omega^{-1} m^{-1}\right)$, is:

$$\chi = \sum_i \lambda_i \cdot z_i \cdot C_i \tag{24}$$

with: λ_i is the equivalent conductivity of the ion (i) in, $S \cdot m^2 \cdot mol.^{-1}$.

The presence of bubbles in the electrolyte solution and on the electrode surfaces causes additional resistances to the ionic transfer and surface electrochemical reactions. One of the accepted theoretical equations to study the bubble effect in the electrolyte is given as follows [41]:

$$\kappa_g = \kappa(1 - 1.5 \cdot f) \tag{25}$$

where κ is the specific conductivity of the gas-free electrolyte solution; f is the volume fraction of gas in the solution [42].

3.5. Transport resistances

Convective mass transfer plays an important role in the ionic transfer, heat dissipation and distribution, and gas bubble behavior in the electrolyte. The viscosity and flow field of the electrolyte determines the mass (ionic) transfer, temperature distribution and bubble sizes, bubble detachment and rising velocity, and in turn influence the current and potential distributions in the electrolysis cell. As the water electrolysis progresses the concentration of the electrolyte increases, resulting in an increase in the viscosity. Water is usually continuously added to the system to maintain a constant electrolyte concentration and thus the viscosity.

4. Alkaline electrolysis

The conductivity of the solution is enhanced by the use of strong electrolytes that deliver ions with high mobility [43], such as sodium, potassium for positive ions, and hydroxide or chlorides as negative ions. During electrolysis, the water molecules move to the cathode by diffusion as they are consumed, and the hydroxide ions move to the anode by migration because they have an opposite charge and diffusion because they are consumed. A diaphragm

separates the two anode and cathode compartments and the gases formed are thus collected: hydrogen at the cathode and oxygen at the anode as shown in **Figure 3**.

Concentrated solutions of potassium hydroxide are generally used as the electrolytic solution because they have very high conductivities and fewer corrosion problems compared with other alkaline electrolytes. The electrode materials often used are based on nickel because of its low cost, high activity [44].

Electrolysis cells can be of two types of configurations: monopolar and bipolar [14]. **Figure 4**(a) gives a schematic of the monopolar configuration. The electrodes are altered in the electrolyzer and are all directly connected to the terminals of the DC power supply: the anodes at the positive terminal and the cathodes at the negative terminal. The total voltage applied to the entire electrolysis cell is essentially the same as that applied to the individual pairs of the electrodes in the cell ($U_{tot} = U_i$), but the current is subdivided between the different unit cells ($I_{tot} = n \times I_i$). **Figure 4**(b) depicts conflation in bipolar mode. Only the two end electrodes are connected directly to the DC power source. The other inner electrodes have a dual role: one side acts as the cathode for a unit cell and the other side acts as the anode for the adjacent unit cell. These cells are electrically linked thanks to their electrodes which are bipolar and ionically via the electrolytic solution. The total voltage of the cell is the sum of the individual voltages of

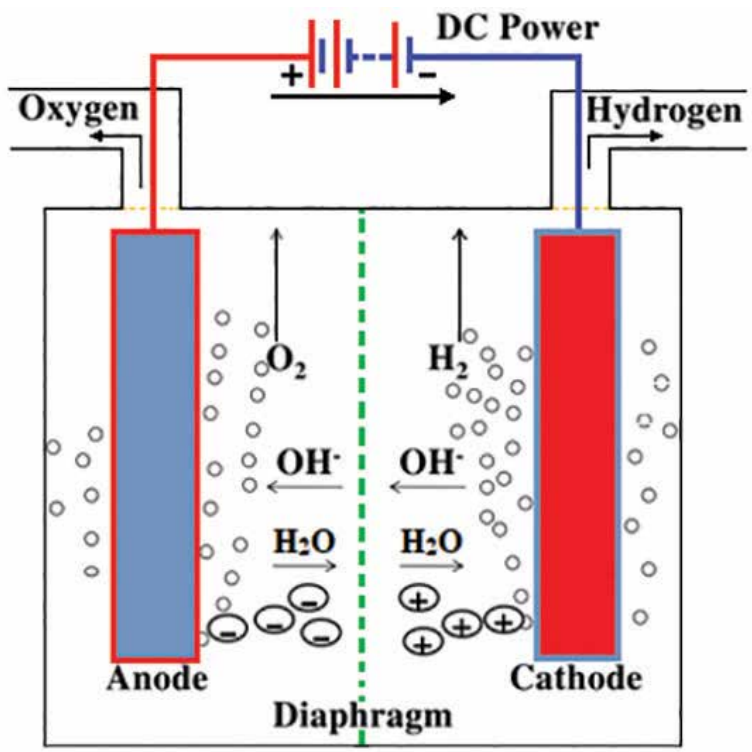

Figure 3. Principle of an alkaline water electrolysis.

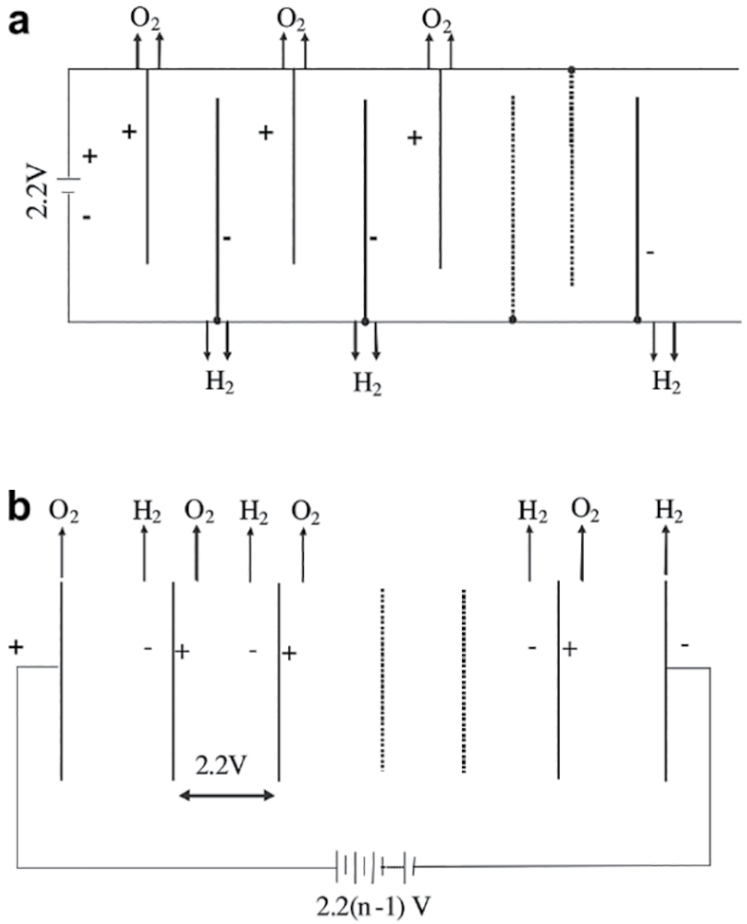

Figure 4. Schematics of cell configurations of monopolar (a) and bipolar (b) electrolyzers [14].

the unit cells ($U_{tot} = n \times U_i$), but the current for each unit cell is equal to the output current of the generator ($I_{tot} = I_i$). The electrical energy consumed is the same in the two configurations.

The wide range of flammability limits of the mixture of hydrogen and oxygen requires a careful design of the electrolyzer system. The separator diaphragm (or membrane) must avoid the mixing of the two gases inside the cell. Furthermore, the corrosive nature of the electrolyte does not allow leaks that are often likely to take place at the connections and seals of the electrolyzer. The bipolar configuration is more risky in mixing oxygen and hydrogen because of their simultaneous productions on the same bipolar electrode (on each side) and also electrolyte leakage as the monopolar design.

Obviously, the life of the system is an important criterion. It is extremely linked to the quality of the materials used. Indeed, these materials must be resistant to high concentrations of the alkaline electrolyte and operating conditions of the electrolyzer (pressure and temperature). In particular, connections and seals are subject to corrosion, which is why it is recommended to use sealing materials that are also stable in this environment [14].

5. PEM electrolyzer

PEM electrolyzers are characterized by their very simple construction and their compactness. The operating principle of electrolysis of water with an electrolyte protons exchange membrane (PEM) is simple. When operating in electrolysis, the water decomposes at the anode into protons and molecular oxygen. The oxygen is evacuated by the water circulation, and the protons migrate to the cathode under the effect of the electric field. There, they are reduced to molecular hydrogen. Each proton carries with it a procession of several molecules of solvation water: it is the electro-osmotic flow.

During the twentieth century, several major innovations have significantly increased the energy and faradic efficiencies of electrolyzers. The concept of zero-gap cells has been developed in order to overcome the disadvantages of the electro-osmotic flow. It consists of pressing porous electrodes against the solid separator in order to reduce the interpolar distance and to reject the gas production at the rear of the interpolar space.

The zero-gap concept with immobilized electrolyte goes even further: it consists of maintaining the electrolyte (acid) in the separator so as to be able to electrolyze the water in the acidic medium while avoiding corrosion problems. Of course, this interesting approach was practically limited by the leakage of electrolyte pushed back into the circuit of the electrolyzer.

The membrane thus serves both electrolyte and separator of electrodes and gases. Therefore, the membrane must have certain physicochemical properties, such as:

- High ionic conductivity to promote proton migration and reduce ohmic drop;
- No electrical conductivity to avoid short-circuits;
- Good chemical stability;
- Low permeability to oxygen and hydrogen;
- Good mechanical and dimensional stability, especially resistance to pressure;
- Good thermal stability, operating temperature up to 80–100°C.

Compared to a liquid electrolyte, we can note some behavioral deference resulting from the properties of this assembly:

- The anionic charges of the membrane are fixed; there can be no concentration gradient in their case.
- The gas evolution is done by the back of the electrodes, the ohmic drop is not disturbed by the reactions to the electrodes, in return, it is necessary to make laying electrodes to allow gas release.
- The nature of the ions also intervenes, but the water content of the membrane, different according to the nature of the ions carried and according to the conditions of preparation and use of the membrane, will condition both its thickness, its mechanical strength, and especially its conductivity.

The appearance of the first ion exchange membranes in the 1940s made it possible to seriously consider industrial applications for this zero-gap concept with immobilized electrolyte. Notably, as early as 1953, at the dawn of the American space program, the US General Electric Company suggested for the first time the use of cation exchange membranes as a solid polymer electrolyte for the production of acid fuel cells. The US solid polymer electrolyte (SPE) concept was born. Applied to the electrolysis of water, it was hoped to be able to operate at a high current density (of the order of an ampere per cm^2). This possibility was interesting for minimizing investment costs and increasing the volume density of production. Unlike fuel cells, the electrolysis of water SPE requires a polymeric material that is very resistant to the oxidizing potential of the anode under the release of native oxygen.

6. Solid oxide electrolyzer

Solid oxide fuel cells are electrochemical devices that can operate reversibly in the electrolysis mode. In the solid oxide electrolyzer, water vapor is reduced to H_2.

Electrolysis at high temperature allows decreasing the electric consumption because with the increase of the temperature offers an additional part of the global energy; which allows high operational efficiencies in the solid oxide electrolyzer.

The main advantage is that a substantial part of the energy required for the electrolysis process is added in the form of heat, which is much cheaper than electrical energy. In addition, the high temperature promotes the conduction of the electrolyte and accelerates the kinetics of the reaction, reducing the energy loss due to the polarization of the electrode. Thus, the efficiency of the electrolysis at high temperature is higher than that obtained at low temperature. The typical high-temperature electrolyzer can achieve an electrical efficiency of 92% while the electrolyzers at low temperature reach a maximum of 85% efficiency.

The high-temperature system uses oxygen ion conducting ceramics as an electrolyte (ZrO_2 stabilized by Y_2O_3, MgO or CaO). The water is brought to a temperature of 200°C to supply steam in the cathode. The electrolysis cell operates at a temperature of 800–1000°C, which ensures the conduction of the solid electrolyte. The water vapor is decomposed into hydrogen gases and oxygen ions (O^{2-}). The oxygen ions are transported through the ceramic solid electrolyte to the anode, where they are oxidized to form gaseous oxygen.

7. Hydrogen station

Hydrogen has a low carbon footprint. It could thus significantly reduce energy-related CO_2 emissions and help limit climate change. Fuel cell electric vehicles (FCEVs) can provide the mobility service of today's conventional cars with potentially very low carbon emissions. Although the potential benefits of hydrogen and fuel cells in end-use applications are promising in terms of environment and energy security, the development of hydrogen production,

Country or region	Existing hydrogen refueling stations	Planned stations	
		2015	2020
Europe	36	~80	~430
Japan	21	100	>100
Korea	13	43	200
United States	9	>50	>10

Table 2. Existing public hydrogen refueling stations and targets announced by hydrogen initiatives [46].

transport, and distribution are difficult. Although the first VECFs were developed in the 1960s, it is only in the last 10 years that the technology of using hydrogen as an energy carrier has begun to develop. Also, some automakers announce the launch of FCEV.

Generally, hydrogen station consists of hydrogen production process including desulfurizer, reformer, water gas shift (WGS) reactor and pressure swing adsorption (PSA) apparatus, and post-treatment process including a compressor, storage, and distributer [45]. Research on the development of the hydrogen station is actively conducted in advanced countries such as the United States, Canada, Japan and Europe. An overview of existing and planned hydrogen refueling stations is given in **Table 2** [46].

Currently, more than 79 hydrogen stations are operating worldwide and others are planned in the future. **Table 3** summarizes the current status of hydrogen station research and development programs and demonstration experiments at home and abroad [45].

Nation	Program	H_2 station	Hydrogen production method
USA	SCAQMD project, CaFCP & freedom CAR etc.	CA, IL, MI, NV, AZ, eastern, etc. [25]	• Electrolysis, liquid H_2, LNG & biomass reforming, photocatalyst, etc. • Compressed H_2 & LH_2 • Air Product Co., Stuart Energy Co. etc.
Japan	WE-NET program, JHFC project, and new H_2 project, etc.	Tokyo & Yokohama, etc. [14]	• Reforming of naphtha, gasoline, LPG, LNG, diesel & methanol, COG, electrolysis, LH_2, etc. • Compressed H_2 • Tokyo gas, Nippon Sanso, Cosmo oil, etc.
Canada	Hydrogenics & Canadian, Transportation FC Alliance, etc.	Toronto, etc. [6]	• Electrolysis of H_2O (alternative energy) • Compressed H_2 • Hydrogenics
EU	CUTE and ECTOS Projects, etc.	Framework (FP5) [32]	• Electrolysis [4], LNG reforming [3], LH_2 [2] Alternative energy, bus • Compressed H_2 & LH_2 • BP Co., Linde Co.
Korea	MOCIE, H_2 & FC Project MOST, 21C Frontier Profect	Goal of MOCIE 1stage (03-05):1 2stage (06-08):10 3stage (09-12):50	• Production by reforming of LNG, LPG & naphtha • Compressed H_2 • SK Co., KIST, KIER, KOGAS, GS Caltex

Table 3. R&D situation of hydrogen station in worldwide [45].

8. Conclusion

Hydrogen economy is a promising instrument for the transformation of the energy system. Hydrogen, ideal fuel for fuel cells, can have several provenances (electrolysis of water, cracking or reforming of petroleum products). The production of hydrogen by the water electrolysis technique gives the concept renewability because it can use a non-greenhouse gas energy source (renewable or nuclear energy). This technique provides applications that require small volumes of high purity hydrogen, including the semiconductor and food industry.

Acid solutions are good electrolytes in water electrolyzers because acidic media show high ionic conductivity and are free from carbonate formation, as compared with alkaline electrolytes. But the acid needs the use of noble metals as electrocatalysts for OER. Consequently, potassium hydroxide is most commonly used in water electrolysis, avoiding the huge corrosion loss caused by acid electrolytes, and the use of noble metals as catalysts. Nickel is a popular electrode material due to its high activity and availability as well as low cost.

PEM electrolyzers are characterized by their very simple construction and their compactness with an electrolyte protons exchange membrane (PEM) is simple. During the twentieth century, several major innovations have significantly increased the energy and faradic efficiencies of electrolyzers.

Solid oxide electrolyzer, operating at high temperature, allows decreasing the electric consumption because with the increase of the temperature offers an additional part of the global energy; which allows high operational efficiencies in the solid oxide electrolyzer. Thus, the efficiency of the electrolysis at high temperature is higher (92%) than that obtained at low temperature (85%).

Research on the development of the hydrogen station is actively conducted in advanced countries such as the United States, Canada, Japan, and Europe. Currently, 70 hydrogen stations are operating worldwide, and demand is expected to increase rapidly in the future.

Author details

Youssef Naimi* and Amal Antar

*Address all correspondence to: youssefnaimi@outlook.com

Faculty of Sciences Ben M'sik, University of Hassan II Casablanca, Casablanca, Morocco

References

[1] United Nations. Transforming Our World: The 2030 Agenda for Sustainable Development. New York: United Nations General Assembly; 2015; A/RES/70/1. Available at: http://www.refworld.org/docid/57b6e3e44.html [accessed 22 April 2018]

[2] Schlör H, Koj J, Zapp P, Schreiber A, Hake J-F. The social footprint of hydrogen production—A social life cycle assessment (S-LCA) of alkaline water electrolysis. Energy Procedia. 2017;**105**:3038-3044

[3] Naimi Y, Pile à combustible à Membrane échangeuse de Protons: Historique, théorie, Etat de l'art et travaux de recherches pour optimiser les performances, Editions universitaires europeennes; 2012. p. 128. ISBN-13: 978–3841788467

[4] Pletcher D, Li X. Prospects for alkaline zero gap water electrolysers for hydrogen production. International Journal of Hydrogen Energy. 2011;**36**:15089

[5] Eliezer D, Eliaz N, Senkov ON, Froes FH. Positive effects of hydrogen in metals. Materials Science and Engineering A. 2000;**280**:220

[6] Lattin WC, Utgikar VP. Transition to hydrogen economy in the United States: A 2006 status report. International Journal of Hydrogen Energy. 2007;**32**:3230

[7] Ramachandran R, Menon RK. An overview of industrial uses of hydrogen. International Journal of Hydrogen Energy. 1998;**23**:593

[8] Barreto L, Makihira A, Riahi K. The hydrogen economy in the 21st century: A sustainable development scenario. International Journal of Hydrogen Energy. 2003;**28**:267

[9] Turner JA. Sustainable Hydrogen Production. Science. 2004;**305**:972

[10] Rosen MA, Scott DS. Comparative efficiency assessments for a range of hydrogen production processes. International Journal of Hydrogen Energy. 1998;**23**:653

[11] Trommer D, Noembrini F, Fasciana M, Rodriguez D, Morales A, Romero M, Steinfeld A. Hydrogen production by steam-gasification of petroleum coke using concentrated solar power—I. Thermodynamic and kinetic analyses. International Journal of Hydrogen Energy. 2005;**30**:605

[12] Momirlan M, Veziroglu TN. Current status of hydrogen energy. Renewable and Sustainable Energy Reviews. 2002;**6**:141

[13] Sato S, Lin SY, Suzuki Y, Hatano H. Hydrogen production from heavy oil in the presence of calcium hydroxide. Fuel. 2003;**82**:561

[14] Stojić DL, Marčeta MP, Sovilj SP, Miljanić SS. Hydrogen generation from water electrolysis—possibilities of energy saving. Journal of Power Sources. 2003;**118**:315

[15] Trasatti S. Water electrolysis: Who first? Journal of Electroanalytical Chemistry. 1999;**476**:90

[16] Dunn S. Hydrogen futures: Toward a sustainable energy system. International Journal of Hydrogen Energy. 2002;**27**:235

[17] De Souza RF, Padilha JC, Goncalves RS, De Souza MO, Rault-Berthelot J. Electrochemical hydrogen production from water electrolysis using ionic liquid as electrolytes: Towards the best device. Journal of Power Sources. 2007;**164**:792

[18] Kinoshita K. Electrochemical Oxygen Technology. 1st ed. New York: John Wiley & Sons; 1992

[19] Zeng K, Zhang D. Recent progress in alkaline water electrolysis for hydrogen production and applications. Progress in Energy and Combustion Science. 2010;**36**:307-326

[20] Bockris JOM, Conway BE, Yeager E, White RE. Comprehensive Treatise of Electrochemistry. New York: Plenum Press; 1981

[21] Viswanath RP. A patent for generation of electrolytic hydrogen by a cost effective and cheaper route. International Journal of Hydrogen Energy. 2004;**29**:1191-1194

[22] Santos DMF, Sequeira CAC, Lobo RFM. Effect of alloys modified by sodium borohydride alkaline solutions on the kinetics of hydrogen evolution reaction at Mm(Ni3.6Co0.7Mn0.4Al0.3)1.15 hydride electrodes. International Journal of Hydrogen Energy. 2010;**35**:9901

[23] Sequeira CAC, Santos DMF, Sousa JR, Brito PSD. Reactively deposited cobalt electrodes for hydrogen evolution in alkaline solution. Materials Technology. 2009;**24**:119

[24] Trasatti S. Work function, electronegativity, and electrochemical behaviour of metals: II. Potentials of zero charge and "electrochemical" work functions. Journal of Electroanalytical Chemistry. 1971;**33**:351

[25] Santos DMF, Sequeira CAC, Figueiredo JL. Hydrogen production by alkaline water electrolysis. Quimica Nova. 2013;**36**(8):1176-1193

[26] Danilovic N, Subbaraman R, Strmcnik D, Stamenkovic VR, Markovic NM. Electrocatalysis of the HER in acid and alkaline media. Journal of the Serbian Chemical Society. 2013;**78**(12):2007-2015

[27] Subbaraman R, Tripkovic D, Strmcnik D, Chang K-C, Uchimura M, Paulikas AP, Stamenkovic V, Markovic NM. Enhancing Hydrogen Evolution Activity in Water Splitting by Tailoring Li+-Ni(OH)2-Pt Interfaces. Science. 2011;**334**:1256

[28] Sequeira CAC, Santos DMF, Cameron E, Brito PSD. Nickel coated electrodes for oxygen evolution in alkaline solution. Materials Technology. 2008;**23**:142

[29] Cappadonia M, Divisek J, von der Heyden T, Stimming U. Oxygen evolution at nickel anodes in concentrated alkaline solution. Electrochimica Acta. 1994;**39**:1559

[30] Damjanovic A, Dey A, Bockris JO'M. Electrode kinetics of oxygen evolution and dissolution on Rh, Ir, and Pt-Rh alloy electrodes. Journal of the Electrochemical Society. 1966;**113**:739

[31] Mozota J, Vukovic M, Conway BE. Enhanced electrocatalysis for chlorine evolution on oxidized Ir and Ru anodes modified by potential cycling. Journal of Electroanalytical Chemistry and Interfacial Electrochemistry. 1980;**114**:153

[32] Gottesfeld S, Srinivasan S. Electrochemical and optical studies of thick oxide layers on iridium and their electrocatalytic activities for the oxygen evolution reaction. Journal of Electroanalytical Chemistry. 1978;**86**:89

[33] Trasatti S. Electrocatalysis: Understanding the success of DSA®. Electrochimica Acta. 2000;**45**:2377

[34] Conway BE. Electrochemical oxide film formation at noble metals as a surface-chemical process. Progress in Surface Science. 1995;**49**:331

[35] Miles MH, Thomason MA. Periodic Variations of Overvoltages for Water Electrolysis in Acid Solutions from Cyclic Voltammetric Studies. Journal of the Electrochemical Society. 1976;**123**:1459

[36] Swette LL, LaConti AB, McCatty SA. Proton-exchange membrane regenerative fuel cells. Journal of Power Sources. 1994;**47**:343

[37] Rivas S, Arriaga LG, Morales L, Fernández AM. Evaluation of Pt-Ru-Ir as bifunctional electrocatalysts for the oxygen electrode in a unitized regenerative fuel cell. International Journal of Electrochemical Science. 2012;**7**:3601

[38] Chen G, Delafuente DA, Sarangapani S, Mallouk TE. Combinatorial discovery of bifunctional oxygen reduction—water oxidation electrocatalysts for regenerative fuel cells. Catalysis Today. 2001;**67**:341

[39] Ioroi T, Kitazawa N, Yasuda K, Yamamoto Y, Takenaka H. Iridium oxide/platinum electrocatalysts for unitized regenerative polymer electrolyte fuel cells. Journal of the Electrochemical Society. 2000;**147**:2018

[40] Crow DR. Principles and Applications of Electrochemistry. 1st ed. London: Chapman and Hall; 1974

[41] Pickett DJ. Electrochemical reactor design. 2nd ed. Amsterdam: Elsevier; 1979

[42] Oldham KB, Myland JC. Fundamentals of Electrochemical Science. San Diego, USA: Academic Press, Inc.; 1994; ISBN: 0125255454, 9780125255455

[43] Leroy RL. Industrial water electrolysis—Present and future. International Journal of Hydrogen Energy. 1983;**8**:401-417

[44] Janjua MBI, Leroy RL. Electrocatalyst performance in industrial water electrolysers. International Journal of Hydrogen Energy. 1985;**10**:11-19

[45] Moon DJ, Lee BG. R&D Trends and Unit Processes of Hydrogen Station. Korean Chemical Engineering Research. 2005;**43**:331-334

[46] International Energy Agency—IEA, Technology Roadmap Hydrogen and Fuel Cell. IEA Publications, printed by CORLET, Paris. 2015. p. 17. Available from: https://www.iea.org/publications/freepublications/publication/TechnologyRoadmapHydrogenandFuelCells.pdf [accessed 22 April 2018]

Chapter 2

Hydrogen Production by Membrane Water Splitting Technologies

Mohd Fadhzir Ahmad Kamaroddin,
Nordin Sabli and Tuan Amran Tuan Abdullah

Additional information is available at the end of the chapter

http://dx.doi.org/10.5772/intechopen.76727

Abstract

Hydrogen production by membrane water splitting technologies is a sustainable method to synthesize hydrogen and provides an alternative to hydrogen production instead of conventional process of synthesizing hydrogen from steam methane reforming. A hybrid polymer electrolyte membrane electrolyzer operational at working temperature of above 80–200°C is advantageous for faster electrochemical kinetics, higher current exchange density, and more resistance to fuel impurities. Phosphoric acid (PA) doping onto polybenzimidazole (PBI) membrane shows significant improvement in proton conductivities, permeability, and thermal stability. PBI-based electrolyzer is relatively new to the hydrogen production technologies as compared to Nafion-based electrolyzer. However, the high cost of purchasing Nafion membrane and inability to execute electrolysis operational above 90°C has sparked new interest on PBI-based membrane, which is known for its good thermal stability.

Keywords: hydrogen production, water splitting, polymer electrolyte membrane, electrolysis, sustainable

1. Introduction

Sustainable energy from renewable resources has become a focal point for many researchers around the world in their search to minimize the carbon emission released to the atmosphere. Hydrogen energy is the cleanest available energy, which only releases heat and water as by-products. Moreover, hydrogen combustion contributes to zero carbon emission. The Kyoto Protocol tabled in 1997 that came into effect in 2005 aimed to reduce the greenhouse gases

(GHG) by 5% (2005–2012) and 18% (2013–2020) against 1990 levels [1]. Unlike a conventional steam methane reforming process, the hybrid polymer electrolyte membrane (PEM) combines with copper (I) chloride and hydrochloric acid electrolytes that have a promising future of providing a sustainable hydrogen production.

Currently, there has been a crucial need for rapid changes from the hydrocarbon-based economy to the one with sustainable and renewable sources [2–4]. Many green technologies are available right now, such as the generation of hydrogen [5], solar electricity [6, 7], and other renewable energy technologies, but the capital expenditure to acquire this technology is very high as compared to conventional energy resources [8, 9]. For example, solar energy is limited by the efficiency of the panel and battery, while the electric vehicle is limited by the lack of charging facility and unsustainable production of electricity generation from coal- and petroleum-based fuel. It has been reported by Nicoletti et al. and Ball and Weeda [10, 11] the by-products from the combustion of hydrocarbon-based fuels are the major factors to the phenomena like global warming, the thinning of the ozone layer, acid rains, and air pollution and its harmful effect on respiratory problems. This is where hydrogen as the vital energy carrier and fuel sources offers sustainable and clean energy for the future [10, 12, 13].

Hydrogen does not exist individually, but it formed water molecules (H_2O) which contain single oxygen atom and dual hydrogen atom makes it an enormous amount of elements in the world. Hydrogen is able to generate sustainable, immaculate and cost-effective energy resources, which can uplift the economic activities of the world with environmentally friendly and secure energy. This is due to no carbon dioxide or carbon monoxide being produced in the process of combusting hydrogen with only water as by-products [14]. Hydrogen production can be synthesized from many types of resources like water, biomass, coal, methane, and others via chemical, thermal, and biological processes [15].

Hydrogen is also an important feedstock for chemical processes [16], and 97% of the world hydrogen supply comes from hydrocarbon-based fuels via reforming process [17] with the world's production of 50 million tons of hydrogen every year [15]. Among the various hydrogen production technologies that are available, electrolysis plays a vital role in producing sustainable hydrogen [18, 19]. Water electrolysis is also acknowledged as a crucial element in the forthcoming energy system [16]. Although this electrolysis technology was invented more than 100 years ago, the hydrogen production from water electrolysis is substantially more costly with the efficiency rate only 18–24% and mainly used when the high purity of hydrogen is needed or in a remote area where methane gas is not available. The cost of producing hydrogen from water electrolysis is more expensive because hydrogen does not exist as an independent gas but occurs naturally in the form of chemical compounds like the hydrocarbons and water [11, 20].

2. Types of membranes for hydrogen production

To date, there are few ways of synthesizing the ion exchange or polymer membranes including sulfonation, polymer blending, acid or base doping, addition of inorganic fillers, pores

filling, in-situ polymerization, and electrospinning [21, 22]. High-performance polymer electrolyte membranes (PEMs) must have the following characteristics [22]:

a. high proton conductivity

b. good electrical insulation

c. high mechanical and thermal stability

d. good oxidative and hydrolytic stability

e. cost-effectiveness

f. low tolerance to ion crossover/good barrier property

g. low swelling stress

h. capability for fabrication of membrane electrode assemblies (MEA)

One of the most important characteristics of the proton exchange membranes is water uptake that influences the electrochemical activity and hydromechanical stability of the membrane. Certainly, water is the fundamental element for proton transfer mechanism from the anode to the cathode in an electrochemical cell including an operation using non-sulfonated membranes in almost anhydrous condition and at a temperature range of 90–160°C [23]. However, the mechanical strength for a membrane with a higher water uptake reduces due to exorbitant swelling of the membrane. As a matter of fact, sulfonated membranes absorb more water molecules per acid group (λ) when compared with phosphonated membranes that make phosphonated membranes more favorable for PEM applications due to higher ionic exchange capacity (IEC) [24].

2.1. Polymer electrolyte membrane

Polymer electrolyte membrane usage in fuel cell technologies (PEM-FC) is widely accepted, and more advanced version of this PEM can significantly transform the energy security for probably 20–30 years from now. It has turned into an attractive research due to its advantages of generating minimum pollution, great power density, and excellent conversion. This is a promising path to be fossil fuel free and to contribute to other sustainable energy sources [25, 26].

Currently, perfluorosulfonic acid polymer membranes like Nafion is accepted as the most widely used applications for both PEM-FC and direct methanol fuel cell (DMFC) because of their superiority and exceptional performance in thermal stability, eminent ionic exchange capacity, and proton conductivity [26, 27]. However, the Nafion is costly, and it experiences huge methanol crossover for DMFC with the addition of depletion of proton conductivity when subjected to working temperature beyond 100°C [27]. Apart from isolating reactants from mixing together, PEM can allow proton to pass through while being nonelectrically conductive. Furthermore, PEMs have other functions of providing high ionic conductivity, good mechanical properties, and minimum to no ion crossover [28]. However, moderate operation

temperature from 80 to 180°C for PEM fuel cells is ideal for heat co-generation. In addition, with current low-temperature operation, a huge capital expenditure is required for acquiring the commercial perfluorosulfonic acid (PFSA) membrane.

Major obstacles for the development of Direct Methanol Fuel Cell (DMFC), PEM-FC, Redox Flow Batteries (RFB) technologies, which have a high crossover of ion via the membrane can be improved and rectified with the use of low feed/water/electrolyte crossover [28]. Multiple approaches and new types of materials have been formulated to mitigate the problem but with serious concerns in the chemical stability and proton conductivity. The membrane ionic conductivity can be enhanced by means of doping with acids such as heteropoly acids (HPA) [28].

In fuel cell development, the PEM needs to have the following characteristics including excellent proton conductivity, favorable mechanical properties, exceptional resistance to chemicals, and durable enough for endurance testing [4]. Nafion-based PEM is used for low temperatures operation <80°C, while for higher temperature of 120–200°C hydrocarbon polymers like polybenzimidazole (PBI), sulfonated poly(arylene ether ether ketone) and poly (bis(phenoxy) phosphazene) are being used as described in the literature. **Table 1** shows some of the proton exchange membranes that are manufactured by established organizations.

Currently, Nafion is used as a common membrane for solid polymer electrolyte although it has disadvantages for being expensive and a fluorinated-based polymer. Thus, recent studies are more focused on the improvement of cheaper and non-fluorinated polymers like polybenzimidazole (PBI), polyethersulfone (PES), sulfonated polysulfone (SPSF), polyaryleneethers, polyphosphazene, sulfonated polyetheretherketone (SPEEK), and polyimides. The advantages of these polymers are that they are cheaper and have good thermal, mechanical, and chemical properties. Out of these polymers, membranes from SPEEK polymer have demonstrated a very good performance for water electrolysis. The proton conductivity can be increased by adjusting the higher degree of sulfonation (DS) for SPEEK polymer due to its excellent mechanical properties. This will allow the optimization of DS onto the polymer

Organization	Type of membranes
US Polyfuel Inc.	Acid-based polyether ether ketone
Toshiba	Acid-based polyether ether sulfone
Sony	OH-modified fullerene based membranes
JSR Corporation, Japan	Polystyrene sulfonic acid-based compounds
Stuttgart University, Germany	Acid-based ionomer blends
Los Alamos National Laboratory (LANL)	Sulfonation sulfone polymer; PVDF-g-SPS
Ballard	Sulfonated F-styrene
DuPont	Modified Nafion
Asahi Glass	PFS/PTFE fibrils

Table 1. Proton exchange membrane of established manufacturers [4].

membrane by manipulating the temperature and immersion time of the sulfonation reaction. The DS of the polymers can also be manipulated by varying the sulfonating agent concentration and the sulfonated monomers content. Furthermore, the sulfonic group ($-SO_3H$) enhances the selectivity, solubility, and water uptake, which contributes to superior chemical properties [29, 30]. Aromatic polymers that are exposed to high sulfonation (higher DS) will have a better proton conductivity. However, higher DS can lead the polymer to become more soluble and swell in water, thus decrease the mechanical strength of the membrane significantly. Therefore, the method used to improve the electrochemical and mechanical properties of the membrane is by forming a composite membrane using the addition of organic and inorganic compounds [29].

Generally, PEM fuel cell working temperature is limited by the Nafion membrane electrochemical properties, which can only operate at a temperature less than 100°C. Although, the ideal working temperature of the PEM-FC based on Pt catalyst should be higher than 100°C as it can significantly mitigate the effect of CO poisoning [27]. Principally, fuel cell consumes oxygen and hydrogen gas to produce electricity, water, and heat as compared to an electrolyzer that produces hydrogen and oxygen as the products.

There are four types of polymer electrolytes for hydrogen economy, which includes fluorinated and partially fluorinated membranes, hydrocarbon membranes, aromatic membranes, and hybrid membranes.

The main polymer chain is used to categorize the type of polymer electrolytes. As a guideline, the primary chain indicates the surface morphology including physical and thermomechanical properties. Apart from that, the supporting chain contributes to the polymer functionality. Typical polymer chains consist of hydrocarbons, perfluorinated and aromatic, as their primary polymer chains. Majority of the polymers used in the research comprise sulfonic acid groups. It is located at supporting chains or as functional groups at the polymer backbone. The sulfonic group functions as a proton conductor in order to promote proton movement across the membrane [31].

2.1.1. Proton exchange membrane

In recent years, there has been an increasing amount of literature on proton exchange membrane particularly focusing on hydrogen production for fuel cells and electrolyzers. Di Noto et al. [32] reported that an excellent proton-conducting membrane for a fuel cell comprises the following attributes:

- **a.** Exceptional stability on electrochemical and chemical properties
- **b.** Great strength and stability on mechanical properties within process temperature limit
- **c.** Membrane chemical properties are suitable for the membrane electrode assembly
- **d.** Exceptionally very little reactant crossover
- **e.** High water retention to maintain electrolyte species and avoid confined drying

f. Superior conductivity of proton to brace high current with the lowest resistance deprivation and minor electronic conductivity

g. Cheap in producing the membrane

Proton Exchange Membrane (PEM) is commonly used in the fuel cells setup. The most popular and widely used PEM is Nafion and Nafion-based membrane because of its excellent proton conductivity and good physicochemical properties. However, Nafion experiences very distinct fuel crossover, tedious process to synthesize, and weak proton conductivity at high temperature in low humidity condition. There are many types of research being conducted to find the alternative membranes for fuel cell systems. Polymers like poly (ether ether ketone), poly (arylene ether ketone), and poly (ether sulfone) have been studied and tested as solid electrolytes in fuel cell applications. All of the studies conducted for PEEK, PAEK, and PES support the fact that aromatic polymer electrolytes are suitable and perform very well in fuel cell systems. The criteria include excellent proton conductivity, good thermomechanical and chemical properties, and reasonable cost. This material is also cheaper and easier to form a membrane as compared to Nafion membranes.

Therefore, the PEEK is chosen as an alternative to Nafion primarily because it is cheaper and easier to synthesize with good electrochemical and stable physicochemical properties [27].

2.1.1.1. Nafion membrane

General Electric Co. (USA) is the first to develop proton exchange membrane (PEM) electrolyzer back in 1966 from a solid polymer electrolyte, which comprises of membrane, anode, and cathode. Nafion membrane produced by DuPont is the most well-known membrane that is made up of perfluorinated polymer with sulfonic acid functionalization as depicted in **Figure 1** [33].

Majority of the available PEM-FC are using proton exchange membranes that originate from perfluorosulfonic acid (PFSA) polymers such as Nafion 115, Nafion 117, and Nafion 212. Nafion has a very good chemical resistance, good mechanical properties, and are very durable [35]. Apart from that, Nafion shows good stability when subjected to radical degradation and

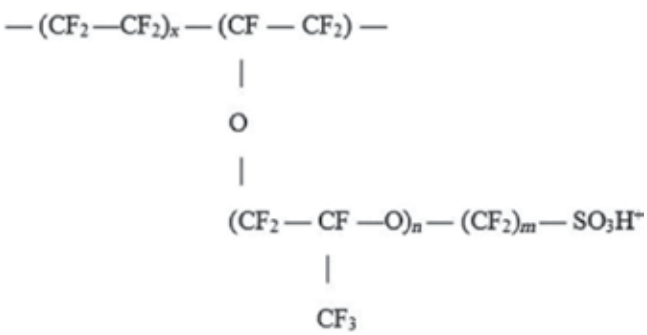

Figure 1. The structural formula of Nafion® membrane by DuPont de Nemours [34].

peroxide ions [36]. Despite all the advantages, Nafion also has few disadvantages such as they cannot function smoothly under dehydrated ambiance and cannot withstand higher operating temperature above 80°C (1 atm pressure) as it will deteriorate its good proton conductivity performance [35]. Moreover, Nafion is not suitable for temperature conditions below 0°C or beyond 100°C, and its proton conductivity is water dependent [36].

Nafion and perfluorinated membranes are considered as the benchmark for other new membrane synthesis [32]. There is also a study being carried out on the modification of Nafion-based membrane with polyaniline (PANI) by varying the membrane thickness. The physical properties such as ion exchange capacity (IEC), proton conductivity, and water uptake are investigated. Moreover, the Cu permeability or Cu crossover phenomena was studied using an ex situ Cu diffusion cell and the performance of the modified membrane was configured using a CuCl electrolytic system [37].

Perfluorosulfonic acid (PFSA) polymer electrolyte membrane conductivity and hydration properties can be enhanced by synthesizing composite membranes with organic fillers such as hygroscopic oxides (SiO_2/TiO_2), zirconium phosphates $Zr(HPO_4)_2 \cdot nH_2O$, ZrP), zirconium sulphophenylphosphates and heteropolyacids. Furthermore, ionic liquids or phosphoric acid can be a substitute for water due to less volatile properties while under dehydrating ambiance in order to sustain high proton conductivity, for example, $10^{-2}S \cdot cm^{-1}$ [38]. However, Nafion membrane is very expensive with the addition of not having adequate conductivity at a higher temperature of 90°C and near anhydrous condition. It is also not environmentally friendly due to the usage of many chemicals in its fabrication, utilization, and discarding processes [32]. In the DMFC system, the Nafion membrane or perfluorinated PEM cannot be directly used due to the high crossover of methanol that can shorten the lifetime and performance of the fuel cells. The high methanol crossover can be explained by the large channel related to the molecular structure that consists of a large ion group [4].

Currently, Nafion and Nafion-based membrane are the most popular and widely used membranes for applications in proton exchange membrane fuel cell, direct methanol fuel cell, and electrolyzers. It has good proton conductivity and fair thermal stability for operating in temperatures below 80°C. However, Nafion is very costly and permeable to fuel, thus allowing diffusion of anolyte to catholyte. In addition, Nafion also loses its good proton conductivity properties at operating temperatures beyond 100°C [27].

2.1.1.2. Polybenzimidazole

Polybenzimidazole (PBI) refers to multiple units of benzimidazole in the structure of aromatic heterocyclic polymers. PBI has a few advantages as compared to Nafion membrane including good tensile strength, fair chemical stability, and exclusive affinity with polyaryletherketone and some other polymers. **Figure 2** presents the synthesis of PBI polymer.

Although Nafion membrane is very good for processes that operate at temperatures from 20 to 80°C, it is not suitable for high-temperature (HT) applications above 100°C due to poor mechanical stability and the significant decrease of proton conductivity [40]. Polybenzimidazole (PBI) was first used by Wainright in 1995 for high-temperature-polymer electrolyte membrane

(HT-PEM) at 150°C and is a very suitable candidate for any process temperature ranging from 120 to 200°C [35, 41].

However, pristine PBI has very low conductivity when compared to Nafion, which makes it unsuitable as a replacement for Nafion. Researches to improve the proton conductivity of pristine PBI have been carried out by treating the PBI with many inorganic acids via PBI composite membrane synthesis. Sulfuric acid (H_2SO_4) and phosphoric acid (H_3PO_4) act as a synergistic effect of contributor and acceptor in transferring the proton, thus allowing for proton transport through the membrane. Phosphoric acid (H_3PO_4) is more favorable when compared to sulfuric acid (H_2SO_4) due to its superiority with process temperatures greater than 150°C in terms of mechanical strength, improved proton conductivity, and thermal durability [35, 42].

When PBI membrane was doped with phosphoric acid (H_3PO_4), its properties improved including low gas permeability, low methanol vapor crossover, and it did not need any humidification. Despite having the advantage of operating at a higher temperature range above 100°C, the doping process is necessary to reinforce the mechanical stability of the membrane due to standard PBI-like Celazole that has a low-to-medium linear molecular weight with poor mechanical stability and poor oxidative resistance. Following are the advantages of HT-PEM-FC that operates above 100°C: ability to use less expensive nonnoble catalyst like cobalt and iron, improved heat rejection rate, enhanced water management, more robust to impurities, and better electrode kinetics [41].

Hybrid membrane from PBI can be prepared by the addition of inorganic fillers such as silicates, titanium dioxide (TiO_2), zirconium dioxide (ZrO_2), heteropolyacids (HPA), and carbon nanotubes (CNT) [22]. Barium zirconium oxide ($BaZrO_3$) was fabricated as a composite membrane from PBI base according to Hooshyari et al. [43] who also researched on the nanocomposite PEM-ZrO_2 nanocluster that was mixed into a solution cast of 2,6-pyridine polybenzimidazole (2,6,Py-PBI) and doped with phosphoric acid with variations from 0 to 10 wt% of ZrO_2 nanocluster [44].

There are few approaches to enhance the properties of PBI-doped H_3PO_4 membrane, which includes a method of preparing ion cross-linked structures such as a mixture of PBI with sulfonated polyether ether ketone (SPEEK), sulfonated polysulfone, or sulfonated partially fluorinated arylene polyether [38]). In addition, improved PBI-doped phosphoric acid membrane can be synthesized by covalently cross-linked structure or composite/hybrid PBI membrane. In PBI/PA, the proton conductivity is strongly dependent on the acid doping level, which is defined as the number of PA molecules per repeating units of the polymer.

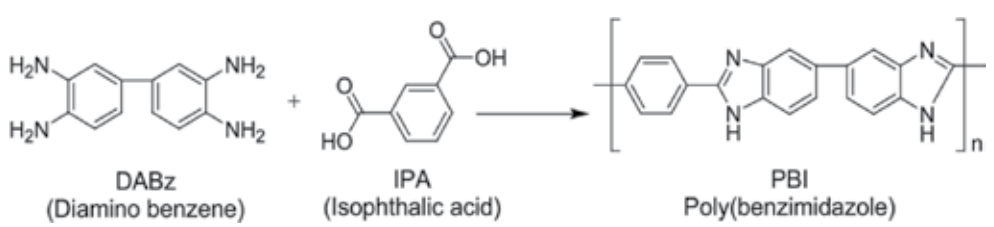

Figure 2. Synthesis of poly(benzimidazole) (PBI) [39].

PBI-based PEM-FC cathode is 70-fold more invulnerable to sulfur content in the air as compared to Nafion®-based PEM-FC cathodes [40]. It is also noted that acid doping in PBI shows a significant effect in the membrane thermal stability and proton conductivities [45]. The proton conductivities of acid-doped PBI membranes were also dependent to the doped acids in the order of $H_2SO_4 > H_3PO_4 > HClO_4 > HNO_3 > HCl$ [45, 46]. Similarly, Oono et al. [47] studied the influence of the phosphoric acid doping level in a PBI membrane by means of immersing the PBI membrane in 85% phosphoric acid solution for 500 min at 20°C and 80 min at 40 and 60°C. Sulfonated PBI showed higher proton conductivity as compared to pristine PBI membrane due to more active acid sites. PBI blending with Nafion, sulfonated polyether, and polyphosphazene were studied to investigate the effect on membrane stability and less permeable to methanol crossover. Moreover, the addition of inorganic fillers enhanced the properties of proton conductivities and physical strength of the modified membrane. However, doping decreased the proton conductivities, but this could be controlled by introducing sulfonated material as reinforcements.

There are numerous methods that have been implemented to enhance the conductivity and stability of PBI membranes, which include membrane fabrication technique for optimization, polymer backbone crosslinking, polymer blending, and creating composite membrane by the introduction of many kinds of organic acids. Factors influencing the proton conductivity of PA-doped PBI and PBI composite membrane are process temperature, acid doping level (ADL), and relative humidity (RH). This was found in PA-doped PBI that had a 5.6 doping level (mole number of H_3PO_4 per repeat unit of PBI) with a conductivity of 6.8×10^{-2} S cm^{-1} and process conditions at 200°C and 5% RH. Moreover, under the similar setting, the PBI composite membrane with 15 wt% of Zirconium Phosphate (ZrP) reported a greater conductivity of 9.6×10^{-2} S cm^{-1} [42]. Nonetheless, the PBI-based membrane still has the disadvantage of poor mechanical properties after doping with a high concentration of acid and poor ability to withstand the long duration of testing [44].

The mechanism in proton conductivity for PA-doped PBI membrane enables PA to transfer the proton contrary to water which helps to increase the temperature span of fuel cell membranes. This is not possible for membranes like Nafion or other sulfonated membranes in an anhydrous condition, which relies heavily on water for proton H^+ movement. However, there is the possibility of PA being detached from the PA-doped PBI membrane if the temperature of the system decreases below 100°C due to water condensation that is forced out of the PA from the membrane. Apart from that, the detached PA can lead to corrosion in the fuel cell system of PA-doped PBI in fuel cell that can chemically deteriorate at operation temperature of 150–200°C, which is crucial in diminishing the poisoning effect to the anode catalyst due to carbon monoxide generation [48]. Titania, TiO_2 and zirconia, and ZrO_2, which are categorized as inorganic fillers can be integrated into the modification of composite PA-doped PBI-based membrane by enhancing the hydromechanical characteristics. This is achieved due to improvement in the proton conductivity and stability of PBI-based membrane in PA-doped medium [44]. Summary of PBI improvement techniques from several types of research is illustrated in **Table 2**.

Previous studies of PBI polymer have demonstrated that PBI derivatives, the 2OH-PBI polymer (dihydroxy function groups), have formed the phosphate linkages between the hydroxyl

No.	Methods	References	Remarks
1.	Optimization of membrane fabrication techniques	[35, 49]	Improvements were found limited demonstrating weakness in mechanical strength when highly loaded with acid and poor endurance when tested for a long term [50]
2.	Crosslinking of polymer backbone	[51–55]	
3.	Blending with other polymers	[56–58]	
4.	Forming a composite structure by incorporation of various inorganic acids	[22, 26, 42, 59]	
5.	Designing composite PA doped PBI-based membranes using ceramic nanoscale and mesoscale fillers such as Titania and Zirconia	[60, 61]	Nanoscale ZrO_2 filler and the accompanied membrane casting is challenged by agglomeration and precipitation [62]
6.	Adding more nitrogen atoms to the polymer molecule structure to enhance acid retention.	[60]	Development of pyridine-polybenzimidazole (Py-PBI), which provides an additional pyridine ring capable of boosting the interaction with PA [60, 63–65]

Table 2. Summary of PBI improvement techniques.

groups of the PBI backbone during polymerization in poly (phosphoric acid) in the cross-linking process. However, the increase in proton conductivity is not translated into better performance of fuel cell. Instead, Pt alloy that has been used as catalysts turned out to give better results, which was 0.49 A/cm^2 at 0.6 V and 0.69 V at 0.2 A/cm^2 with operation temperatures at 180°C and pressure of 1 atm in H_2/air environment [66].

2.1.1.3. Polyether ether ketone

Today, Victrex is the leading manufacturer of PEEK polymer in the world. The sulfonation process for its PEEK membrane is introduced using sulfonic acid groups (SO_3H) via alteration or polymerization of sulfonated monomers onto the backbone structure of the polymer. The hydrophilic nature of the PEEK polymer is developed from the accumulation of sulfonic acid groups. It has been reported that the membranes developed the carrier for proton charge as the consequences of the segregation of the sulfonic acid groups and proton conductivity with the help of water movement in PEEK hydrated state [27]. This is supported by the fact that polymer with aromatic rings like polyether ether ketone (PEEK), polybenzimidazoles (PBI), polyoxadiazole, polysulfone (PSf), and polyimides can contribute to cheaper production cost and deliver sufficient physicochemical properties [67].

To date, previous studies have shown that alteration of PEEK polymer properties can replace Nafion membrane in PEM-FC and DEMFC systems. Significant mechanisms are critically used to prepare the PEM from PEEK like PEEK electrophilic sulfonation (S-PEEK), S-PEEK and nonfunctional polymers blending, and S-PEEK heteropolycompounds with polyetherimide doping with organic acids [27]. Therefore, it is crucial to regulate the degree of sulfonation (DS) as it is affecting the thermochemical stability of PEEK membranes by keeping the DS low [68]. It has been reported that the workability of proton exchange membranes

from sulfonated polyether ether ketone (SPEEK) are strengthened by unaltered silica (SiO_2) and altered silica (SiO_2–SO_3H) nanoparticles. The characterization of sulfonated membranes includes the degree of sulfonation (DS), water uptake, and thermostability properties. The SiO_2 fusion elevates the degree of hydrophilic tendency, hence admitting a higher degree of water retention that promotes better route for proton transfer. However, we can observe that there is a decrement of the proton conductivity. The steady synergy of –SO_3H/-SO_3H within SiO_2-SO_3H and SPEEK chains results in ion cross-linked membrane framework which balances the reduction in proton conductivity. The SPEEK/SiO_2-SO_3H membrane with nanoparticles fillers has the ability to function as a competent PEM from the performance study conducted for fuel cell application [69].

3. Electrolyzer technologies

The chemical reaction equation for an electrolyzer is presented in Eq. (1):

$$2CuCl(s) + 2HCl(aq) \rightarrow H_2(g) + 2CuCl_2(aq) \quad (1)$$

The Atomic Energy of Canada Limited (AECL) has succeeded in generating hydrogen from the above step using CuCl/HCl electrolyzer and suggesting an alteration to the existing CuCl cycle [70, 71]. The operating parameters, appropriate membrane selection, and electrochemical cell's scheme are important factors to be tackled in order to have a functional electrolyzer. AECL has tested and determined that the CuCl electrolyzer needs to have these characteristics [72]:

i. Optimum pressure 24 bar, temperature range 70–80°C

ii. 0.1 A cm^{-2} of current density

iii. 0.6–0.7 V range of cell voltage

iv. 1.23 V of reversible cell potential

v. 75% of potential conversion

vi. 0.5 M CuCl and 11 M HCl as recommended concentration for operation

vii. ΔH = 93.76 kJ/mol [71]

Research conducted by Naterer et al. confirmed that the CuCl/HCl electrolysis reaction rate enhances with the increment of reaction temperature and the concentration of CuCl [72] and greater current density at 80°C when compared to 25°C for the same cell voltage [17]. The schematic diagram of proton exchange membrane (PEM) water electrolysis cells is presented in **Figure 3**. The solid polymer electrolyte that conducts proton ion is sandwiched between two electrodes to construct a membrane electrode assembly (MEA). The MEA is submerged in pure water (18 μ cm) and the proton movement stays within the membrane's boundary.

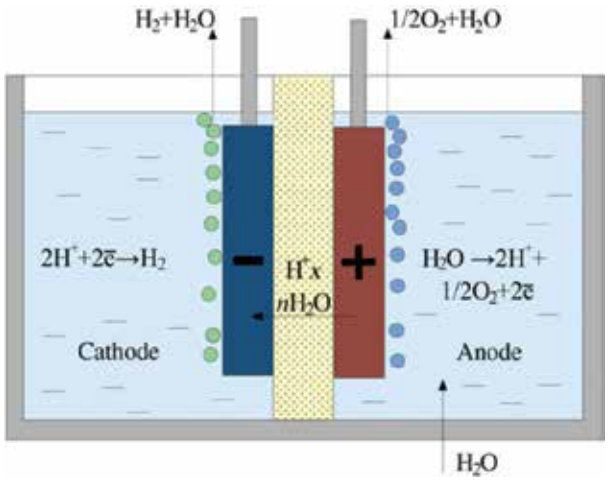

Figure 3. Schematic diagram of PEM electrolysis cell [33].

The efficiency of a PEM cell is dependent on the current density during operation. While a higher current density is crucial to cut down the start-up cost, a lower current density is needed to cut down the cost of operation. Both factors have to be taken into consideration [33]. Different types of electrolytes can be deployed in an EL cell: an alkaline electrolysis (AEL) cell works with a basic liquid electrolyte. In a proton exchange membrane (PEM) EL cell, an acidic ionomer—a process often called solid polymer electrolysis (SPE)—is used, and a high-temperature (HT) EL cell has a solid oxide as the electrolyte. The schematic diagram of the alkaline electrolysis cell is presented in **Figure 4**.

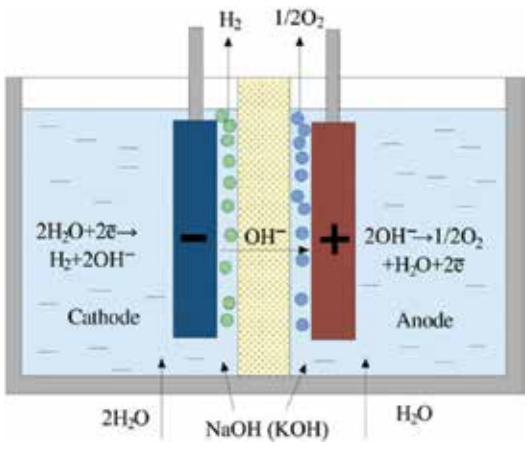

Figure 4. Schematic diagram of the alkaline electrolysis cell [34].

Technology	Advantages	Disadvantages
Alkaline electrolysis	Technology: oldest and well established	Current density: low
	Cost: cheapest and effective	Degree of purity: low (crossover of gases)
	Catalyst type: Noble	Electrolyte: liquid and corrosive
	Durability: Long term	Dynamics: low dynamic operation
	Stacks: MW range	Load range: low for partial load
	Efficiency: 70%	Pressure: Low operational pressure
	Commercialized	
PEM electrolysis	Current density: high	Technology: new and partially establish
	Voltage efficiency: high	Cost: high cost of components
	Load range: Good partial load range	Catalyst: noble catalyst
	System design: compact	Corrosion: acidic environment
	Degree of purity: high gas purity	Durability: comparatively low
	Dynamics: high dynamics operation	Stack: Below MW range
	Response: rapid system response	Membrane: limited and costly
		Commercialization in near term
High-temperature steam electrolysis	Efficiency: 100%	Technology: in laboratory phase
	Thermal neutral efficiency >100% with hot steam	Durability: low due to high heat, ceramics
	Catalyst: Nonnoble	System design: bulk system design
	Pressure: High-pressure operation	

Table 3. A comparison between alkaline, PEM, and high-temperature electrolysis [73–75].

To ensure a sufficiently high ionic conductivity, every electrolyte requires minimum temperatures. The upper temperature limit is determined mostly by the stability of the cell materials and components. More details are provided in later in this chapter.

Currently, three most used electrolysis technologies are being used. A comparison between alkaline, PEM, and high-temperature electrolysis is presented in **Table 3**.

4. Conclusion

In this chapter, hydrogen production from membrane electrolysis is discussed in detail. Hydrogen production from membrane water splitting technologies possesses great potential as a sustainable hydrogen source. Previous research focused mainly on Nafion-based membrane, but with the advancement in the research, a better and cheaper membrane can be used without compromising on the output of hydrogen production. Composite membrane provides better performance in terms of durability, heat resistance, hydrogen production, and purity.

Acknowledgements

The authors would like to express appreciation for the financial support provided by the Ministry of Higher Education Malaysia under the Universiti Putra Malaysia project number 9452000 GP-IPM Putra Grant and Universiti Teknologi Malaysia project number 03G10 Flagship Research University Grant.

Author details

Mohd Fadhzir Ahmad Kamaroddin[1,2], Nordin Sabli[2]* and Tuan Amran Tuan Abdullah[2]

*Address all correspondence to: nordin_sab@upm.edu.my

1 Universiti Putra Malaysia, Selangor, Malaysia

2 Universiti Teknologi Malaysia, Johor, Malaysia

References

[1] Oh TH, Hasanuzzaman M, Selvaraj J, Teo SC, Chua SC. Energy policy and alternative energy in Malaysia: Issues and challenges for sustainable growth – An update. Renewable and Sustainable Energy Reviews. 2018;**81**(P2):3021-3031

[2] Wang Z, Roberts RR, Naterer GF, Gabriel KS. Comparison of thermochemical, electrolytic, photoelectrolytic and photochemical solar-to-hydrogen production technologies. International Journal of Hydrogen Energy. 2012:16287-16301

[3] Apak S, Atay E, Tuncer G. Renewable hydrogen energy regulations, codes and standards: Challenges faced by an EU candidate country. International Journal of Hydrogen Energy. 2012;**37**(7):5481-5497

[4] Shi D, Guo Z, Bedford N, Shi D, Guo Z, Bedford N. 10—Nanoenergy materials. In: Nanomaterials and Devices. 2015. pp. 255-291

[5] Dincer I. Green methods for hydrogen production. International Journal of Hydrogen Energy. 2012;**37**(2):1954-1971

[6] Razykov TM, Ferekides CS, Morel D, Stefanakos E, Ullal HS, Upadhyaya HM. Solar photovoltaic electricity: Current status and future prospects. Solar Energy. 2011;**85** (8):1580-1608

[7] Mekhilef S, Safari A, Mustaffa WES, Saidur R, Omar R, Younis MAA. Solar energy in Malaysia: Current state and prospects. Renewable and Sustainable Energy Reviews. 2012;**16**(1):386-396. Available from: http://www.sciencedirect.com/science/article/pii/S1364032111004138

[8] Timilsina GR, Kurdgelashvili L, Narbel PA. Solar energy: Markets, economics and policies. Renewable and Sustainable Energy Reviews. 2012;**16**(1):449-465

[9] Reichelstein S, Yorston M. The prospects for cost competitive solar PV power. Energy Policy. 2013;**55**:117-127

[10] Nicoletti G, Arcuri N, Nicoletti G, Bruno R. A technical and environmental comparison between hydrogen and some fossil fuels. Energy Conversion and Management. 2015;**89**:205-213

[11] Ball M, Weeda M. The hydrogen economy—Vision or reality? International Journal of Hydrogen Energy. 2015;**40**(25):7903-7919. DOI: 10.1016/j.ijhydene.2015.04.032

[12] Mazloomi K, Gomes C. Hydrogen as an energy carrier: Prospects and challenges. Renewable and Sustainable Energy Reviews. 2012;**16**:3024-3033

[13] Dutta S. A review on production, storage of hydrogen and its utilization as an energy resource. Journal of Industrial and Engineering Chemistry. 2014;**20**:1148-1156

[14] Stiegel GJ, Ramezan M. Hydrogen from coal gasification: An economical pathway to a sustainable energy future. International Journal of Coal Geology. 2006;**65**(3-4):173-190

[15] Zhang F, Zhao P, Niu M, Maddy J. The survey of key technologies in hydrogen energy storage. International Journal of Hydrogen Energy. 2016;**41**(33):14535-14552

[16] Smolinka T, Ojong ET. Chapter 8 – Hydrogen production from renewable energies—Electrolyzer technologies. In: Electrochemical Energy Storage for Renewable Sources and Grid Balancing. 2015. pp. 103-128

[17] Naterer G, Suppiah S, Lewis M, Gabriel K, Dincer I, Rosen MA, et al. Recent Canadian advances in nuclear-based hydrogen production and the thermochemical Cu-Cl cycle. International Journal of Hydrogen Energy. 2009;**34**(7):2901-2917

[18] Rashid MM, Mesfer MK, Al Naseem H, Danish M. Hydrogen production by water electrolysis: A review of alkaline water electrolysis, PEM water electrolysis and high temperature water electrolysis. International Journal of Engineering and Advanced Technology. 2015;**3**:2249-8958

[19] Aghahosseini S, Dincer I, Naterer GF. Linear sweep voltammetry measurements and factorial design model of hydrogen production by HCl/CuCl electrolysis. International Journal of Hydrogen Energy. 2013;**38**(29):12704-12717

[20] Lewis MA, Masin JG, O'Hare PA. Evaluation of alternative thermochemical cycles, Part I: The methodology. International Journal of Hydrogen Energy. 2009;**34**(9):4115-4124

[21] Ran J, Wu L, He Y, Yang Z, Wang Y, Jiang C, et al. Ion exchange membranes: New developments and applications. Journal of Membrane Science. 2016;**522**:267-291 Available from: http://linkinghub.elsevier.com/retrieve/pii/S0376738816307980

[22] Mishra AK, Bose S, Kuila T, Kim NH, Lee JH. Silicate-based polymer-nanocomposite membranes for polymer electrolyte membrane fuel cells. Progress in Polymer Science. 2012;**37**(6):842-869

[23] Labalme E, David G, Souquet J, Buvat P, Bigarre J. Use of a new crosslinking method to obtain semi-IPN membranes with phosphonic acid groups for a PEMFC application. Journal of Materials Chemistry A. 2014;**2**(25):9792 Available from: http://xlink.rsc.org/?DOI=c4ta01472c

[24] Shao Z, Sannigrahi A, Jannasch P. Poly(tetrafluorostyrenephosphonic acid)-polysulfone block copolymers and membranes. Journal of Polymer Science Part A: Polymer Chemistry. 2013;**51**(21):4657-4666

[25] Simon S, Zhou F, Liso V, Lennart S, Rabjerg J, Thomas S, et al. A comprehensive review of PBI-based high temperature PEM fuel cells. International Journal of Hydrogen Energy. 2016:1-35

[26] Seo K, Seo J, Nam K-H, Han H. Polybenzimidazole/inorganic composite membrane with advanced performance for high temperature polymer electrolyte membrane fuel cells. Polymer Composites [Internet]. 2017;**38**(1):87-95. DOI: 10.1002/pc.23563

[27] Iulianelli A, Basile A. Sulfonated PEEK-based polymers in PEMFC and DMFC applications: A review. International Journal of Hydrogen Energy. 2012;**37**(20):15241-15255

[28] Abouzari-Lotf E, Nasef MM, Ghassemi H, Zakeri M, Ahmad A, Abdollahi Y. Improved methanol barrier property of Nafion hybrid membrane by incorporating nanofibrous interlayer self-immobilized with high level of phosphotungstic acid. ACS Applied Materials & Interfaces. 2015;**7**(31):17008-17015

[29] Kim DJ, HChoi DH, Park CH, Sam SY. Characterization of the sulfonated PEEK/sulfonated nanoparticles composite membrane for the fuel cell application. 2016;**41**:5793-5802

[30] Seetharaman S, Raghu SC, Mahabadi KA. Enhancement of current density using effective membranes electrode assemblies for water electrolyser system. Journal of Energy Chemistry. 2016;**25**(1):77-84

[31] Ahmad H, Kamarudin SK, Hasran UA, Daud WRW. Overview of hybrid membranes for direct-methanol fuel-cell applications. International Journal of Hydrogen Energy. 2010;**35**(5):2160-2175

[32] Di Noto V, Zawodzinski TA, Herring AM, Giffin GA, Negro E, Lavina S. Polymer electrolytes for a hydrogen economy. International Journal of Hydrogen Energy. 2012;**37**(7):6120-6131

[33] Millet P, Grigoriev S. Water electrolysis technologies. In: Renewable Hydrogen Technologies: Production, Purification, Storage, Applications and Safety. 2013. pp. 19-41

[34] Millet P, Grigoriev S. Water electrolysis technologies. Renewable Hydrogen Technologies: Production, Purification, Storage, Applications and Safety. 2013. pp. 19-41

[35] Li Q, Jensen JO, Savinell RF, Bjerrum NJ. High temperature proton exchange membranes based on polybenzimidazoles for fuel cells. Progress in Polymer Science. 2009;**34**(5):449-477

[36] Kraytsberg A, Ein-Eli Y. Review of advanced materials for proton exchange membrane fuel cells. Energy & Fuels [Internet]. 2014;**28**(12):7303-7330. DOI: 10.1021/ef501977k

[37] Abdo N, Bradley Easton E. Nafion/polyaniline composite membranes for hydrogen production in the Cu-Cl thermochemical cycle. International Journal of Hydrogen Energy. 2016;**41**(19):7892-7903

[38] Aili D, Hansen MK, Pan C, Li Q, Christensen E, Jensen JO, et al. Phosphoric acid doped membranes based on Nafion®, PBI and their blends—Membrane preparation, characterization and steam electrolysis testing. International Journal of Hydrogen Energy. 2011;**36**(12):6985-6993

[39] Hwang K, Kim JH, Kim SY, Byun H. Preparation of polybenzimidazole-based membranes and their potential applications in the fuel cell system. Energies. 2014;**7**(3):1721-1732

[40] Garsany Y, Gould BD, Baturina OA, Swider-Lyons KE. Comparison of the sulfur poisoning of PBI and Nafion PEMFC cathodes. Electrochemical and Solid-State Letters. 2009;**12**(9):B138-B140 Available from: http://link.aip.org/link/ESLEF6/v12/i9/pB138/s1&Agg=doi%5Cnhttp://esl.ecsdl.org/cgi/doi/10.1149/1.3168516

[41] Araya SS, Zhou F, Liso V, Sahlin SL, Vang JR, Thomas S. A comprehensive review of PBI-based high temperature PEM fuel cells. International Journal of Hydrogen Energy. 2016;**41**(46):21310-21344

[42] He R, Li Q, Xiao G, Bjerrum NJ. Proton conductivity of phosphoric acid doped polybenzimidazole and its composites with inorganic proton conductors. Journal of Membrane Science. 2003;**226**(1-2):169-184

[43] Hooshyari K, Javanbakht M, Shabanikia A, Enhessari M. Fabrication $BaZrO_3$/PBI-based nanocomposite as a new proton conducting membrane for high temperature proton exchange membrane fuel cells. Journal of Power Sources. 2015;**276**:62-72. DOI: 10.1016/j.jpowsour.2014.11.083

[44] Nasef MM, Fujigaya T, Abouzari-Lotf E, Nakashima N, Yang Z. Enhancement of performance of pyridine modified polybenzimidazole fuel cell membranes using zirconium oxide nanoclusters and optimized phosphoric acid doping level. International Journal of Hydrogen Energy. 2016;**41**(16):6842-6854

[45] Suryani, Liu Y-L. Preparation and properties of nanocomposite membranes of polybenzimidazole/sulfonated silica nanoparticles for proton exchange membranes. Journal of Membrane Science. 2009;**332**(1-2):121-128

[46] Xing B, Savadogo O. The effect of acid doping on the conductivity of polybenzimidazole (PBI). Journal of New Materials for Electrochemical Systems. 1999;**2**(2):95-101

[47] Oono Y, Sounai A, Hori M. Influence of the phosphoric acid-doping level in a polybenzimidazole membrane on the cell performance of high-temperature proton exchange membrane fuel cells. Journal of Power Sources. 2009;**189**(2):943-949

[48] Mack F, Aniol K, Ellwein C, Kerres J, Zeis R. Novel phosphoric acid-doped PBI-blends as membranes for high-temperature PEM fuel cells. Journal of Materials Chemistry A [Internet]. 2015;**3**(20):10864-10874 Available from: http://pubs.rsc.org/en/Content/ArticleLanding/2015/TA/C5TA01337B

[49] Xiao L, Zhang H, Scanlon E, Ramanathan LS, Choe E-W, Rogers D, et al. High-temperature polybenzimidazole fuel cell membranes via a sol-gel process. Chemistry of Materials [Internet]. 2005;**17**(21):5328-5333. DOI: 10.1021/cm050831

[50] Li X, Chen X, Benicewicz BC. Synthesis and properties of phenylindane-containing polybenzimidazole (PBI) for high-temperature polymer electrolyte membrane fuel cells (PEMFCs). Journal of Power Sources. 2013;**243**:796-804

[51] Li Q, Pan C, Jensen JO, Noye P, Bjerrum NJ. Cross-linked polybenzimidazole membranes for fuel cells. Chemistry of Materials. 2007;**15**(21):350-352

[52] Zhai Y, Zhang H, Zhang Y, Xing D. A novel H_3PO_4/Nafion-PBI composite membrane for enhanced durability of high temperature PEM fuel cells. Journal of Power Sources. 2007;**169**(2):259-264

[53] Noye P, Li Q, Pan C, Bjerrum NJ. Cross-linked polybenzimidazole membranes for high temperature proton exchange membrane fuel cells with dichloromethyl phosphinic acid as a cross-linker. Polymers for Advanced Technologies. 2008;**19**:1270-1275

[54] XU N, GUO X, FANG J, XU H, YIN J. Synthesis of novel Polybenzimidazoles with pendant amino groups and the formation of their crosslinked membranes for medium temperature fuel cell applications. Journal of Polymer Science Part A: Polymer Chemistry. 2009;**47**:6992-7002

[55] Zhai Y, Zhang H, Xing D, Shao ZG. The stability of Pt/C catalyst in H_3PO_4/PBI PEMFC during high temperature life test. Journal of Power Sources. 2007;**164**(1):126-133

[56] Arunbabu D, Sannigrahi A, Jana T. Blends of polybenzimidazole and poly(vinylidene fluoride) for use in a fuel cell. The Journal of Physical Chemistry. B. 2008;**112**(17):5305-5310

[57] Li QF, Rudbeck HC, Chromik A, Jensen JO, Pan C, Steenberg T, et al. Properties, degradation and high temperature fuel cell test of different types of PBI and PBI blend membranes. Journal of Membrane Science. 2010;**347**(1-2):260-270

[58] Cho H, Hur E, Henkensmeier D, Jeong G, Cho E, Kim HJ, et al. Meta-PBI/methylated PBI-OO blend membranes for acid doped HT PEMFC. European Polymer Journal. 2014;**58**:135-143

[59] Staiti P, Minutoli M, Hocevar S. Membranes based on phosphotungstic acid and polybenzimidazole for fuel cell application. Journal of Power Sources. 2000;**90**(2):231-235

[60] Quartarone E, Magistris A, Mustarelli P, Grandi S, Carollo A, Zukowska GZ, et al. Pyridine-based PBI composite membranes for PEMFCs. Fuel Cells. 2009:349-355

[61] Di Noto V, Piga M, Giffin GA, Quartarone E, Righetti P, Mustarelli P, et al. Structure-property interplay of proton conducting membranes based on PBI5N, SiO_2-Im and H_3PO_4 for high temperature fuel cells. Physical Chemistry Chemical Physics. 2011;**13**(26):12146-54. Available from: http://www.ncbi.nlm.nih.gov/pubmed/21594297

[62] Quartarone E, Villa DC, Angioni S, Mustarelli P. Facile and green assembly of nanocomposite membranes for fuel cells. Chemical Communications [Internet]. 2015;**51**(10):1983-1986 Available from: http://xlink.rsc.org/?DOI=C4CC08347D

[63] Xiao L, Zhang H, Jana T, Scanlon E, Chen R, Choe EW, et al. Synthesis and characterization of pyridine-based polybenzimidazoles for high temperature polymer electrolyte membrane fuel cell applications. Fuel Cells. 2005;**5**(2):287-295

[64] Sannigrahi A, Ghosh S, Maity S, Jana T. Structurally isomeric monomers directed copolymerization of polybenzimidazoles and their properties. Polymer (Guildf). 2010;**51**(25):5929-5941

[65] Maity S, Jana T. Soluble polybenzimidazoles for PEM: Synthesized from efficient, inexpensive, readily accessible alternative tetraamine monomer. Macromolecules. 2013;**46**(17):6814-6823

[66] Yu S, Benicewicz BC. Synthesis and properties of functionalized polybenzimidazoles for high-temperature PEMFCs. Macromolecules. 2009;**42**(22):8640-8648

[67] Jang I-Y, Kweon O-H, Kim K-E, Hwang G-J, Moon S-B, Kang A-S. Application of polysulfone (PSf)– and polyether ether ketone (PEEK)–tungstophosphoric acid (TPA) composite membranes for water electrolysis. Journal of Membrane Science. 2008;**322**(1):154-161

[68] Burgal JP da S. Development of poly (ether ether ketone) nanofiltration membranes for organic solvent nanofiltration in continuous flow systems [A Thesis Submitt Degree Dr Philos Imp Coll London Diploma Imp Coll London]. 2016

[69] Unnikrishnan L, Mohanty S, Nayak SK. Proton exchange membranes from sulfonated poly(ether ether ketone) reinforced with silica nanoparticles. High Performance Polymers. 2013;**25**(7):854-867. Available from:. DOI: http://hip.sagepub.com/cgi/doi/10.1177/0954008313487392

[70] Naterer GF, Suppiah S, Stolberg L, Lewis M, Wang Z, Daggupati V, et al. Canada's program on nuclear hydrogen production and the thermochemical Cu–Cl cycle. International Journal of Hydrogen Energy. 2010;**35**(20):10905-10926

[71] Ferrandon MS, Lewis MA, Alvarez F, Shafirovich E. Hydrolysis of $CuCl_2$ in the Cu-Cl thermochemical cycle for hydrogen production: Experimental studies using a spray reactor with an ultrasonic atomizer. International Journal of Hydrogen Energy. 2010;**35**(5):1895-1904

[72] Naterer GF. Recent Canadian advances in the thermochemical Cu-Cl cycle for nuclear hydrogen production. In: Fourth Information Exchange Meeting; April 2009. 2010. pp. 14-16

[73] Holladay JD, Hu J, King DL, Wang Y. An overview of hydrogen production technologies. Catalysis Today. 2009;**139**(4):244-260

[74] Carmo M, Fritz DL, Mergel J, Stolten D. A comprehensive review on PEM water electrolysis. International Journal of Hydrogen Energy. 2013;**38**:4901-4934

[75] Zeng K, Zhang D. Recent progress in alkaline water electrolysis for hydrogen production and applications. Progress in Energy and Combustion Science. 2010;**36**(3):307-326

Chapter 3

Hydrogen Production from Light Hydrocarbons

Ahmed Aidid Ibrahim

Additional information is available at the end of the chapter

http://dx.doi.org/10.5772/intechopen.76813

Abstract

Recognizing and procurement of a sustainable energy system are among the supreme important problems that today's scientists should tackle. Interchanging the existing fossil fuels and transforming them into a sustainable fuel is one of the vital pieces in that system. Hydrogen as an energy carrier, obtained from light hydrocarbons, can take an essential role in the matters of sustainability, eco-friendly emissions, and energy saving. Our enthusiasm in stirring toward a hydrogen economy has its root in the vision of securing energy requirements at a satisfactory price, with larger competence and small environmental destruction associated with the utilization of traditional fuels. Hydrogen production pathways and relevant issues are discussed here. This chapter highlights the recent technological progress in the light hydrocarbons toward sustainable hydrogen production.

Keywords: light hydrocarbons, hydrocarbon reforming, H_2 production

1. Introduction

The atmospheric emission of greenhouse gases as result of the constant burning of fossil fuels put a grave risk to the worldwide environs and subsequent climate variation [1]. Greenhouse gases such as CH_4, CO_2, N_2O, and others organic pollutants result from the burning of carbon-based fuels [2]. Fossil fuel combustion affects negatively the climate change [3]. Furthermore, the mounting energy requirement has necessitated the price rise of conventional fuel which is diminishing. It is estimated that coal reserves will be depleted in around 200 years [4]; however, the world's growing population and industrialization are driving an ever-increasing demand for energy [5, 6]. With the pressure of climate change and the structural problems in the energy sector, discovering and developing renewable energies to replace current dominant energy sources is necessary to ensure a sustainable energy future [7]. Because hydrogen has

significant advantages as an energy transporter, a hydrogen-based economy has been emerging as a clean, efficient, zero-carbon alternative to current energy structures [8].

Hydrogen is not easily available in nature like fossil fuels. Though it might be obtained from any main energy source, it can be then employed as a straight fuel to the internal combustion engine in a fuel cell. The by-product of hydrogen is the water by-product [8–12]. The crucial trouble challenged by the modern world is the shortage of fossil. Therefore, it is indispensable to work out an alternative fuel that can substitute non-renewable fossil fuels. Hydrogen gas is one of the extremely versatile, efficient and sustainable clean energy carriers that may be used to substitute the fossil fuels due to its high energy yield when compared to conventional hydrocarbon fuels [13, 14]. The energy storage capacity of hydrogen is superb because a unit weight of it can generate nearly 33 kWh of energy [15]. Substituting hydrogen for fossil fuels in ultimate energy uses could bring this key environmental welfare [16] into accordance with the technical, green and cost challenges, and it is easy to overcome the difficulties in, for instance, production, storage and transport of hydrogen [17–19]. Hydrogen can be considered to be a secondary energy source since it can be converted to energy in the form of heat or electricity through either combustion or electrochemical reactions. The chief problem in using hydrogen fuel roots from its absence in nature and the requirement of cheap production systems [20, 21]. Extensive processes exist for H_2 production which depends on the kind of the raw materials considered. The processes could be separated into two main classes viz., traditional and technology that can be renewed. Class one process is the fossil fuels and comprises the techniques of pyrolysis and hydrocarbon reforming. In the latter process, hydrocarbon reforming process, involve the chemical methods of reforming: steam, dry, partial oxidation, autothermal steam and hydrocarbon decomposition.

The former class includes the techniques that bring hydrogen from biomass and water. The primary feeds of biomass are partitioned into two biological and thermochemical processes.

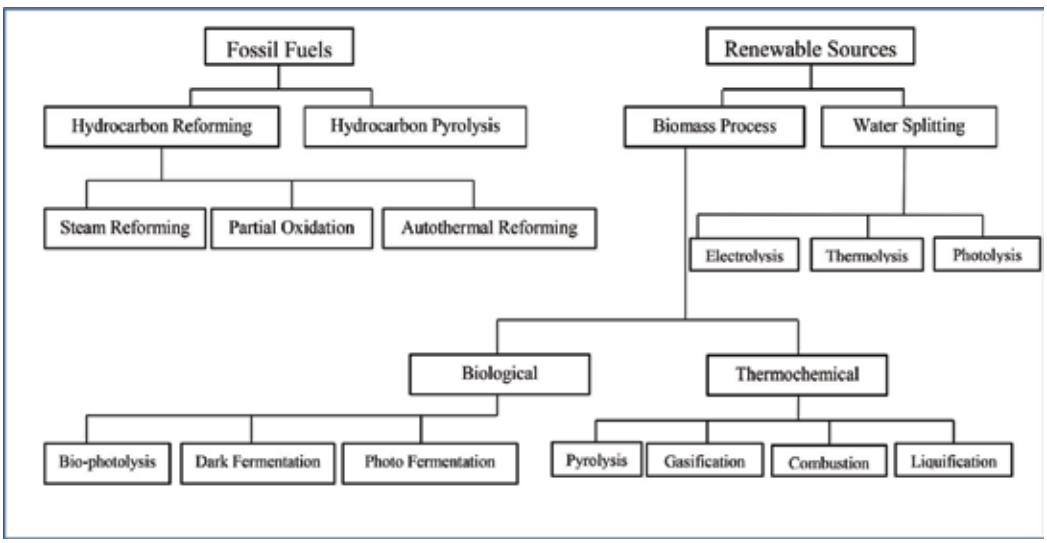

Figure 1. Hydrogen production methods.

The technology that concerns the thermochemical: primarily comprises combustion, gasification, pyrolysis, and liquefaction, while the biological processes are associated with photo-fermentation, bio-photolysis, dark fermentation, and sequential dark. The renewable knowhow involves the systems, which produces H_2 from electrolysis, photo-electrolysis and thermolysis. The material input to these technologies is water only. **Figure 1** displays the numerous pathways for hydrogen production.

Hydrogen can be obtained from different processes. Microorganisms for instance algae and bacteria through biological processes generate hydrogen [8]. Splitting of water into oxygen and hydrogen employing solar or electrolysis is another process. Chemical reactions and heat are used to discharge hydrogen from organic materials like biomass and fossil fuels via thermochemical processes.

2. Hydrogen and the environment

Hydrogen is regarded as a renewable and sustainable solution for mitigating global fossil fuel utilization and destroying the global warming [22]. The purpose of producing hydrogen as "Green Hydrogen" is to cause zero or low environmental impact. For this purpose all CO_2 and other pollutants must be removed when hydrogen is extracted from fossil fuels. Not only the environmental concern, but also the increase in energy demand inclines the researchers to develop new and current techniques and seek new energy sources. However, to ensure the sustainability of modern societies, hydrogen is a promising future energy carrier since it is a very important and environment friendly substitute to fossil fuels [23]. Hydrogen is counted as a green fuel since it is carbon-free henceforth CO_2 emission free. However, it can be generated from an extensive collection of fossil fuel and viable energy origin, so the type of hydrogen production process determines the emissions that will occur. Besides being abundance in the universe, hydrogen is not consumed like hydrocarbons; because it changes state from water to hydrogen back and forth when used as a fuel. However, production of hydrogen is not always CO_2 free. There exist various production methods such as gasification, electrolysis, and biological routes while these production methods can be performed using different feedstocks like water, biomass, or coal [24]. Some of these routes use non-renewable sources, some use extreme chemicals, and others have unknown life cycles. For the purpose of finding a clean energy route from the beginning of the circle to the end, a systematic approach to analysis is essential. This analysis should assess the whole production in such terms: terminating the dependency on non-renewable resources, reducing wastes, increasing efficiency or implementation of renewable sources to the systems.

3. Properties of hydrogen

Hydrogen is an element that possesses one proton and one electron. It is greatly plentiful and owns chemical properties that are exclusive and significant. Hydrogen is among the most available element in the world, which is chemically tied to the earth in great quantities and

has to be free from an extensive assortment of feedstock. Other than water, the feed includes all hydrocarbon origin, namely natural gas, oil, biomass, and coal [25]. Currently, capital and maintenance costs, hazard and safety risk control, conversion performance, operation and design process flexibility are the key norms for the generating hydrogen. The selection of the feedstock and the minimization of the waste production play important role in setting criteria for maximizing hydrogen production.

3.1. Physical properties of hydrogen

Hydrogen is the simplest element chemically present. Hydrogen possesses only one proton, atomic number of unity, and average atomic weight of about 1 amu. H is the hydrogen symbol. Hydrogen is the most abundant chemical substance in the universe, particularly in planets and stars. Nevertheless, it is rare to find monoatomic hydrogen on Earth since it combines with other elements by covalent bonds. Hydrogen as such is not poisonous. It is nonmetal, tasteless, colorless, odorless, and highly flammable gas. The molecular formula is H_2. On the Earth, hydrogen compounds exist as hydrocarbons and water. The most familiar isotope of hydrogen is protium, (1H). It has a single proton and a single electron with no neutron. Hydrogen is characterized by melting point of -259.14°C, a boiling point of -252.87°C, and density of 0.08988 g/L. Hydrogen is lighter than air. It has two separate oxidation states, (+1, -1), that facilitate it to react as both a reducing agent and an oxidizing agent. There are two separate spin isomers of hydrogen diatomic molecules, viz. orthohydrogen and parahydrogen. In the room temperature, the orthohydrogen constitutes 3/4 of hydrogen gas while the parahydrogen forms 1/4. Hydrogen is obtainable in different states, like compressed gas, liquid, slush, and solid and metallic forms [26, 27].

3.2. Chemical properties of hydrogen

Hydrogen is extremely combustible gas and burns in the air starting from low concentration of 4–75%. The enthalpy for the combustion reaction for hydrogen is -286 kJ/mol., and is defined by the equation:

$$2H_2(g) + O_2(g) \leftrightarrow 2H_2O(l) \quad \Delta H = -572 \text{ kJ} \tag{1}$$

Moreover, a mixture of chlorine and hydrogen from 5 to 95% can cause an explosion. The explosion of these mixtures can be easily triggered by sunlight, heat and spark [28, 29]. The temperature at which the hydrogen autoignition happens is at 500°C. Invisible ultraviolet light to bare eyes are radiated by flames of pure hydrogen-oxygen. Therefore, a flame detector is essential to monitor the leak of burning. Because hydrogen floats in air, its flames cause less harm than hydrocarbon fires, and rises rapidly. H_2 reacts with oxidizing elements, like chlorine and fluorine to form the corresponding hydrogen halides. Since hydrogen is an effective reducing agent, compounds of hydrogen halides are easily formed from the reaction of hydrogen and chlorine and fluorine. H_2 commonly forms compounds with a lot of elements in spite of its stability. In the case of reaction, hydrogen can react with more electronegative elements like oxygen or halogens and therefore can have a partial positive charge. On the other hand, it

can react with more electropositive elements like alkali metals and assume a partial negative charge. In addition, there is an intermolecular bonding known as hydrogen bonding that exists between hydrogen and elements like oxygen, fluorine, or nitrogen. This type of bonding is vital for the stability of many biological units. Hydrogen compounds with metals and metalloids are known as hydrides. H^+ ion is formed when hydrogen is oxidized its electron is removed. Frequently, the H^+ in aqueous solutions is termed as the hydronium ion, which is crucial in the chemistry of acid–base. There are three hydrogen isotopes in the universe: tritium, deuterium, and protium denoted as ^3H, ^2H, and ^1H respectively. Compounds of hydrides are characterized by the participation of one or more hydrogen anions that possess reducing, nucleophilic, or basic properties. The bonding of hydrogen to a more electropositive element or group generates hydrides. While hydrides compounds usually react as reducing agent or Lewis bases by giving electrons, other metal hydrides react as hydrogen- atom donors and acids and. For example, the common drying reaction of calcium hydride:

$$CaH_2 + 2H_2O \rightarrow 2H_2 + Ca(OH)_2 \quad (2)$$

Categories of hydrides are as follows:

a) Saline or ionic, these hydrides are formed by the bond between a very electropositive metal, mostly an alkaline earth or an alkali metal and hydrogen atom. Reducing reagents and heterogeneous bases are good examples of the uses of ionic hydrides in organic synthesis.

b) Covalent hydrides, often seen in the complex metal hydride, transition metal hydrides, are hydrogen centers that form hydrides, or those that are nucleophilic.

c) Interstitial hydrides usually occur in metals or alloys. They are often characterized by metallic bonding. Interstitial binary hydrides are formed when hydrogen gets in contact with transition metals.

3.3. Barriers fuel hydrogen

A major hurdle in the hydrogen economy lies in its transport and storage. Though H_2 is characterized by very low volumetric energy density, but it possesses high energy density based on mass. At ambient conditions molecular hydrogen is present as a gas, which is difficult. Liquefied or pressurized hydrogen gas is required to get sufficient fuel energy. When the gas pressure increased definitely the volumetric energy density will improve, however this entails a larger amount of energy be used to pressurize the gas. Otherwise, slush or liquid hydrogen can be employed [30–32]. An extensive amount of energy must be used to liquefy the hydrogen, which is cryogenic and hence boils at 20 K. Hydrogen is not suitable to be stored in tanks since hydrogen diffuses through any liner material arranged to preserve it, which eventually leads to the wearying of the container. Hydrogen is often kept in compound form like chemical hydride. The compounds can be shifted from place to place fairly easily and then decomposed into hydrogen gas. The requirements of compound to form at high pressure and temperatures and for the hydrogen to be desorbed lead the current barriers to practical storage. The surface of solid storage material adsorbs hydrogen and then be desorbed when needed. This technology is yet to be improved. Hydrogen has one of the widest explosive/

ignition mixes ranges with air. The leak of hydrogen from its mixture with air will most probable cause an explosion, since the mixture of air and hydrogen form a broad explosive/ignition when it gets contact with flame or spark. The utilization of hydrogen as a fuel is confined by this issue, particularly in non-open areas like underground parking or tunnels. The burning flames of pure hydrogen in the UV range are unseen; therefore flame detector is essential to sense the hydrogen leakage. Moreover, hydrogen can be detected by smelling since it is odorless. While the hydrogen economy is expected to make a smaller carbon footprint, there are lots complexities regarding the ecological matters of hydrogen manufacturing. Fossil fuel reforming represents the main source of hydrogen; nonetheless this technique eventually leads to larger carbon dioxide emissions when compared to fossil fuel used in an internal combustion engine. Other problems comprise hydrogen production through electrolysis entails a larger energy input than straight using renewable energy and the likelihood of other lateral outputs [33].

4. Hydrogen technology

Climate variation and fossil fuel exhaustion are the chief reasons leading to hydrogen technology. Various technologies are available for the production of hydrogen: These include electrical, thermal, hybrid and biological methods. Thermal conversion processes are the most utilized processes, with steam reforming becoming the best [34, 35]. Several reforming technologies are performed in industry. Hydrogen is also obtained from splitting water by electrolysis. Nevertheless, because of the strong bonds in water molecules, a 39.3 kWh of electrical energy is theoretically required to split 1 kg of water. Moreover, for hydrocarbon feedstock solar energy accomplishes most of the thermal conversion processes. Currently, in the refinery hydrogen is used as a raw material, rather than as an energy carrier. Often, hydrogen is transported via pipelines when it generated on-site. On the other hand, the procurement of an efficient, safe, and compact storage technology is vital for the transition from the fossil fuel-based energy carriers toward hydrogen. In recent days fuel cell applications are operated with liquefied hydrogen, kept in cryogenic tanks. Enormous research investigations are currently carried out in the arena of hydrogen solid-state storage. Nevertheless, the appropriate materials regarding the hydrogen storage capacity, cost, and thermodynamics are not yet enough. Lifetime, high storage density, prolonged cycle ability, satisfactory sorption kinetics and thermodynamics are the essential parameters for a hands-on storage material. No doubt hydrogen is a future energy carrier needed to have the proper the infrastructural technologies and logistics. Fossil fuel has the potential to balance between hydrogen as energy carrier of the future and the famous fossil fuel energy carriers. Hydrogen production processes are categorized as conventional and alternative energy resources like solar and wind, natural gas, coal, nuclear, biomass. There are several techniques for hydrogen generation from diverse raw materials and energy input selections. Having environmentally friendly properties, hydrogen became an eminent choice for an alternative fuel. The combustion techniques of fossil fuel destroy the environment and these days, less than 15% of total energy consumption of the world is not based on these techniques [36]. Consequently, hydrogen utilization as an alternative fuel is ideal since it is not an unsafe, poisonous or uncertain mode of production.

5. Hydrogen production from fossil fuels

Hydrogen is generated from fossil fuels using numerous technologies, the principal of which are pyrolysis and hydrocarbon reforming. These techniques are the most advanced and normally employed, recovering virtually the whole hydrogen needs. About 48% of hydrogen is obtained from natural gas, 18% from coal, and 30% from naphtha and heavy oils [37–39]. Currently, the fuels from the fossil possess the principal role in the world hydrogen resource. Membrane reactors are used in the chemical and biochemical industries, to produce H_2 from traditional fuels. A membrane frame permits mass transfer by the influence of driving forces of pressure, concentration, electric potential, temperature, and other driving forces. Membranes are classified into biological and synthetic based on their nature. A high selectivity and permeability, excellent chemical and stability are the required characteristics of the efficient H_2-production membrane. Consequently, for a composite membrane, indispensable parts include a permeable support permitting the gases crossing, blended with a barrier restrictive to the inter-diffusion in the metallic support.

5.1. Methods for hydrocarbon reforming

The process by which the hydrocarbon fuel is changed to produce hydrogen via reforming systems is termed hydrocarbon reforming. During the hydrocarbon reforming other components are employed along with the hydrocarbon. These include carbon dioxide and the system is termed as CO_2 reforming or dry reforming. Moreover steam may include as reactants in the reforming system of the hydrocarbon. This system is branded as steam reforming. Both dry and steam reforming reactions are endothermic, Therefore, it necessary to furnish energy. Reforming the hydrocarbon with oxygen is known as partial oxidation, and the reaction is exothermic. When the steam and partial oxidation reactions are combined the system is called autothermal reforming [40].

5.1.1. Method of steam reforming

In the steam reforming process, the catalytic conversion of hydrocarbon into hydrogen and carbon monoxide is carried out in the presence of steam in the feed. The reforming procedure comprises gas purification, methanation, water-gas shift and synthesis gas production. Most feedstock contains natural gas, methane, and a mixture of light hydrocarbons, which include propane, butane, ethane, pentane, and both light and heavy naphtha. When the feed is contaminated with organic sulfur compounds, a desulphurization stage should precede the reforming step to circumvent the deactivation of the reforming catalyst which CO_2 is seized and put in the ocean or geological reservoirs [41]. The primary chemical reaction that occurs during the steam reforming is:

$$C_nH_m + nH_2O \rightarrow \{n + 1/2m)H_2 + nCO \tag{3}$$

Depending on the values n and m dictate the hydrocarbon type. For instance, methane reforming n and m are equal to 1 and 4 respectively. The methane steam reforming is the best and well- advanced method employed for extensive hydrogen output. The conversion performance amounts to 74–85%. When natural gas and steam are reacted over a nickel-based catalyst

to generate synthesis, the reaction temperature is usually set to 850–900°C. About 30–35% of the entire amount of natural gas as a process fuel provides the needed energy of 63.3 kJ/mol of H_2. To inhibit coke deposition on the catalyst and achieve a purified H_2 output, the process operation is adjusted to 3.5 MPa pressure, steam-to-carbon ratios of 3.5, and high temperatures [42]. After the reformer, the mixture of gases goes through a heat recovery, and water gas shift reactor where an additional H_2 is produced from the reaction between the steam and carbon monoxide then, the mixture of gases goes through either a pressure swing adsorption or through a CO_2-removal and methanation producing virtually pure H_2 [43]. Membrane reactors offer a remarkable solution. Since the topmost process of producing huge amounts of H_2, SMR has been broadly evidenced by incorporating a delicate membrane which is operated right inside the reaction environs or downstream to reaction units (**Figures 2** and **3**).

Palladium-based membrane reactors of the second method provide considerable advantages by uniting the gas separation and chemical reaction in a unit. Generated H_2 adsorbed and dissociated atomically on one side of the membrane in the reformer, diffuses, and lastly desorbs on the other side [44]. Similar reactant conversion is permitted by the Pb-based membrane reactors. Contrary to normal SMR which operate at high temperature 850–900°C, the membrane reactors operate at a lower temperature of 450–550°C and produce methane conversions up to 90–95% [45].

5.1.2. Partial oxidation technique

Partial oxidation (POX) technique chiefly comprises the reaction transformation of hydrocarbons, oxygen, and steam, to synthesis gas which consists of hydrogen, carbon monoxide, and carbon dioxide. Feedstocks starting from methane to naphtha are often used in the catalytic process at about 950°C, while the process operation takes place at 1150–1315°C for non-catalytic systems [44]. Pure O_2 is used to incompletely oxidize the hydrocarbon feedstock, after the elimination of sulfur content in the feed removal. The generated synthesis is additionally

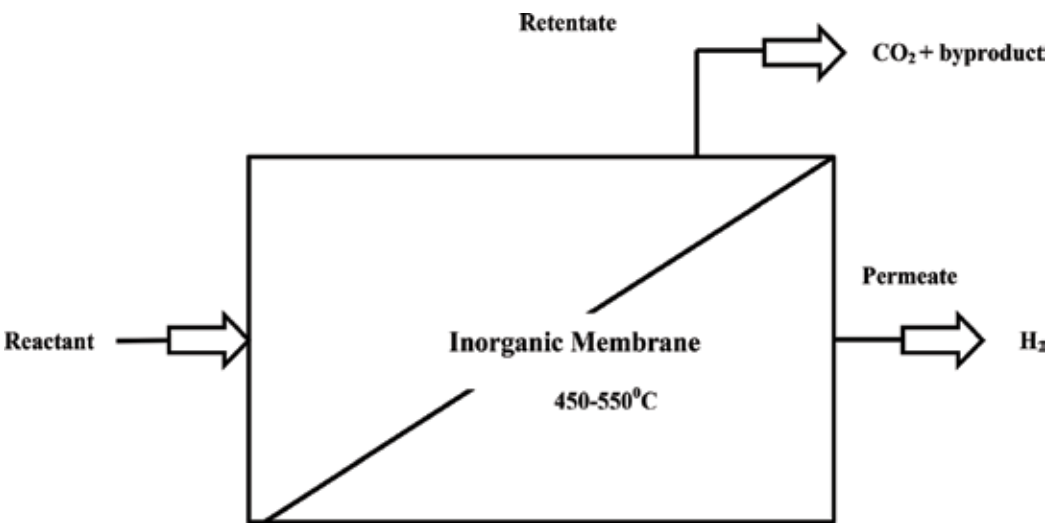

Figure 2. Flow illustration of steam methane reforming unified-membrane process.

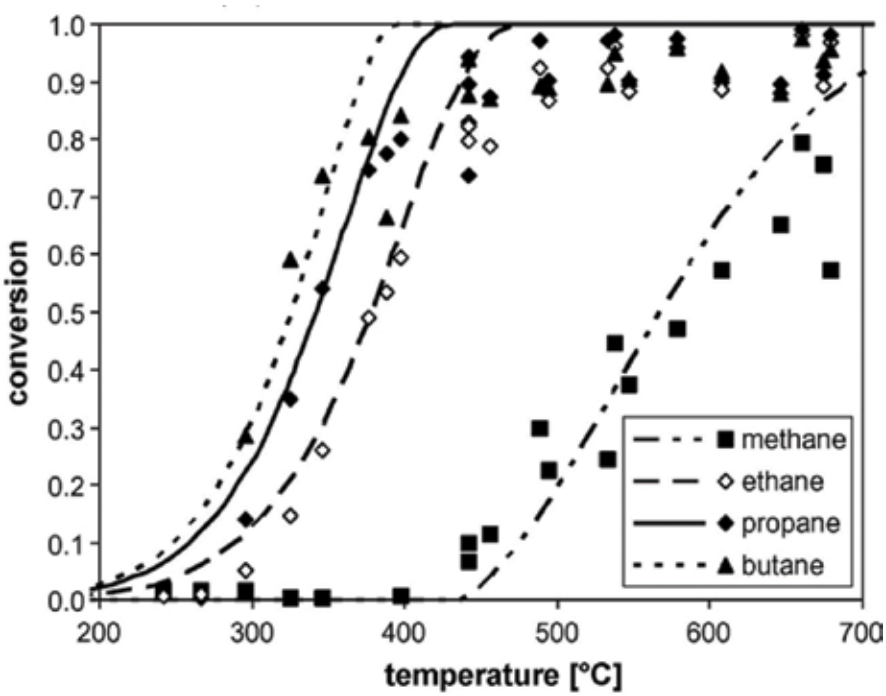

Figure 3. Methane (•), ethane (◊), propane (♦), and butane (▲) conversion as function of temperature for S/C 2.5 in SR of natural gas (catalyst with 900 cpsi); symbols: Experiment; lines: Model predictions [58].

purified and separated in a similar way as the output gas of the steam reforming method. The formidable price of the oxygen manufacturing and the extra expenses of desulphurization perform the process significantly expensive. In the process dealing with catalyst, the heat is delivered through the monitored combustion. Eq. (4), presents the catalytic reforming, while Eqs. (5) and (6) represent the chemical reactions of water gas shift and methanation.

$$C_nH_m + \frac{1}{2}nO_2 \rightarrow \frac{1}{2}mH_2 + nCO \tag{4}$$

$$CO + H_2O \rightarrow H_2 + CO_2 \tag{5}$$

$$3H_2 + CO \rightarrow H_2O + CH_4 \tag{6}$$

Heavier feedstock like coal and heavy oil residues are suitable resources for the production of hydrogen when partial oxidation technique is applied.

5.1.3. Autothermal reforming technique

In the process of autothermal reforming technique (ATR), the endothermic steam reforming receives heat from the combined exothermic partial oxidation to promote the production of hydrogen. Fundamentally, steam, air, and oxygen are fed to the reformer, starting the oxidation reactions as well as the reforming to happen simultaneously, as presented in Eq. (8).

$$C_nH_m + \frac{1}{2}nH_2O + \frac{1}{4}nO_2 \rightarrow nCO + \left(\frac{1}{2}n + \frac{1}{2}m\right)H_2 \quad (7)$$

When methane is autothermally reformed at 700°C inlet temperature and the proper ratios of steam to carbon and oxygen to carbon, a thermal efficiency of 60–75% and maximum hydrogen yield of about 2.8 are achieved [42]. The investment cost is about 50% lower than coal gasification. A small improvement is reported when the ATR reactor is combined with a Pd membrane. The high operating temperature of 900°C needed by the system ruins the efficiency improvement brought by the membrane [43].

5.1.4. Dry reforming

The dry reforming is a chemical process that consists of converting hydrocarbon and carbon dioxide, considered as one of the world's most abundant greenhouse gases to synthesis gas with a proper H_2/CO molar ratio [46]. As a result, this process has the potentials to alleviate the environmental challenges related to greenhouse gases emissions and to transform biogas and natural gas to synthesis gas. Furthermore, the produced H_2/CO ratio synthesis gas is suitable for the production of hydrocarbons via Fischer-Tropsch synthesis, in addition to the synthesis of oxygenated chemicals [47]. The dry reforming reaction is:

$$C_nH_m + n\,CO_2 \rightarrow \left\{\frac{1}{2}m\right\}H_2 + 2nCO \quad (8)$$

Being an extremely endothermic reaction, dry reforming requires high operating temperatures, usually in the range of 900–1273 K, to achieve the desired conversion levels. The forward reaction is favored at low pressures as dictated by stoichiometry. Additionally, it has been observed that an nCO_2/C_nH_m molar ratio higher than the stoichiometric requirement of unity can also provide high synthesis gas yields. The positive effects of high reaction temperatures, low pressures, and high nCO_2/C_nH_m molar.

5.2. Pyrolysis of hydrocarbon

The pyrolysis of hydrocarbon is a famous method where hydrogen solely comes from the hydrocarbon subjected to thermal decomposition via the following universal reaction:

$$C_nH_m \rightarrow nC + \frac{1}{2}mH_2 \quad (9)$$

Light liquid hydrocarbons having boiling points 200°C are decomposed thermo-catalytically to generate elemental carbon and hydrogen, however, dealing with residual fractions having boiling temperatures above 350°C, the production of hydrogen requires hydrogasification and cracking of methane. The direct reduction of carbon content in the natural gas known as often de-carbonization, which constitutes mainly methane, is performed at 980°C temperature and atmospheric pressure in the environment, where there is no water and air. Furthermore, pyrolysis does not involve CO_2 removal steps and water gas shift. Carbon control and

sequestration, which is energy intensive stage is replaced by carbon control that could be employed in the chemical industries and metallurgy. Therefore, the processes of partial oxidation or steam conversion are higher than investments for big plants causing 25–30% hydrogen production cost [45]. The price of hydrogen would be less if markets are found for the extensive amounts of carbon resulting from the natural gas decomposition. From the environmental perspective it would be more beneficial to dissociate catalytically natural gas to carbon and hydrogen, instead of H_2 production by steam reforming of methane attached with CO_2 sequestration [48]. For a specified temperature, the reduction of carbon content is increased by the constant elimination of hydrogen by membrane separation. For H_2 separation, Pd-Ag alloys, which operate at lower temperatures and mitigate the carbon deposition, are normally used. The chief disadvantages of the present method are attributed to the very low hydrogen separation, which results from the membrane stability influenced by high temperatures required for the equilibrium of the reduction of the carbon content and the low H_2 partial pressures in the reaction mixture [43].

6. Light hydrocarbons (LHs)

Hydrocarbons, as their name denotes, are compounds of hydrogen and carbon. They represent one of the vital classes of organic chemistry. They exist in gaseous states such as propane and methane, a liquid state like benzene and hexane, and solid state as paraffin wax, polystyrene, naphthalene, and polyethylene.

Hydrocarbons are classified into:

a. Saturated hydrocarbons which are formed completely of single bonds between carbon–carbon and are saturated with hydrogen. The compound formula with a linear structure, alkanes are C_nH_{2n+2}. The universal formula of saturated hydrocarbons is $C_nH_{2n+2(1-r)}$, where r represents the number of rings. One ring hydrocarbons are termed cycloalkanes. Linear and branched species of saturated hydrocarbons are the sources of petroleum.

b. Unsaturated hydrocarbons have one or more double or triple bonds between carbon atoms. Those with double bond are called alkenes. Those with one double bond and non-cyclic structure have the formula C_nH_{2n}. Those having triple bonds are named alkyne. Those with one triple bond have the formula C_nH_{2n-2}.

c. Aromatic hydrocarbons are hydrocarbons that have at least one aromatic ring. The hydrocarbon is characterized by strong covalent (sigma) bonds and delocalized pi electrons between carbon atoms forming a circle. Some simple hydrocarbons and their variations are given in **Table 1**.

Hydrocarbons are a primary energy source for current civilizations. The predominant use of hydrocarbons is as a combustible fuel source. In their solid form, hydrocarbons take the form of asphalt (bitumen) [49]. Methane and ethane are gaseous at ambient temperatures and cannot be readily liquefied by pressure alone. Propane is however easily liquefied and exists in 'propane bottles' mostly as a liquid. Butane is so easily liquefied that it provides a safe,

Alkadiene	Cycloalkane	Alkyne (triple bond)	Alkene (double bond)	Alkane (single bond)
—	—	—	—	Methane
—	—	Ethyne	Ethene	Ethane
Propadiene	Cyclopropane	Propyne	Propene	Propane
Butadiene	Cyclobutane	Butyne	Butene	Butane
Pentadiene	Cyclopentane	Pentyne	Pentene	Pentane
Hexadiene	Cyclohexane	Hexyne	Hexene	Hexane
Heptadiene	Cycloheptane	Heptyne	Heptene	Heptane
Octadiene	Cyclooctane	Octyne	Octene	Octane
Nonadiene	Cyclononane	Nonyne	Nonene	Nonane
Decadiene	Cyclodecane	Decyne	Decene	Decane
Undecadiene	Cycloundecane	Undecyne	Undecene	Undecane

Table 1. Simple hydrocarbons and their variations.

volatile fuel for small pocket lighters. Pentane (C_5H_{12}) is a clear liquid at room temperature, commonly used in chemistry and industry as a powerful nearly odorless solvent of waxes and high molecular weight organic compounds, including greases. Hexane (C_6H_{14}) is also a widely used non-polar, non-aromatic solvent, as well as a significant fraction of common gasoline. The C^6 through C^{10} alkanes, alkenes and isomeric cycloalkanes are the chief components of gasoline, naphtha, jet fuel and specialized industrial solvent mixtures. Hydrocarbons with low molecular weight such as methane, ethane, propane and ethane are termed as light hydrocarbons (LHs). Light hydrocarbons are the largest petroleum fraction which in between C_l and C_9. They are catagenic products, formed between 75 and 140°C. The higher hydrocarbons are too stable to generate the LHs at these temperatures. Additionally, LHs are different from cracking products [50]. Many are structurally like bio-precursors. Basically, all isomers are found within the alkanes, cycloalkanes and aromatics with no visible preference for natural structures. It is improbable that the LHs are formed without support. The LHs constitute well over 50% of the carbon in petroleum. They seem to be a random mixture of classes (isoalkanes, cyclopentanes, cyclohexanes, and aromatics). For instance, the gasoline fraction of different crudes may be branded by identifying the relative amounts of the following five classes of hydrocarbons: normal paraffins, isoparaffins, alkylcyclopentanes, alkylcyclohexanes, and aromatics. Of analogous significance to hydrogen, is the production of its mixture with carbon monoxide (H_2 + CO), normally named synthesis gas or syngas, which is a valuable raw material for numerous industrial uses. The significant natural sources of light hydrocarbons comprise leakage from oil and gas reservoirs and anaerobic production of methane. There are some reports of low molecular weight hydrocarbons in open ocean water. The coastal waters act as a source for atmospheric methane. The vital man-derived sources of methane in the coast are ports with their accompanying shipping and industrial activity, offshore petroleum drilling and production operations, and open ocean shipping activity. In 2010 almost, 50% of global

anthropogenic methane emissions came from sources like agriculture, coal mines, landfill, oil and natural gas systems and waste water. Mobile sources in specific are famous to give meaningfully to urban hydrocarbon and nitrogen oxide levels. For instance the vehicle exhaust accounts for most of the non-methane hydrocarbon concentrations in metropolitan cities [51–53].

6.1. Production of hydrogen from liquefied petroleum gas

Steam reforming of liquefied petroleum gas (LPG) is a practical choice for producing hydrogen in isolated regions where there is no pipeline natural gas supply. The most common LPG gases include propane, butane (n-butane) and isobutane (i-butane), as well as mixtures of these gases. Fuel processing converts LPG into hydrogen and carbon dioxide. Lopez-Ortiz et al. elaborated the utilization of cobalt tungstate in a chemical looping partial oxidation of methane process to generate syngas [54]. They carried out simulations and thermodynamic analysis. Results acquired indicated no carbon formation and syngas yield (89.6%) were calculated. Wang et al. investigated the autothermal reforming of LPG in a fixed-bed reactor by changing essential parameters like steam-to-carbon ratio (S/C), the oxygen-to-carbon ratio (O/C), reforming temperature, and catalyst [55]. It was established that temperature, S/C, and O/C were the most key parameters for fuel conversion and lowering carbon deposition. Similarly, steam reforming is applied to convert LPG to hydrogen using Rh, Ru, Pt, and other noble metal catalysts. For instance, Laosiripojana et al., used Ni- and Rh-based catalysts supported on $GdCeO_2$ (CGO) and Al_2O_3 in steam reforming of LPG at 750–900°C [56]. They obtained that Rh/CeO_2 catalyst gave the highest H_2 yield. Steam reforming of LPG employing nickel-based perovskites (La-Ni-O) partly replaced with cobalt was examined [57]. The suitable selection of water/LPG feed ratio together with the proper Co/Ni ratio in the synthesis of perovskite precursors was vital to retain the catalyst active during LPG steam reform and hence the hydrogen production.

6.2. Production of hydrogen from alkanes

A broad experimental study of steam reforming (SR) of alkane components: methane, ethane, propane, butane, and natural gas for the catalytic conversion over a Rh-based catalyst was carried out and compared to numerically predicted conversion and selectivity [58]. The result established a mechanism for predicting product distribution in steam reforming of natural gas mixtures with varying compositions. Likewise, the developed simulation, permit the numerical calculation of chemical species profiles and surface coverage within catalytic monoliths. Steam reforming of ethane, propane, and butane display virtually same conversion and selectivity as a function of temperature and steam to carbon ratio (S/C).

Rhodium-based catalyst with different Rh content (1, 2.5 and 5 wt. %) and high surface area alumina support were tested for steam reforming of propane [59]. All catalysts exhibited complete conversion at 750°C with hydrogen selectivity over 98% and high stability for more than 140 hours' time on stream. In the work of Ferrandon et al., Mono-metallic nickel and rhodium catalysts and bimetallic Ni-Rh catalysts supported on $La\text{-}Al_2O_3$, $CeZrO_2$, and $CeMgO_x$ were arranged and assessed for catalyzing the steam and autothermal reforming of n-butane [60]. The bimetallic Ni-Rh supported on $La\text{-}Al_2O_3$ catalysts with low weight loading of rhodium showed higher H_2 yields than Ni or Rh alone. The $Ni\text{-}Rh/CeZrO_2$ catalyst

exhibited higher performance and no coke formation, in comparison to similar metals on other supports. Hydrogen was produced from butane steam reforming using Ni/Ag loaded $MgAl_2O_4$ catalyst to substitute the conventional fast catalytic deactivation and lower H_2 production from the hydrocarbon steam-reforming reaction [61]. The Ag-loaded catalyst showed considerably higher reforming reactivity than $Ni/MgAl_2O_4$ catalyst. The silver-containing catalyst diminished the carbon formation and boosted the hydrogen product and selectivity. The production of H_2 was enhanced up to 68% at 700°C for 1 h and this high efficiency sustained for up to 53 h.

Mesoporous nanocrystalline Ni/Al_2O_3 catalysts were used to examine the Partial oxidation (POX) of methane, ethane, and propane [62]. Different feed conditions were considered during the study. 5 wt. % Ni/Al_2O_3 catalysts displayed the maximum catalytic activity in the temperature range of 500–700°C. The catalyst was substantially stable for 48 h time on stream in methane partial oxidation. Moreover, increased carbon deposition on the catalysts was observed when ethane and propane in stoichiometric feed ratio were considered. Alternatively, the performance of CO_2-reforming of methane over mesoporous Co-Ni/SBA-15-x (x = Mg, La, and Sc) was tested in continuous fixed bed at 700–800°C reaction temperature [63]. When the catalyst support was modified by adding Mg and Sc, the CH_4 conversion was improved markedly by 28 and 26%, respectively at 700°C higher than the corresponding bare SBA-15 supported catalysts. TEM and TGA/GTA characterizations of spent catalyst established that the coke resistance was considerably upgraded as a result of the support alteration, leading to the formation of amorphous carbon. Consequently, Co-Ni/SC-SBA-15 catalyst remarkably promoted the stability and catalytic activity to produce synthesis gas.

6.3. Production of hydrogen from ethane

With the increased production of shale gas through a new drilling technology of hydraulic fracturing significant attention has been paid to the utilization of ethane which accounts for about 7% of shale gas [64]. Jeong et al. proposed a pathway for using ethane to generate hydrogen [65]. The investigators performed the analysis of membrane reactor using techno-economic analysis and process simulation using Aspen HYSYS® for ethane steam reforming. The process simulation indicated high H_2 selectivity. In ethane steam reforming, synthesis gas is produced as:

$$C_2H_6 + 2H_2O \rightarrow 5H_2 + 2CO \tag{10}$$

Alternatively, Veranitisagul et al. studied ceria and gadolinia doped ceria catalysts to produce syngas from ethane at the temperature range of 800–900°C via the steam reforming reaction [66]. The catalytic activity was enhanced with the addition of 0.15 Gd. It could generate a substantial amount of hydrogen and the carbon formation that deactivates at high temperature was prevented. Hypothetically, the carbon formation could take place through the reforming of ethane, as result of these reactions:

$$C_2H_6 \leftrightarrow 2C + 3H_2 \tag{11}$$

$$C_2H_4 \leftrightarrow 2C + 2H_2 \tag{12}$$

$$CH_4 \leftrightarrow C + 2H_2 \tag{13}$$

$$CO_2 + 2H_2 \leftrightarrow C + 2H_2O \tag{14}$$

$$2CO+ \leftrightarrow C + CO_2 \tag{15}$$

$$CO + H_2 \leftrightarrow C + H_2O \tag{16}$$

6.4. Production of hydrogen from methane

Methane (CH_4) is a light hydrocarbon and the most important component of natural gas. Methane is also a strong and plentiful greenhouse gas (GHG), which makes it a significant contributor to climate change. Methane like other LHs can be converted to hydrogen using different methods as mentioned. The natural gas comprising C_1, C_2, C_3, and C_{4+} have been widely used to produce hydrogen. As presented in **Table 2**, methane is a primary component in natural gas followed by ethane and propane [67].

Catalytic carbon dioxide reforming of methane (CO_2 reforming of CH_4), also called dry reforming of methane to distinguish this process from steam reforming, has attracted rigorous research interest during the last decades. The interest is ascribed to the fact that CO_2 reforming of CH_4 mitigates carbon emissions. The reaction is endothermic:

$$CO_2(g) + CH_4(g) \rightarrow 2H_2(g) + 2CO(g)\Delta H_{298K} = +247\text{KJ/mole} \tag{17}$$

The equilibrium conversion and the equilibrium product composition are influenced by the reaction temperature, pressure, initial reactant ratio, and the content of the inert gas. Nevertheless, catalysts must be employed to allow the reaction to take place in reasonable kinetics. Ni catalyst is found suitable for this reaction. Aluminum oxide (Al_2O_3), particularly γ-Al_2O_3, is one of the best generally used catalyst support materials for CO_2 reforming of CH_4. Liao and Horng studied methane dry reforming to generate synthesis gas [68]. Their work concentrated

Elements	**Volumetric composition (%)**	
	Wet	**Dry**
Methane	84.6	96.0
Ethane	6.4	2.00
Propane	5.3	0.60
Isobutane	1.2	0.18
n-butane	1.4	0.12
Isopentane	0.4	0.14
n-Pentane	0.2	0.06
Hexanes	0.4	0.10
Heptanes	0.1	0.80

Table 2. Universal composition of dry and wet natural gas.

on the heat recovery of the designed reformers. An oven was employed for the simulation of the heat recovery. The results specified that the oven temperature is proportional to the reforming reaction temperature and hence promote the energy of the reformer. When the energy of reformer was increased the synthesis gas production enhanced and efficiency of reforming and CO_2 conversion was obviously raised. The production of hydrogen and carbon from the catalytic decomposition of methane via iron catalyst was explored [69]. The

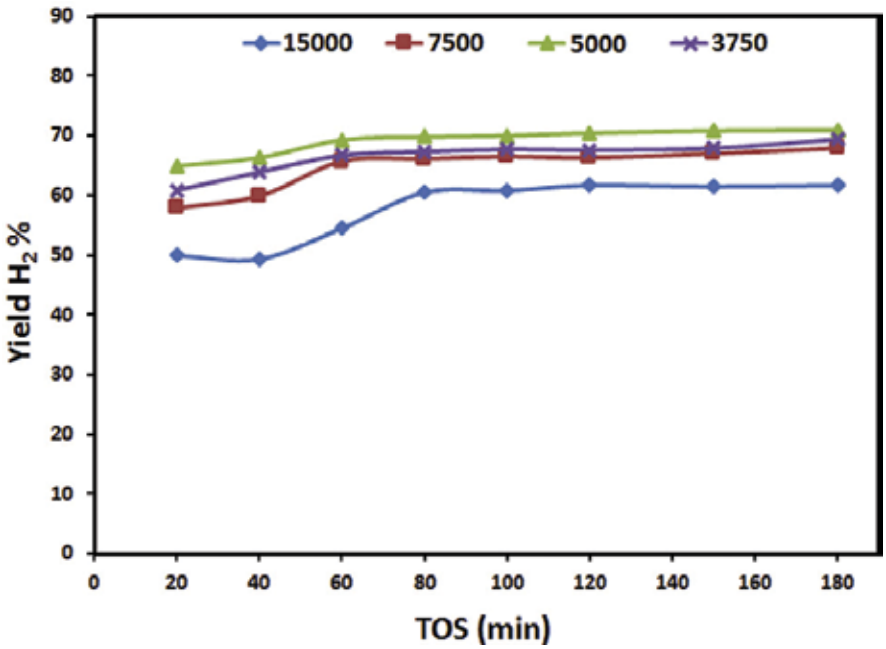

Figure 4. Stability performances in terms of H_2 yield (%) over 15Co-30Fe/Al catalysts as a function of TOS at 700°C at different GHSVs.

Hydrogen production techniques	Temperature (°C)	Hydrogen yield (%)	References
Dry reforming	750	43.0	[71]
	850	78.0	
Steam Reforming	500	98.7	[72]
Steam Reforming	750	85.0	[73]
Partial Oxidation	850	88.9	[74]
Partial Oxidation	750	36.8	[75]
Autothermal	700	83.0	[76]
Autothermal	850	78.0	[77]
Decomposition	700	75	[78]
	800	90	

Table 3. Summary of hydrogen yield from methane for various hydrogen production techniques.

investigation covered the utilization of alumina supported catalysts over various iron loadings. Multiwall nanotubes were formed and as the % loading of Fe was increased, the hydrogen yield increased. When 60% Fe/Al_2O_3 catalyst was employed, the highest H_2 yield of 77.2% was acquired. Similarly, mono-, bi- and tri-metallic catalysts obtained from iron-nickel-cobalt supported over alumina was examined for the decomposition of methane to hydrogen and value-added carbon. The catalytic activity of 30 wt. % Fe and 15 wt.% Co displayed the highest performance overall investigated catalysts. **Figure 4** illustrates the hydrogen yield versus time on stream (TOS). It is apparent that the gas hourly space velocity (GHSV) has some effect on the hydrogen yield [70]. **Table 3** reviews the technologies along with their reaction temperatures and percentage of hydrogen yield. It is important to note that hydrogen yield depends on the type of catalyst, pretreatment and operating conditions [71–78].

7. Future perspective

Currently, about 1/5 of global energy is utilized as electricity, whereas 80% is utilized as fuel. Hydrogen energy is a clean and alternative energy that has been suggested as the energy carrier of the future. Solar-driven microalga hydrogen production is both a favorable and inspiring biotechnology, which play a significant role in the global drive to decrease GHG emissions. One of the major barriers with regard to the hydrogen economy is its production cost and inefficient storage methods, which need to be resolved. Current research efforts are focused on strain improvement by systems metabolic engineering and finding suitable conditions to increase the levels of hydrogen production. In the near future, it may be possible to perform knockouts and insertions based on the data available by modeling previous studies. The advent of synthetic biology necessitates such models since it aims at standardizing biology, which should give predicted responses. With all these advancements, the commercial feasibility of H_2 production may rely on efficient production strategies with elevated yield, well-organized transport and storage systems ensuring the secured supply of hydrogen. Moreover, the prospect of light hydrocarbon hydrogen production is determined by the research advances such as enhancement of productivity through catalytic engineering and the advance of chemical reactors, the economic attentions like the price of fossil fuels, social appreciation, and use of hydrogen energy systems in our society. Today, hydrogen is being used to power a fleet of busses in some countries. More industries will accept hydrogen energy when a renewable economically viable process of hydrogen production is achieved. Last but not least, the integrated effort of both scientists and engineers is needed to fully implement hydrogen energy as the energy for the future. Mass hydrogen production is the foundation for the transition to a "hydrogen economy", which has the potential to enable the development of distributed power generation networks [79].

8. Conclusions

The global crisis of fossil fuels has greatly stimulated worldwide interest to develop sustainable sources of energy carriers. Light hydrocarbons can be used as a potential source of hydrogen energy due to their inherent capacity to decompose the hydrocarbon into H_2 using

the thermochemical energy. Photo-biological hydrogen production is considered as a more efficient and less energy-intensive process. Hydrogen powered fuels can be used in different types of fuel cells as a clean energy to generate electricity with high efficiency. At present, hydrogen energy from microalgae is economically less feasible due to its high production cost. Nevertheless, efficient bio-hydrogen production from microalgae may be accelerated by recent technological advancements in metabolic and genetic engineering approaches.

Biography

Dr. Ibrahim is renowned for his pioneering work on fossil fuel conversion energy technologies; he has authored and co-authored more than a seventy refereed journal and conference papers. His main research interests include catalysis, hydrogen energy technologies.

Author details

Ahmed Aidid Ibrahim

Address all correspondence to: aidid@ksu.edu.sa

Chemical Engineering, Faculty of Engineering, King Saud University, Saudi Arabia

References

[1] Planton S, Deque M, Chauvin F, Terray L. Expected impacts of climate change on extreme climate events. Comptes Rendus Geoscience. 2008;**340**:564-574 https://doi.org/10.1016/j.crte.2008.07.009

[2] Midilli A, Dincer I. Hydrogen as a renewable and sustainable solution in reducing global fossil fuel consumption. International Journal of Hydrogen Energy. 2008;**33**:4209-4222 https://doi.org/10.1016/j.ijhydene.2008.05.024

[3] Cormos CC. Hydrogen production from fossil fuels with carbon capture and storage based on chemical looping systems. International Journal of Hydrogen Energy. 2011;**36**: 5960-5971 https://doi.org/10.1016/j.ijhydene.2011.01.170

[4] Venkata Raman SV, Iniyan S. Goic. A review of climate change, mitigation and adaptation. Renewable and Sustainable Energy Reviews. 2012;**16**:878-897 https://doi.org/10.1016/j.rser.2011.09.009

[5] Koroneos C, Dompros A, Roumbas G, Moussiopoulos N. Advantages of using hydrogen as compared to kerosene. Resources, Conservation and Recycling. 2005;**44**:99-113 https://doi.org/10.1016/j.resconrec.2004.09.004

[6] Nojoumi H, Dincer I, Naterer GF. Greenhouse gas emissions, assessment of hydrogen and kerosene-fueled aircraft propulsion. International Journal of Hydrogen Energy. 2009;**34**: 1363-1369 https://doi.org/10.1016/j.ijhydene.2008.11.017

[7] Teichmann D, Arlt W, Wassersche P. Liquid organic hydrogen carriers as an efficient vector for the transport and storage of renewable energy. International Journal of Hydrogen Energy. 2012;**37**:18118-18132 https://doi.org/10.1016/j.ijhydene.2012.08.066

[8] Valavaniidis A, Vlachogianni T. Green chemistry and green engineering from theory to practice for the protection of the environment and sustainable development. Synchrona Themata, Athens 2012. ISBN: ISBN: 978–960–9695-00-8

[9] Ratlamwala TAH, Dincer I. Comparative energy and exergy analyses of two solar-based integrated hydrogen production systems. International Journal of Hydrogen Energy. 2015; **40**:7568-7578 https://doi.org/10.1016/j.ijhydene.2014.10.123

[10] Dincer I, Zamfirescu C. Chapter-3 hydrogen production by electrical energy. Sustainable Hydrogen Production. 2016:99-161 https://doi.org/10.1016/B978-0-12-801563-6.00003-0

[11] Ding C, Yang KL, He J. Handbook of Biofuels Production. 2nd ed. New York: Longman; 2016 ISBN: 9780081004562

[12] Marban G, Valdes-Solis T. Towards the hydrogen economy? International Journal of Hydrogen Energy. 2007;**32**:1625-1637 https://doi.org/10.1016/j.ijhydene.2006.12.017

[13] Hosseini SE, Wahid MA. Hydrogen production from renewable and sustainable energy resources: Promising green energy carrier for clean development. Renewable and Sustainable Energy Reviews. 2016;**57**:850-866 https://doi.org/10.1016/j.rser.2015.12.112

[14] Aziz M. Integrated hydrogen production and power generation from microalgae. International Journal of Hydrogen Energy. 2016;**41**:104-112 https://doi.org/10.1016/j.ijhydene.2015.10.115

[15] Sharma S, Ghoshal SK. Hydrogen the future transportation fuel: From production to applications. Renewable and Sustainable Energy Reviews. 2015;**43**:1151-1158 https://doi.org/10.1016/j.rser.2014.11.093

[16] Veras TS, Mozer TS, Santos DCRM, Cesar AS. Hydrogen: Trends, production and characterization of the main process worldwide. International Journal of Hydrogen Energy. 2017;**42**:2018-2033 http://dx.doi.org/10.1016/j.ijhydene.2016.08.219

[17] Voldsund M, Jordal K, Anantharaman R. Hydrogen production with CO2 capture. International Journal of Hydrogen Energy. 2016:4969-5023 http://dx.doi.org/10.1016/j.ijhydene.2016.01.009

[18] Weger L, Abanedes A, Butler T. Methane cracking as a bridge technology to the hydrogen economy. International Journal of Hydrogen Energy. 2017;**42**:720-731 https://doi.org/10.1016/j.ijhydene.2016.11.029

[19] Momirlan M, Veziroglu TN. The properties of hydrogen as fuel tomorrow, in sustainable energy system for a cleaner planet. International Journal of Hydrogen Energy. 2005;**30**: 795-802. DOI: 10.1016/j.ijhydene.2004.10.011

[20] Kapdan IK, Kargi F. Bio-hydrogen production from waste materials. Enzyme and Microbial Technology. 2006;**38**:569-582. DOI: 10.1016/j.enzmictec.2005.09.015

[21] Rastogi RP, Madamwar D, Pandey A. Algal Green Chemistry-Recent Progress in Biotechnology. Amsterdam: Elsevier; 2017 978-0-444-64041-3

[22] Huang W, Chen W, Anandarajah G. The role of technology diffusion in a decarbonizing world to limit global warming to well below 2°C: An assessment with application of global TIMES model. Applied Energy. 2017;**208**:291-301 http://dx.doi.org/10.1016/j.apenergy.2017.10.040

[23] Milano J, Ong HC, Masjuki HH, Chong WT, Vellayan V. Microalgae biofuels as an alternative to fossil fuel for power generation. Renewable and Sustainable Energy Reviews. 2016;**58**:180-197 http://dx.doi.org/10.1016/j.rser.2015.12.150

[24] Çelik D, Yıldız M. Investigation of hydrogen production methods in accordance with green chemistry principles. International Journal of Hydrogen Energy. 2017;**42**:23395-23401 http://dx.doi.org/10.1016/j.ijhydene.2017.03.104

[25] Simpson JA, ESC W. Hydrogen. Oxford English Dictionary. 2nd ed. Clarendon Press; 1989. p. 7 ISBN 0-19-861219-2

[26] Hydrogen. Van Nostrand's Encyclopedia of Chemistry. Wylie-Interscience; 2005. pp. 797-799 ISBN 0-471-61525-0

[27] Grayson M. Kirk-Othmer Encyclopedia of Chemical Technology 3rd ed, 1980, 12, 938. New York, Chichester: John Wiley and Sons. [General information on hydrogen energy including chemical and physical properties of hydrogen.] ISBN: 978–0–471-48496-7

[28] Carcassi MN, Fineschi F. Deflagrations of H_2–air and CH_4–air lean mixtures in a vented multi-compartment environment. Energy. 2005;**30**:1439-1451. DOI: 10.1016/j.energy.2004.02.012

[29] Committee on Alternatives and Strategies for Future Hydrogen Production and Use, US National Research Council, US National Academy of Engineering. The Hydrogen Economy: Opportunities, Costs, Barriers, and R&D Needs. National Academies Press; 2004. p. 240. ISBN 0-309-09163-2

[30] Zuttel A, Borgschulte A, Schlapbach L. Hydrogen storage. In: Hydrogen as a Future Energy Carrier. Weinheim: Wiley-VCH Verlag GmbH & Co; 2008 https://doi.org/10.1002/9783527622894.ch6

[31] Ross DK. Hydrogen storage: The major technological barrier to the development of hydrogen fuel cell cars. Vacuum. 2006;**80**:1084-1089 https://doi.org/10.1016/j.vacuum.2006.03.030

[32] Dillon AC, Heben MJ. Hydrogen storage using carbon adsorbents: Past, present and future. Applied Physics A: Materials Science & Processing. 2001;**72**:133-142 https://doi.org/10.1007/s003390100788

[33] Hollemann/Wiberg 2007: Arnold Hollemann, Egon Wiberg, Lehrbuch der Anorganischen Chemie, 102nd ed. Munchen 2007. ISBN: 9783110177701

[34] Demirbas MF. Hydrogen from various biomass species via pyrolysis and steam gasification processes. Energy Sources A. 2007;**28**:245-252 https://doi.org/10.1080/009083190890003

[35] Bromberg L, Cohn DR, Rabinovich A, Alexeev N. Plasma catalytic reforming of methane. International Journal of Hydrogen Energy. 1999;**24**:1131-1137 https://doi.org/10.1016/S0360-3199(98)00178-5

[36] Thomas SCE, Lloyd AC. Stopping climate change: The case for coal and hydrogen. International Journal of Hydrogen Energy. 2017;**42**:8406-8407 http://dx.doi.org/10.1016/j.ijhydene.2017.01.053

[37] Kothari R, Buddhi D, Sawhney RL. Comparison of environmental and economic aspects of various hydrogen production methods. Renewable and Sustainable Energy Reviews. 2008;**12**:553-563. DOI: 10.1016/j.rser.2006.07.012

[38] Balat H, Kirtay E. Hydrogen from biomass – Present scenario and future prospects. International Journal of Hydrogen Energy. 2010;**35**:7416-7426. DOI: 10.1016/j.ijhydene.2010.04.137

[39] Dincer I, Acar C. Review and evaluation of hydrogen production methods for better sustainability. International Journal of Hydrogen Energy. 2015;**40**:11094-11111 http://dx.doi.org/10.1016/j.ijhydene.2014.12.035

[40] Chen HL, Lee HM, Chen SH, Chao Y, Chang MB. Review of plasma catalysis on hydrocarbon reforming for hydrogen production-interaction, integration, and prospects. Applied Catalysis B: Environmental. 2008;**85**:1-9. DOI: 10.1016/j.apcatb.2008.06.021

[41] Damen K, Van Troost M, Faaij A, Turkenburg W. A comparison of electricity and hydrogen production systems with CO2 capture and storage. Part A: Review and selection of promising conversion and capture technologies. Progress in Energy and Combustion Science. 2006;**32**:215-246. DOI: 10.1016/j.pecs.2007.02.002

[42] Ersoz A. Investigation of hydrocarbon reforming processes for micro-cogeneration systems. International Journal of Hydrogen Energy. 2008;**33**:7084-7094. DOI: 10.1016/j.ijhydene.2008.07.062

[43] Boon J, Cobden PD, van Dijk HAJ. van Sint Annaland, M. High-temperature pressure swing adsorption cycle design for sorption-enhanced water–gas shift. Chemical Engineering Science 2015; 122:219-231. http://dx.doi.org/10.1016/j.ces.2014.09.034

[44] Koros WJ, Fleming GK. Membrane-based gas separation. Journal of Membrane Science. 1993;**83**:1-80 https://doi.org/10.1016/0376-7388(93)80013-N

[45] Zhang J, Wu X, Qian Y, Wang J. Formation behaviors of gas and liquid products during the two-stage hydrogasification of low-rank coal. Fuel. 2015;**150**:217-225 http://dx.doi.org/10.1016/j.fuel.2015.02.037

[46] Naeem MA, Al-Fatesh AS, Fakeeha AH, Abasaeed AE. Hydrogen production from methane dry reforming over nickel-based nanocatalysts using surfactant-assisted or polyol method. International Journal of Hydrogen Energy. 2014;**39**:17009-17023 https://doi.org/10.1016/j.ijhydene.2014.08.090

[47] Srinivas S, Malik RK, Mahajani SM. Fischer-Tropsch synthesis using bio-syngas and CO_2. Energy for Sustainable Development. 2007;**11**:66-71 https://doi.org/10.1016/S0973-0826(08)60411-1

[48] Misyura SY, Donskoy IG. Dissociation of natural and artificial gas hydrate. Chemical Engineering Science. 2016;**148**:65-77 http://dx.doi.org/10.1016/j.ces.2016.03.021

[49] McMurry J. Organic Chemistry 5th ed. Brooks/Cole: Thomson Learning; 2000. 75–81. ISBN 0-495-11837-0

[50] Yu C, Gong D, Huang S, Liao F, Sun Q. Characteristics of light hydrocarbons of tight gases and its application in the Sulige gas field, Ordos basin, China. Energy Exploration and Exploitation. 2014;**32**:211-226 https://doi.org/10.1260/0144-5987.32.1.211

[51] Wang JL, Ding WH, Chen TY. Source determination of light non-methane hydrocarbons by simultaneous multi-site sampling in a metropolitan area. Chemosphere: Global Change Science. 2000;**2**:11-22 https://doi.org/10.1016/S1465-9972(99)00057-4

[52] McKay WA, Turner MF, Jones BMR, Halliwell CM. Emissions of hydrocarbons from marine phytoplankton-some results from controlled laboratory experiments. Atmospheric Environment. 1996;**30**:2583-2593 https://doi.org/10.1016/1352-2310(95)00433-5

[53] Blake DR, Rowland FS. Urban leakage of liquefied petroleum gas and its impact on Mexico City air quality. Science 1995; **269**:953-956. https://doi.org/10.1126/science.269.5226.953

[54] Lopez-Ortiz A, Gonzalez-Vargas PE, Melendez-Zaragoza MJ, Collins-Martinez V. Thermodynamic analysis and process simulation of syngas production from methane using $CoWO_4$ as oxygen carrier. International Journal of Hydrogen Energy. 2017;**42**:30223-30236 http://dx.doi.org/10.1016/j.ijhydene.2017.07.119

[55] Wang W, Turn SQ, Keffer V, Douette A. Study of process data in auto thermal reforming of LPG using multivariate data analysis. Chemical Engineering Journal. 2007;**129**:11-19. DOI: 10.1016/j.cej.2006.10.027

[56] Laosiripojana N, Sutthisripok W, Charojrochkul S, Assabumrungrat S. Steam reforming of LPG over Ni and Rh supported on Gd-CeO_2 and Al_2O_3: Effect of support and feed composition. Fuel. 2011;**90**:136-141. DOI: 10.1016/j.fuel.2010.07.053

[57] Avila-Neto CN, Oliveira KD, Oliveira KF, Aline MM, Arouca AMM, Ferreira RAR, Hori CE. Interconnection between feed composition and Ni/Co ratio in (La-Ni-Co-O)-based perovskites and its effects on the stability of LPG steam reforming. Applied Catalysis A: General. 2018;**550**:184-197 https://doi.org/10.1016/j.apcata.2017.11.011

[58] Schadel BT, Duisberg M, Deutschmann O. Steam reforming of methane, ethane, propane, butane, and natural gas over a rhodium-based catalyst. Catalysis Today. 2009;**142**:42-51. DOI: 10.1016/j.cattod.2009.01.008

[59] Zapf R, Thiele R, Wichert M, OConnell M, Ziogas A, Kolb G. Application of rhodium nanoparticles for steam reforming of propane in microchannels. Catalysis Communications. 2013;**41**:140-145. http://dx.doi.org/10.1016/j.catcom.2013.07.018

[60] Ferrandon M, Kropf AJ, Krause T. Bimetallic Ni-Rh catalysts with low amounts of Rh for the steam and auto-thermal reforming of n-butane for fuel cell applications. Applied Catalysis A: General. 2010;**397**:121-128. DOI: 10.1016/j.apcata.2010.03.013

[61] Jeong H, Kang M. Hydrogen production from butane steam reforming over Ni/Ag loaded $MgAl_2O_4$ catalyst. Applied Catalysis B: Environmental. 2010;**95**:446-455. DOI: 10.1016/j.apcatb.2010.01.026

[62] Peymani M, Alavi SM, Rezaei M. Synthesis gas production by catalytic partial oxidation of methane, ethane and propane on mesoporous nanocrystalline Ni/Al_2O_3 catalysts. International Journal of Hydrogen Energy. 2016;**41**:19057-19069 http://dx.doi.org/10.1016/j.ijhydene.2016.07.072

[63] Al-Fatesh AS, Arafat Y, Atia H, Ibrahim AA, Quan Luu Manh Ha QLM, M. Schneider M, M-Pohl M, Fakeeha AH. CO2-reforming of methane to produce syngas over CO-Ni/SBA-15 catalyst: Effect of support modifiers (Mg, La and Sc) on catalytic stability, Journal of CO_2 Utilization 2017;**21**:395–404. http://dx.doi.org/10.1016/j.jcou.2017.08.001

[64] Freeman C, Moridis GJ, Michael GE, Blasingame TA. Measurement, modeling, and diagnostics of flowing gas composition changes in shale gas wells. SPE Latin America and Caribbean petroleum engineering conference. Society of Petroleum Engineers. 2012 https://doi.org/10.2118/153391-MS

[65] Jeong S, Sehwa Kim S, Lee B, Ryi S-K, Lim H. Techno-economic analysis: Ethane steam reforming in a membrane reactor with H2 selectivity effect and profitability analysis. International Journal Hydrogen Energy. 2017 In press. http://dx.doi.org/10.1016/j.ijhydene.2017.07.202

[66] Veranitisagul C, Koonsaeng N, Laosiripojana N, Laobuthee A. Preparation of gadolinia doped ceria via metal complex decomposition method: Its application as catalyst for the steam reforming of ethane. Journal of Industrial and Engineering Chemistry. 2012;**18**:898-903. DOI: 10.1016/j.jiec.2012.01.047

[67] Lee S, Speight JG, Loyalka SK. Handbook of Alternative Fuel Technologies. CRC Press; 2014. ISBN: 9781466594579

[68] Liao CH, Horng RF. Experimental study of syngas production from methane dry reforming with heat recovery strategy. International Journal of Hydrogen Energy. 2017; **42**:25213-25224 https://doi.org/10.1016/j.ijhydene.2017.01.238

[69] Ibrahim AA, Fakeeha AH, Al-Fatesh AS, Abasaeed AE, Khan WU. Methane decomposition over iron catalyst for hydrogen production. International Journal of Hydrogen Energy. 2015;**40**:7593-7600 https://doi.org/10.1016/j.ijhydene.2014.10.058

[70] Al-Fatesh AS, Fakeeha AH, Khan WU, Ibrahim AA, He S, Seshan K. Production of hydrogen by catalytic methane decomposition over alumina supported mono-, bi- and

tri-metallic catalysts. International Journal of Hydrogen Energy. 2016;**41**:22932-22940 https://doi.org/10.1016/j.ijhydene.2016.09.027

[71] Abdullah B, Abd Ghani NA, Vo DVN. Recent advances in dry reforming of methane over Ni-based catalysts. Journal of Cleaner Production. 2017;**162**:170-185 https://doi.org/10.1016/j.jclepro.2017.05.176

[72] Kim CH, Han JY, Lim H, Lee KY, Ryi SK. Methane steam reforming using a membrane reactor equipped with a Pd-based composite membrane for effective hydrogen production. International Journal of Hydrogen Energy. 2018;**43**:5863-5872 https://doi.org/10.1016/j.ijhydene.2017.10.054

[73] Akbari-Emadabadi S, Rahimpour MR, Hafizi A, Keshavarz P. Production of hydrogen-rich syngas using Zr modified Ca-Co bifunctional catalyst-sorbent in chemical looping steam methane reforming. Applied Energy. 2017;**206**:51-62 https://doi.org/10.1016/j.apenergy.2017.08.174

[74] Wang HY, Ruckenstein E. Conversions of methane to synthesis gas over Co/γ-Al_2O_3 by CO_2 and/or O_2. Catalysis Letters. 2001;**75**:13-18 https://doi.org/10.1023/A:1016719703118

[75] Basile F, Fornasari G, Trifiro F, Vaccari A. Rh–Ni synergy in the catalytic partial oxidation of methane: Surface phenomena and catalyst stability. Catalysis Today. 2002;**77**:215-223 https://doi.org/10.1016/S0920-5861(02)00247-X

[76] Yan Y, Li H, Li L, Li Z, Zhang J. Properties of methane autothermal reforming to generate hydrogen in membrane reactor based on thermodynamic equilibrium model. Chemical Engineering and Processing. 2018;**125**:311-317 https://doi.org/10.1016/j.cep.2018.01.010

[77] Mota N, Ismagilov IZ, Matus EV, Kuznetsov VV, Kerzhentsev MA, Ismagilov ZR, Navarro RM, Fierro JLG. Hydrogen production by autothermal reforming of methane over lanthanum chromites modified with Ru and Sr. International Journal of Hydrogen Energy. 2016;**41**:19373-19381 https://doi.org/10.1016/j.ijhydene.2016.05.029

[78] Pinilla JL, Utrilla R, Lazaro MJ, Moliner R, Suelves I, Garcia AB. Ni- and Fe-based catalysts for hydrogen and carbon nanofilament production by catalytic decomposition of methane in a rotary bed reactor. Fuel Processing Technology. 2011;**92**:1480-1488 https://doi.org/10.1016/j.fuproc.2011.03.009

[79] Michael B, Marcel W. The hydrogen economy vision or reality? International Journal of Hydrogen Energy. 2015;**40**:7903-7919 http://dx.doi.org/10.1016/j.ijhydene.2015.04.032

Chapter 4

Production of Hydrogen and their Use in Proton Exchange Membrane Fuel Cells

Flavio Colmati, Christian Gonçalves Alonso,
Tatiana Duque Martins, Roberto Batista de Lima,
Antonio Carlos Chaves Ribeiro,
Leandro de Lima Carvalho,
André Mychell Barbieux Silva Sampaio,
Monah Marques Magalhães,
José William Diniz Coutinho,
Geovany Albino de Souza, Lucas Fernandes Aguiar,
Diericon de Sousa Cordeiro,
Adão Marcos Ferreira Costa,
Thiago Soares Silva Ribeiro,
Pedro Henrique Machado Godoy and
Guilherme Botelho Meireles de Souza

Additional information is available at the end of the chapter

http://dx.doi.org/10.5772/intechopen.76663

Abstract

This work will show an overview of the hydrogen production from ethanol by steam reforming method, using distinct catalysts, resulting in low carbon monoxide content in H2 produced; a thermodynamic analysis of reforming employing entropy maximization, the ideal condition for ethanol, and other steam reforming reactions, the state of the art of steam reforming catalysts for H2 production with low CO content. Moreover, in the second part, there will be an overview of the use of hydrogen in a proton exchange membrane fuel cell (PEMFC), the fuel cell operational conditions, a thermodynamic analysis of PEMFC, the catalysts used in the electrodes of the fuel cell, consequences of the CO presence in the hydrogen fuel feed in PEMFC, and the operation conditions for maximum output power density.

Keywords: production of hydrogen, ethanol steam reforming, PEMFC, electrochemical energy, electrocatalysts

1. Introduction

This chapter shows the hydrogen production from ethanol-steam reformation and from photocatalysis and photoelectrochemical processes and the use of the hydrogen in a proton exchange membrane fuel cell (PEMFC) to convert chemical energy into electrical energy. The photocatalysis and photoelectrochemical processes use the solar energy for direct conversion of solar energy into renewable hydrogen fuel; moreover, solar energy is the unique renewable source that can fulfill the world's needs for the future to produce hydrogen fuel and generate the electricity. Hydrogen production can feed a PEMFC which converts chemical energy into electric energy by an electrochemical reaction. H_2 is oxidized at the anode and O_2 (often in the form of air) is reduced at the cathode, which results in electrical work. This system presents the advantage that it can be used in remote place to convert electrical energy without ambient degradation.

2. Hydrogen production from ethanol-steam reformation

The development of efficient technologies for the production and use of hydrogen, an alternative source for clean energy generation from the conversion of renewable biomass, has been presented as one of the most attractive possibilities for the gradual adaptation of the energy matrix to the global management policies of air pollutant emissions and to the sustainable use of natural resources.

The use of hydrogen in fuel cells, a clean and energy-efficient technology, has been promoted throughout the twenty-first century for the improvement of hydrogen production processes with low levels of carbon monoxide (CO). In particular, the ethanol-steam reforming reaction, a biomass-derived renewable product, has been considered extremely important for the advancement of PEM non-stationary fuel cell technology. The coupling of an ethanol reformer system to PEMFC results in a significant environmental advantage since it promotes a cycle of zero carbon emission when considering the fixation of CO_2 in the growth and development of sugarcane crops, feedstock for ethanol production [1].

The ethanol-steam reforming reaction is ideally characterized by the stoichiometric vapor-phase feed of 1 mole of ethanol and 3 moles of water in a catalytic reactor. The reaction produces 6 moles of H_2 and 2 moles of CO_2. This reaction is fundamentally endothermic and thus requires a source of energy external to the system for its realization. In addition, the process hardly occurs without the formation of byproducts and intermediates by the means of parallel reactions on the catalytic surface.

In a thermodynamic study via the minimization of Gibbs free energy using a non-stoichiometric method, Rossi et al. [2] verified that temperatures lower than 700 K do not favor the formation of CO; however, the maximum production of hydrogen notably occurs at higher temperatures. This result exposes the complexity of the process and the necessity to develop new highly selective catalysts to H_2 and CO_2 leading to the minimization of CO concentration via shift reaction. In general, according to Furtado et al. [3], the ethanol-steam reforming reaction involves numerous steps and usually competes with various reactions, which generate byproducts resulting in a lower H_2 yield. The breakdown of the carbon-carbon bond of ethanol multiplies the possible paths in the reaction network represented in **Table 1**, which requires higher temperatures, typically in the range from 623 to 923 K [4]. Although thermodynamic predictions indicate that it is possible to carry out the steam reforming reaction of ethanol at temperatures in the order of 523 K, the development of catalysts for the technological establishment of the process involves the understanding of many variables that can influence directly or indirectly in its viability. According to these studies, the temperature, pressure, composition and flow of reagents are variables that have a direct influence on the catalytic performance of the process. On the other hand, the use of different catalysts leads to different reaction paths so that the catalyst is a direct process variable and its composition (active phase, support), precursors and method of preparation are considered indirect variables but essentially important.

$C_2H_5OH + 3H_2O \rightarrow 2CO_2 + 6H_2$	Ethanol steam reforming
$C_2H_5OH + H_2O \rightarrow 2CO + 4H_2$	Incomplete steam reforming
$C_2H_5OH \rightarrow CH_3CHO + H_2$	Ethanol dehydrogenation
$C_2H_4O \rightarrow CO + CH_4$	Acetaldehyde decomposition
$2C_2H_4O + H_2O \rightarrow CH_3COCH_3 + CO_2 + 2H_2$	Aldol condensation
$C_2H_5OH \rightarrow CO + CH_4 + H_2$	Ethanol decomposition
$C_2H_5OH \rightarrow C + CO + 3H_2$	Ethanol decomposition
$2C_2H_5OH \rightarrow (C_2H_5)_2 + H_2O$	Ethanol dehydration
$C_2H_5OH \rightarrow C_2H_4 + H_2O$	Ethanol dehydration to ethylene
$C_2H_4 \rightarrow 2C + 2H_2$	Ethylene decomposition
$C_2H_4 + H_2 \rightarrow C_2H_6$	Ethylene hydrogenation
$C_2H_6 + H_2 \rightarrow 2CH_4$	Cracking reaction
$CH_4 + H_2O \rightarrow CO + 3H_2$	Methane steam reforming
$2CO \rightarrow CO_2 + C$	Boudouard reaction
$C + H_2O \rightarrow CO + H_2$	Gasification
$CO + H_2O \rightarrow CO_2 + H_2$	Water-gas shift reaction

Table 1. Thermodynamically possible reactions in the steam reforming process.

Alternatives for purification of the reformate for the removal of CO and feed in PEMFC have been proposed by several researchers [3–10]. According to Rosseti et al. [5, 6], there are well-established routes, such as high- and low-temperature water-gas shift (WGS) and methanation, which can be integrated into the hydrogen production unit. Chen et al. [8] experimentally investigated a reaction system composed of two stages, an ethanol vapor reforming reactor (Ni/Al_2O_3 catalyst) followed by a water-gas shift reactor (Fe/Cr_2O_3 catalyst) to purify the hydrogen stream. In this study, four operational parameters including liquid flow, H_2O/C molar ratio, reactor temperature and water-gas shift (WGS) reactor temperature were evaluated. The results indicated that the molar ratio H_2O/C is the factor that most influences the performance of the system, which can be optimized to minimize CO formation.

Another alternative widely evaluated in the available literature [9, 10] considers the use of reactive systems of hydrogen-permeable catalytic membranes, which can lead to the production of highly pure hydrogen and therefore enable direct integration between the reformer unit and PEMFC. Koch et al. [11] studied the ethanol-steam reforming process aiming to feed a PEM fuel cell to produce clean energy. The process consists of two stages as shown in **Figure 1**; the first stage produces a high hydrogen content gas via ethanol steam reformation. The second stage, a palladium-based membrane, separates the hydrogen from the rest of the reformed gas, producing high-purity hydrogen (>99.9999%), which prevents poisoning produced by impurities or fuel shortage. Koch et al. concluded that ethanol-steam reformer process was able to generate a pure hydrogen stream of up to 100 mm/min to feed the PEM fuel cell [11].

Based on the feasibility of energy cogeneration through fuel cells from biomasses such as ethanol, Rossetti et al. [6] performed the simulation and optimization of the H_2 production process from the ethanol reformation with water vapor. The layout of the system was inspired by an existing unit in combined heat and power generation, with the purpose of evaluating the

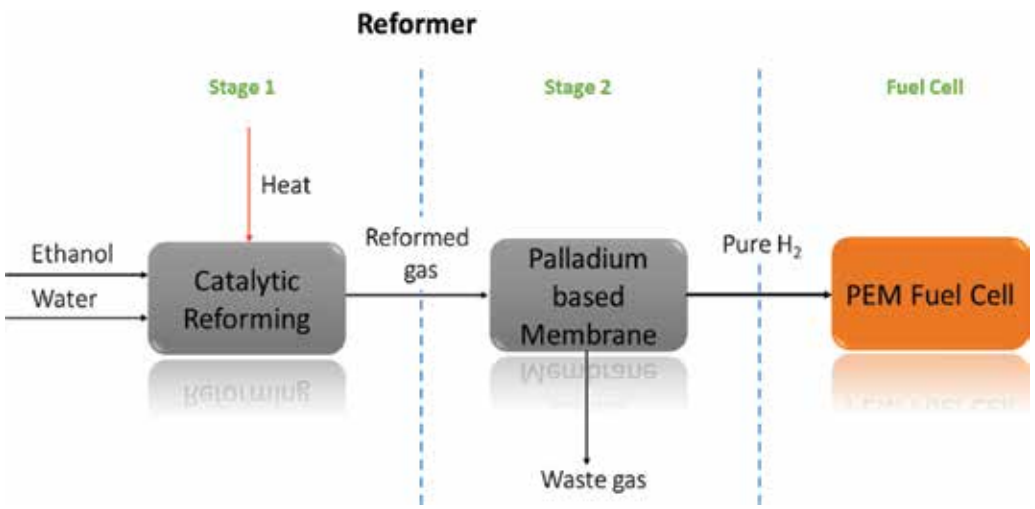

Figure 1. Simplified scheme of the reformer processes [11].

efficiency of the process and the possibility of operating with diluted bioethanol feed, reducing the cost with the purification step. The system consisted of six reactors connected in series for production and purification of hydrogen, containing a fuel processor, which includes a steam reformer, two water-heating gases and a serial methanation reactor, in addition to the fuel cell. The heat was generated by burning part of the reformate. During the process, it was verified that the change in water/ethanol ratio in the feed of the reactor had a direct impact on the production of H_2, that is, the increase in the ratio also increased the H_2 yield.

In view of the earlier information, it can be concluded that the ethanol-vapor reforming process combined with PEMFC is undefined between the two technological options presented, namely: reforming reactor and WGS systems in contrast to the use of membranes in the ethanol-steam reforming process. Finally, the technological development of the PEMFCs will possibly define the commercial choice for one of the two technologies.

3. The role of photophysics and photochemistry on water split process

3.1. Principles

Solar energy is the unique renewable source that can fulfill the world's needs for the future [12]. The direct conversion of solar energy into renewable hydrogen fuel is done basically by two methods, photocatalysis and photoelectrochemical (PEC) water splitting. The first method relies on photocatalytically active particles suspended in aqueous electrolyte solutions, where one or both water-splitting half reactions take place. The second method uses photocatalytically active particles or thin films deposited on electrodes [13].

Photocatalysis involves photophysical processes, initiated by photon absorption, followed by the generation of excited states and finalized as a photochemical or electrochemical redox reaction. These excited states permit that a prohibitive reaction under certain conditions can occur by the use of a photocatalyst, and this reason makes photocatalysis interesting for solar energy conversion technologies [14].

On search (and development) of new materials/catalysts for water-splitting processes, a common approach is to mimic natural processes and/or analogue materials. In case of water splitting, the natural process is photosynthesis. Under this point of view, the central role of natural water-splitting process is occupied by an enzyme complex, known as photosystem II (PS II), capable to split water using sunlight [15].

Photons absorbed by this enzymatic complex are transferred to the catalyst core, where a single charge separation takes place [4]. This catalyst core in PS II is a Mn_4CaO_5 oxo-bridged complex, represented by two similar models in **Figure 2**, but its exact reaction mechanism is still obscure [16].

Chlorophyll fluorescence is used to provide information on many aspects of photosynthesis. There are two different quenching mechanisms for chlorophyll fluorescence, a photochemical and a non-photochemical quenching. The first one is caused by charge separation at PS II reaction centers and can be considered a reliable measure of the PS II charge separation rate.

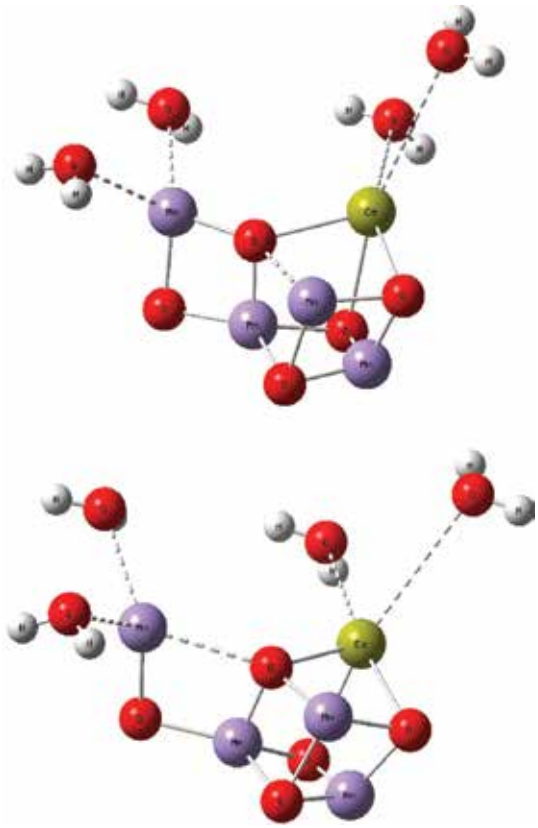

Figure 2. Representations of PS II core catalyst [16].

The second one may be due to a number of other non-radiative de-excitation processes in PS II [17].

Pijpers et al. punctuate that is necessary to separate light collection/conversion from catalysis. Whereas light collection/conversion generates one electron/hole pair at a time, water splitting is a four-electron/hole global process 4 as shown in reaction (1). This part of the process is particularly demanding once it involves the formation of double bonds between oxygen, four protons and four electrons [18]. Reaction (1) is known as oxygen evolution reaction (OER).

$$2H_2O \rightarrow O_2 + 4H^+ + 4e^- \quad (1)$$

The subsequent, less demanding process is the reduction of H^+ into two hydrogen molecules, as shown by reaction (2), and known as hydrogen evolution reaction (HER).

$$4H^+ + 4e^- \rightarrow 2H_2 \quad (2)$$

It is important to point that, different from artificial processes, that usually have high over-potentials, this natural multi-protein complex uses only small driving forces and moderate activation energies [19].

3.2. Artificial design

Pijpers et al. affirm that an artificial photosynthesis design must guarantee that one electron-hole pair of a semiconductor be integrated with the catalyst to perform OER [4]. A general representation of an ideal photocatalyst, as proposed by Hisatomi, Takanabe and Domen, is represented in **Figure 3**.

3.3. Catalysts

Focusing on artificial processes, the evolution of oxygen, by UV-illuminated single crystals of TiO_2, suspended in water, was firstly reported by Frank and Honda et al. [22], in 1972. Further investigations in the photoelectrochemical behavior of TiO_2 leads to an increase in the interest on metal-oxide-based materials such as catalysts and with some time the development of a mixed catalyst for the mediation of water cleavage by visible light (Pt/RuO_2 is cited as an example). In parallel, some earth-abundant (Mn, Fe, Co, Ni) 3d-metal-based materials were developed [20]. By now, the interest on TiO_2 particles resides in its use as support material for water splitting [21].

Photoanodes of CdS were also used to cleavage water molecules induced by visible light 11 following the reactions represented in Eqs. (3) and (4).

$$\text{PHOTOANODE} : CdS + 2H^+ \rightarrow Cd^{2+} + S \tag{3}$$

$$\text{PHOTOCATHODE} : 2e^- + 2H_2O \rightarrow H_2 + 2OH^- \tag{4}$$

One associated issue of these electrodes is the photocorrosion in the time which deactivates these electrodes, increasing cost and causing maintenance to be difficult. These photoanodes were improved by coating with polypirrole-inhibiting photocorrosion of CdS anodes into Cd^{2+}

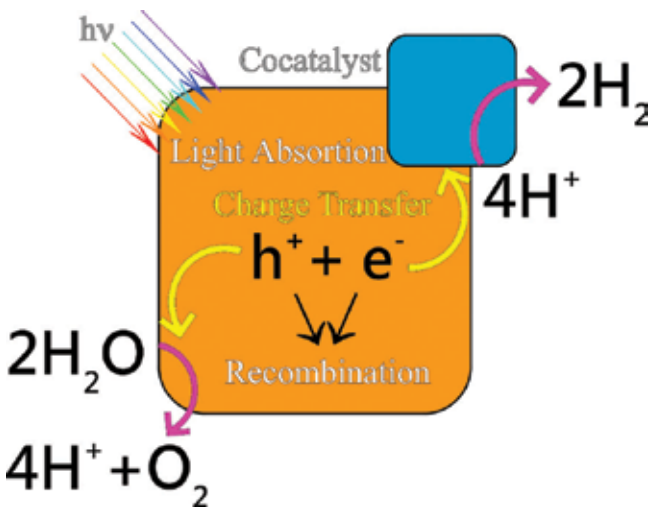

Figure 3. General representation of a photocatalyst [14].

ions, following the equations represented in reaction (5), more complex kinetically and thermodynamically less favorable [22].

$$2H_2O + 4H^+ \rightarrow O_2 + 4H^+ \quad (5)$$

Inert anodes are also applied on water oxidation, usually coated by a catalyst. One example is the use of ITO or FTO electrodes, coated by a self-assembled amorphous film, generated by electrodeposition of cobalt salts into phosphate, methyl phosphonate or borate electrolytes [18]. That approach has as a characteristic the need of an electrolyte medium that is a key factor for activity, selectivity and formation of the self-assembled amorphous film. The selection for cobalt resides on the fact that its tetranuclear oxo core mimics the natural oxygen-evolving complex (OEC) of PSII [23]. Regarding cobalt, thin films of Co-Pi (cobalt-phosphate) are deposited on Fe_2O_3, WO_3 and ZnO electrodes, focusing on reducing the onset potential for water oxidation leading to performing the process in neutral pH conditions. A posterior approach deposits Co-Pi thin films on the ITO film attached to an np-Si solar cell, directing the voltage produced by the solar cell to reduce the cited over-potential [15].

Cobalt is also reported to be associated with molybdenum-based polyoxometalates with the limitations that this system must contain tris(2,2′-bipyridine)ruthenium (II) ($Ru(bpy)_3^{2+}$) and sodium persulfate ($S_2O_8^{2-}$) in an aqueous borate buffer solution at pH 8.0 [24]. Berardi et al. [23] presents a new class of isostructural cubane-shape catalysts Cobalt-based, Hydrogen substituted by Me, t-Bu, OMe, Br, COOMe and CN, capable to water oxidation under dark or illuminated conditions, unfortunately again under highly basic conditions (pH = 8.0) in the presence of ($Ru(bpy)_3^{2+}$) as photosensitizer and sodium persulfate ($S_2O_8^{2-}$) as electrolyte. The best quantum efficiency (QE) decrescent substituent order is determined as OMe > COOMe > Me ≈ H ≈ Br ≈ CN > t-Bu. In conclusion, the combination of semiconductor-electrocatalyst-electrolyte interfaces is mandatory on water-splitting photocatalysis.

Yellow scheelite monoclinic $BiVO_4$ is also used as a photocatalyst for O_2 evolution under visible light, in the presence of an appropriate electron acceptor. But due to its conduction band bottom limit is located on a more positive potential than the potential of water reduction; it is incapable of evolving into hydrogen [25]. However, $BiVO_4$ doped with In and Mo produces a $Bi(1-X)In(X)V(1-X)Mo(X)O_4$ catalyst, with a more negative conduction band than H^+/H_2, making it capable of water splitting at neutral pH-evolving hydrogen with no use of any sacrificial agent [25].

Following additional layers' approach, Si electrodes gain focus again in 2014, with Kaiser and Jaegermann's [12] work. The electrochemical properties of single-crystalline p-type 3C-SiC films on p-Si and n-Si substrates are investigated as electrodes in H_2SO_4 aqueous solutions, under dark and light conditions. The photoelectrochemical measurements on different wavelengths indicate the p-SiC film on p-Si substrate which can generate a cathodic photocurrent, corresponding with hydrogen production, and can also generate an anodic photocurrent, for oxygen evolution. Iron nickel oxide (FeNiOx) is also used for water splitting. One remarkable example is reported by Morales et al. on which an amorphous layer of the oxide is oxidatively

electrodeposited on hematite, capable of evolving oxygen and practically transparent. This optical transparency property permits the composition of the oxide catalyst into a hematite/perovskite tandem water-splitting cell. Solar-to-hydrogen conversion efficiencies are reported to be around 2%. The development of the catalyst and its integration into photoanodes open new possibilities in solar fuel production [26].

Following a nanostructuring and morphology control approach [13], numerous efforts have been taken to investigate morphologies and nanostructures of the NiCo-oxide and also the relationship between the nanostructure and the electrocatalytic activity. Compared to NiCo oxides, NiCo sulfides appear as promising electrocatalysts [13]. More recent works show nickel cobalt selenide (NiCo-selenide) as a better electrocatalyst candidate when compared to its oxide-based and sulfide-based species [20].

Cocatalysts are combined to catalysts in order to increase its efficiency [13]. It is concluded that the role of cocatalysts is different in photocatalysis and in photoelectrochemical water splitting for $LaTiO_2N/Co_3O_4$ systems. Cocatalyst is not only material and concentration dependant, but it also depends of the size distribution of particles. Small particles are favorable for photocatalysis due to kinetic effects. In PEC, larger cocatalyst particles are better, probably due to avoiding charge recombination. Under this point of view, the design of a cocatalyst size must be function to the solar light energy conversion process [13].

Recently, Garcia-Esparza et al. [27] report the manufacture of an oxygen insensitive system ($MoOx/Pt/SrTiO_3$), that, when coated on metal surfaces, can evolute hydrogen and avoid recombination of H_2 and O_2 onto water, maintaining H_2 evolution at high taxes. Catalyst candidates can also be proposed using computational chemistry tools. Many distinct properties such as optical and transport properties electronic-band structure, density of states, and others, can be accurately determined by distinct levels of theory. Recently, Reshak [28] proposed that $Tl_{10}Hg_3Cl_{16}$ single crystals can be used as a catalyst in water splitting due to electronic and optical properties calculated by density functional theory/mBJ. Its results are compared to experimental data to conclude that these computational tools can be used with good levels of precision, helping to elucidate internal details of these systems.

4. Proton exchange membrane fuel cell

The proton exchange membrane fuel cell (PEMFC) is a device that converts chemical energy into electrical energy through an electrochemical reaction [29]. At the anode, the hydrogen or other fuel that may produce pure hydrogen like the ethanol-steam reforming process is oxidized and releases protons and electrons. The protons are carried out to the cathode side through electrolyte and the electrons produce electrical current in an external circuit. At the cathode, the electrons and the protons are associated with oxygen (often from atmospheric air) producing water and energy as a final product from PEMFC; thus, the fuel cell system does not produce pollutants and is ambient compatible.

The chemical reactions are:

$$\text{Anode} : H_2(g) \rightarrow 2H^+ + 2e^- \tag{6}$$

$$\text{Cathode} : O_2(g) + 2e^- + 4H^+ \rightarrow H_2O \tag{7}$$

The global reaction of the fuel cell system can be written as Eq. (8). The theoretical potential (E) of this reaction is 1.23 V, but at the operational condition the potential is around 0.7 V. This potential result at the maximum output power density is about 1 W cm^2 [30, 31].

$$\text{PEMFC} : H_2(g)\ (\text{at anode}) + O_2(g)\ (\text{at cathode}) \rightarrow H_2O(l) + \text{energy} \tag{8}$$

Figure 4 shows a representative schema of the PEMFC operation. The fuel is fed at the anode site and the oxygen is fed at the cathode side. The electrons from anode to cathode are used in an external electrical circuit to produce electrical work.

An alternative source of hydrogen can be the steam reformation of liquid substances like alcohols of small chairs. Ethanol, for example, is low density and nontoxic alcohol obtained from fermentation of renewable resources like sugarcane. This has been studied as a possible fuel in direct alcohol fuel cell (DAFC) systems [32]. However, its direct use is difficult due to the rupture of C—C bond on platinum or platinum alloy electrodes. The ethanol-steam reforming reactions take place in different steps with endothermic/exothermic reactions [33, 34].

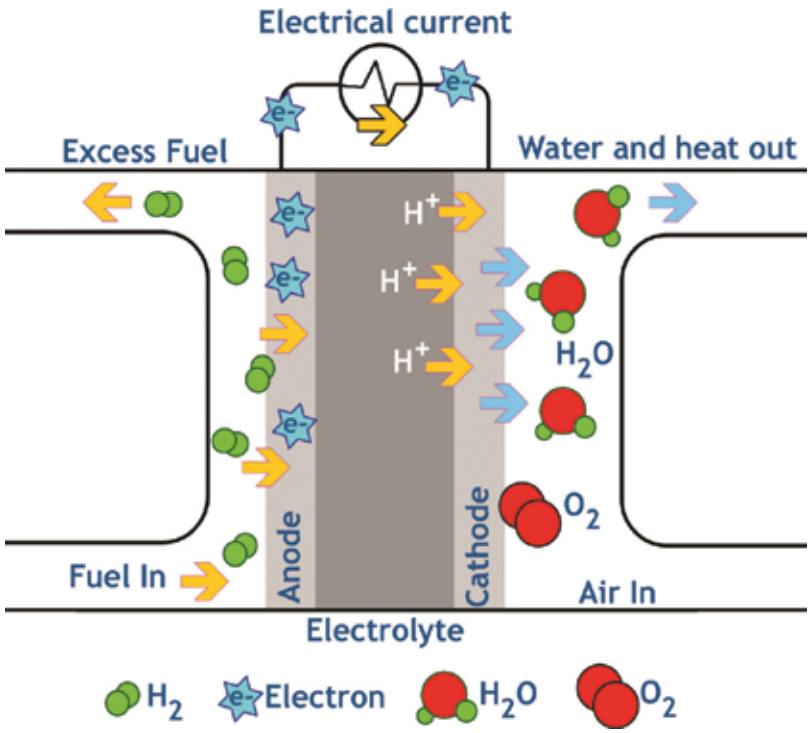

Figure 4. Proton exchange membrane fuel cell (PEMFC), anode fed with H_2 and cathode fed with O_2. Protons are carried out from anode to cathode through membrane electrolyte and the electrons produce working in an external circuit.

For ethanol-steam reforming reaction the chemical reactions are:

$$C_2H_5OH + 3H_2O \rightarrow 2CO_2 + 6H_2 \quad (9)$$

$$CO + H_2O \leftrightarrow CO_2 + H_2 \quad (10)$$

$$CO + ½O_2 \rightarrow CO_2 \quad (11)$$

The PEMFC works at low temperature due to electrolyte that is hydrated (lower than 100°C), which is an advantage, as well as other new materials that enable the cell to work at high temperature [35]. At low temperatures, the catalytic material that presents high efficiency is platinum, for both anode and cathode electrodes. But, as demonstrated previously, hydrogen obtained from steam presents low-content CO, which adsorbs strongly on platinum surface and poisons the electrode. To outline this problem, a second metal is included into the electrode. This second metal often is a transition and not a noble metal which dissociated in water at low potential and provides oxygenated species to oxidize the adsorbed CO at a lower potential. This pathway is known as the Langmuir-Hinshewood mechanism [36], where two adsorbed species react and form a final product; some studies show that PtRu is the more efficient electrocatalyst [37–39]. The use of pure Pt as anode of PEMFC fed with H_2 , presenting 100 ppm of CO, results in more than 50% of loss of efficiency due to electrode poisoning effect [37].

The research of PEMFC focuses on minimizing the amount of Pt used in the electrodes, due to high cost of this material; moreover, the oxygen reduction reaction which happens at the cathode electrode presents low kinetic and parallel pathways producing H_2O_2, resulting in loss of power density output. The use of the different cathode material improves the performance of the fuel cell. The development of a membrane working at high temperatures can improve the kinetics of chemical reactions also and results in better fuel cell performance.

The main advantage of the fuel cell system, notably PEMFC, is the efficiency in energy conversion, once the efficiency of electrochemical systems is above the other converter; however, the source of hydrogen is important [40, 41]. The hydrogen obtained from water electrolysis is very pure, but it results in energy deficit [42]; the H_2 from steam hydrocarbons contains CO. Thus, the tendency is an aggregate of the system to convert energy. Solar photovoltaic can be used to produce highly pure H_2 for PEMFC and moreover, solar energy can charge batteries [43] for later use.

5. Conclusions

Solar energy is a renewable source that can fulfill the world's needs for the future. The direct conversion of solar energy into renewable hydrogen fuel is done basically by two methods: photocatalysis and photoelectrochemical processes. The hydrogen obtained from photocatalysis and/or photoelectrochemical process can feed PEMFCs to convert chemical energy into electrical energy with high efficiency and without degradation of the ambient. PEMFC fed with H_2 obtained from ethanol-steam reforming reaction (which contains CO) must use Pt-based alloy catalysts to increase the poisoning tolerance and improve the lifetime of the PEMFC.

Acknowledgements

The authors thank CNPq, Capes, FAPEG and FAPEMA for research support.

Conflict of interest

The authors state that there is no conflict of interest associated with this work.

Author details

Flavio Colmati[1]*, Christian Gonçalves Alonso[1], Tatiana Duque Martins[1], Roberto Batista de Lima[2], Antonio Carlos Chaves Ribeiro[3], Leandro de Lima Carvalho[1], André Mychell Barbieux Silva Sampaio[1], Monah Marques Magalhães[1], José William Diniz Coutinho[2], Geovany Albino de Souza[1], Lucas Fernandes Aguiar[1], Diericon de Sousa Cordeiro[1], Adão Marcos Ferreira Costa[1], Thiago Soares Silva Ribeiro[1], Pedro Henrique Machado Godoy[1] and Guilherme Botelho Meireles de Souza[1]

*Address all correspondence to: colmati@ufg.br

1 Universidade Federal de Goiás (UFG), Instituto de Química, Goiânia, Goiás, Brazil

2 Universidade Federal do Maranhão (UFMA), Instituto de Química, São Luís, Maranhão, Brazil

3 Instituto Federal de Educação, Ciência e Tecnologia Goiano (IFGoiano), Morrinhos, Goiás, Brazil

References

[1] Alonso CG, Furtado AC, Cantão MP, Santos OAA, Fernandes-Machado NRC. Reactions over Cu/Nb_2O_5 catalysts promoted with Pd and Ru during hydrogen production from ethanol. International Journal of Hydrogen Energy. 2009;**34**:3333-3341. DOI: 10.1016/j.ijhydene.2009.02.021

[2] Rossi CCRS, Alonso CG, Antunes OAC, Guirardello R, Cardozo-Filho L. Thermodynamic analysis of steam reforming of ethanol and glycerine for hydrogen production. International Journal of Hydrogen Energy. 2009;**34**:323-332. DOI: 10.1016/j.ijhydene.2008.09.071

[3] Furtado AC, Alonso CG, Cantão MP, Fernandes-Machado NRC. Bimetallic catalysts performance during ethanol steam reforming: Influence of support materials. International Journal of Hydrogen Energy. 2009;**34**:7189-7196. DOI: 10.1016/j.ijhydene.2009.06.060

[4] Li D, Li X, Gong J. Catalytic reforming of oxygenates: State of the art and future prospects. Chemical Reviews. 2016;**116**:11529-11653. DOI: 10.1021/acs.chemrev.6b00099

[5] Rosseti I, Compagnoni M, Torli M. Process simulation and optimisation of H_2 production from ethanol steam reforming and its use in fuel cells. 1. Thermodynamic and kinetic analysis. Chemical Engineering Journal. 2015;**281**:1024-1035. DOI: 10.1016/j.cej.2015.08.025

[6] Rosseti I, Compagnoni M, Torli M. Process simulation and optimisation of H_2 production from ethanol steam reforming and its use in fuel cells. 2. Process analysis and optimization. Chemical Engineering Journal. 2015;**281**:1036-1044. DOI: 10.1016/j.cej.2015.08.045

[7] Tripodi A, Compagnoni M, Ramis G, Rosseti I. Process simulation of hydrogen production by steam reforming of diluted bioethanol solutions: Effect of operating parameters on electrical and thermal cogeneration by using fuel cells. International Journal of Hydrogen Energy. 2017;**42**:23776-23783. DOI: 10.1016/j.ijhydene.2017.04.056

[8] Chen C, Tseng H, Lin Y, Chen W. Hydrogen production and carbon dioxide enrichment from ethanol steam reforming followed by water gas shift reaction. Journal of Cleaner Production. 2017;**162**:1430-1441. DOI: 10.1016/j.jclepro.2017.06.149

[9] Viviente JL, Meléndez J, Tanaka DAP, Gallucci F, Spallina V, Manzolini G, Foresti S, Palma V, Ruocco C, Roses L. Advanced m-CHP fuel cell system based on a novel bio-ethanol fluidized bed membrane reformer. International Journal of Hydrogen Energy. 2017;**42**: 13970-13987. DOI: 10.1016/j.ijhydene.2017.03.162

[10] Serra M, Ocampo-Martinez C, Li M, Llorca J. Model predictive control for ethanol steam reformers with membrane separation. International Journal of Hydrogen Energy. 2017;**42**: 1949-1961. DOI: 10.1016/j.ijhydene.2016.10.110

[11] Koch R, López E, Divins NJ, Allué M, Jossen A, Riera J, Llorca J. Ethanol catalytic membrane reformer for direct PEM FC feeding. International Journal of Hydrogen Energy. 2013;**38**:5605-5615. DOI: 10.1016/j.ijhydene.2013.02.107

[12] Ma QB, Kaiser B, Jaegermann W. Novel photoelectrochemical behaviors of p-SiC films on Si for solar water splitting. Journal of Power Sources. 2014;**253**:41-47. DOI: 10.1016/j.jpowsour.2013.12.042

[13] Pokrant S, Dilger S, Landsmann S, Trottmann M. Size effects of cocatalysts in photoelectrochemical and photocatalytic water splitting. Materials Today Energy. 2017;**5**:158-163. DOI: 10.1016/j.mtener.2017.06.005

[14] Hisatomi T, Takanabe K, Domen K. Photocatalytic water-splitting reaction from catalytic and kinetic perspectives. Catalysis Letters. 2015;**145**:95-108. DOI: 10.1007/s10562-014-1397-z

[15] Pijpers JJH, Winkler MT, Surendranath Y, Buonassisi T, Nocera DG. Supporting information light-induced water oxidation at silicon electrodes functionalized with a cobalt oxygen evolving catalyst. Proceedings of the National Academy of Sciences of the United States of America. 2011;**108**:10056-10061. DOI: 10.1073/pnas.1106545108/-/DCSupplemental.www.pnas.org/cgi/doi/10.1073/pnas.1106545108

[16] Bovi D, Narzi D, Guidoni L. Magnetic interactions in the catalyst used by nature to split water: A DFT + U multiscale study on the Mn_4CaO_5 core in photosystem II. New Journal of Physics. 2014;**16**:1-13. DOI: 10.1088/1367-2630/16/1/015020

[17] Neubauer C, Schreiber U. Photochemical and non-photochemical quenching of chlorophyll fluorescence induced by hydrogen peroxide. Zeitschrift für Naturforschung. 1989; **44c**:262-270

[18] Surendranath Y, Dincă M, Nocera DG. Electrolyte-dependent electrosynthesis and activity of cobalt-based water oxidation catalysts. Journal of the American Chemical Society. 2009; **131**:2615-2620. DOI: 10.1021/ja807769r

[19] Barber J, Rutherford AW. Introduction. Philosophical Transactions of the Royal Society B: Biological Sciences. 2008;**363**:1125-1128. DOI: 10.1098/rstb.2007.2227

[20] Zhao X, Yang Y, Li Y, Cui X, Zhang Y, Xiao P. NiCo-selenide as a novel catalyst for water oxidation. Journal of Materials Science. 2016;**51**:3724-3734. DOI: 10.1007/s10853-015-9690-9

[21] Duonghong D, Borgarello E, Grätzel M. Dynamics of light-induced water cleavage in colloidal systems. Journal of the American Chemical Society. 1981;**103**:4685-4690. DOI: 10.1021/ja00406a004

[22] Frank A, Honda K. Visible-light-induced water cleavage and stabilization of n-type cadmium sulfide to photocorrosion with surface-attached polypyrrole-catalyst coating. The Journal of Physical Chemistry. 1982;**86**:1933-1935. DOI: 10.1021/j100208a005

[23] Berardi S, La Ganga G, Natali M, Bazzan I, Puntoriero F, Sartorel A, Scandola F, Campagna S, Bonchio M. Photocatalytic water oxidation: Tuning light-induced electron transfer by molecular Co_4O_4 cores. Journal of the American Chemical Society. 2012;**134**: 11104-11107. DOI: 10.1021/ja303951z

[24] Tanaka S, Annaka M, Sakai K. Visible light-induced water oxidation catalyzed by molybdenum-based polyoxometalates with mono- and dicobalt(iii) cores as oxygen-evolving centers. Chemical Communications. 2012;**48**:1653-1655. DOI: 10.1039/C2CC16821A

[25] Jo WJ, Kang HJ, Kong K-J, Lee YS, Park H, Lee Y, Buonassisi T, Gleason KK, Lee JS. Phase transition-induced band edge engineering of $BiVO_4$ to split pure water under visible light. Proceedings of the National Academy of Sciences. 2015;**112**:13774-13778. DOI: 10.1073/pnas.1509674112

[26] Morales-Guio CG, Mayer MT, Yella A, Tilley SD, Grätzel M, Hu X. An optically transparent iron nickel oxide catalyst for solar water splitting. Journal of the American Chemical Society. 2015;**137**:9927-9936. DOI: 10.1021/jacs.5b05544

[27] Garcia-Esparza AT, Shinagawa T, Ould-Chikh S, Qureshi M, Peng X, Wei N, Anjum DH, Clo A, Weng TC, Nordlund D, Sokaras D, Kubota J, Domen K, Takanabe K. An oxygen-insensitive hydrogen evolution catalyst coated by a molybdenum-based layer for overall water splitting. Angewandte Chemie, International Edition. 2017;**56**:5780-5784. DOI: 10.1002/anie.201701861

[28] Reshak AH. Photophysical, transport and structure properties of $Tl_{10}Hg_3Cl_{16}$ single crystals: Novel photocatalytic water-splitting solar-to-hydrogen energy conversion. Journal of Catalysis. 2017;**352**:142-154. DOI: 10.1016/j.jcat.2017.04.028

[29] Wang Y-J, Long W, Wang L, Yuan R, Ignaszak A, Fang B, Wilkinson D. Unlocking the door to highly active ORR catalysts for PEMFC applications: Polyhedron-engineered Pt-based nanocrystals. Energy & Environmental Science. 2018;**11**:258-275. DOI: 10.1039/C7EE02444D

[30] Das V, Padmanaban S, Venkitusamy K, Selvamuthukumaran P, Blaabjerg F, Siano P. Recent advances and challenges of fuel cell based power system architectures and control —A review. Renewable and Sustainable Energy Reviews. 2017;**73**:10-18. DOI: 10.1016/j.rser.2017.01.148

[31] Youssef EM, Amin RS, El-khatib KM. Development and performance analysis of PEMFC stack based on bipolar plates fabricated employing different designs. Arabian Journal of Chemistry, in press. DOI: 10.1016/j.arabjc.2015.07.005

[32] Braunchweiga B, Hibbittsb D, Neurockb M, Wieckowski A. Electrocatalysis: A direct alcohol fuel cell and surface science perspective. Catalysis Today. 2013;**202**:197-209. DOI: 10.1016/j.cattod.2012.08.013

[33] Duan S, Senkan S. Catalytic conversion of ethanol to hydrogen using combinatorial methods. Industrial and Engineering Chemistry Research. 2005;**44**:6381-6386. DOI: 10.1021/ie049202k

[34] Chen J, Xu D. Hydrogen production by the steam reforming of bio-ethanol over nickel-based catalysts for fuel cell applications. International Journal of Sustainable and Green Energy. 2017;**6**:28-38. DOI: 10.11648/j.ijrse.20170603.11

[35] Rosli RE, Sulong AB, Daud WRW, Zulkifley MA, Husaini T, Rosli MI, Majlan EH, Haque MA. A review of high-temperature proton exchange membrane fuel cell (HT-PEMFC) system. International Journal of Hydrogen Energy. 2017;**42**:9293-9314. DOI: 10.1016/j.ijhydene.2016.06.211

[36] Baxter RJ, Hu P. Insight into why the Langmuir-Hinshelwood mechanism is generally preferred. The Journal of Chemical Physics. 2002;**116**:4379-4381. DOI: 10.1063/1.1458938

[37] Colmati F, Lizcano-Valbuena WG, Camara GA, Ticianelli EA, Gonzalez ER. Carbon monoxide oxidation on Pt-Ru electrocatalysts supported on high surface area carbon. Journal of the Brazilian Chemical Society. 2002;**13**:474-482

[38] Calderón-Cárdenas A, Ortiz-Restrepo JE, Mancilla-Valencia ND, Torres-Rodriguez GA, Lima FHB, Bolaños-Rivera A, Gonzalez ER, Lizcano-Valbuena WH. CO and ethanol electro-oxidation on Pt-Rh/C. Journal of the Brazilian Chemical Society. 2014;**25**:1-8

[39] Lopes PP, Ticianelli EA. The CO tolerance pathways on the Pt-Ru electrocatalytic system. Journal of Electroanalytical Chemistry. 2010;**644**:110-116. DOI: 10.1016/j.jelechem.2009.06.011

[40] Piela P, Mitzel J. Polymer electrolyte membrane fuel cell efficiency at the stack level. Journal of Power Sources. 2015;**292**:95-103. DOI: 10.1016/j.jpowsour.2015.05.043

[41] Amphlett JC, Mann RF, Peppley BA, Roberge PR, Rodrigues A, Salvador JP. Simulation of 250 kW diesel processor/PEM fuel cell system. Journal of Power Sources. 1998;**71**:179-184. DOI: 10.1016/S0378-7753(97)02752-3

[42] Lamy C. From hydrogen production by water electrolysis to its utilization in a PEM fuel cell or in a SO fuel cell: Some considerations on the energy efficiencies. International Journal of Hydrogen Energy. 2016;**41**:15415-15425. DOI: 10.1016/j.ijhydene.2016.04.173

[43] Ezzat MF, Dincer I. Development, analysis and assessment of a fuel cell and solar photovoltaic system powered vehicle. Energy Conversion and Management. 2016;**219**:284-292. DOI: 10.1016/j.enconman.2016.10.025

Chapter 5

Iodine Doped Graphene for Enhanced Electrocatalytic Oxygen Reduction Reaction in PEM Fuel Cell Applications

Adriana Marinoiu, Elena Carcadea,
Mircea Raceanu and Mihai Varlam

Additional information is available at the end of the chapter

http://dx.doi.org/10.5772/intechopen.76495

Abstract

Although doped graphene based materials have been intensively investigated, as electrocatalysts for oxygen reduction reaction (ORR), there is still a number of challenges to be explored in order to design a highly active, durable, thermodynamically stable and low-cost catalyst with full recognized technological importance. The application of iodine-doped graphene in fuel cells (FC) has been recently examined as innovative nanomaterial for cathode fabrication. Up to date microscopic and spectroscopic techniques have been combined with structural and electrochemical investigations for a compendious characterization of developed ORR catalysts. The unique structure of doped graphenes is ascertained by the presence of mesopores, vacancies and high surface area, and favors the ions/electrons transportation at nanometric scale. The chapter discusses (a) how to use the existing knowledge in respect to synthesized doped graphenes and (b) how to improve the FC by taking into account these materials and have an enhanced electrochemical performance as well as long-term durability.

Keywords: fuel cell, cathode, doped graphenes, oxygen reduction reaction, iodine

1. Introduction

Due to diminishing fossil fuel resources and climate change, sustainable renewable energy sources are sought. Among the proposed clean energy sources, fuel cells are the latest developed energy conversion devices that convert the chemical energy of a fuel directly into electrical

energy. Fuel cells technology has recently evolved to address the challenges of global energy. Among them, proton exchange membrane fuel cells (PEMFC) have attracted a considerable attention as a potential power source for automotive and stationary applications due to its low temperature operation conditions, high power density and high energy conversion efficiency. Hydrogen is regarded as the most attractive fuel for PEM FC, demonstrating excellent electrochemical reactivity, highest power density, zero emissions characteristics.

The standard structure of a fuel cell consists in a solid electrolyte in contact to a porous anode and cathode on either side. A fuel cell consists of a fuel-fed anode and an oxygen-filled cathode separated by a solid polymer membrane. Diffusion layers for the reactants and product, bipolar plates to transport the reactants/product to/from the catalytic layers; end plates with current collectors and sealing gaskets are other basic components of a fuel cell. This configuration allows the transfer of ions between the two electrodes (components constituting the membrane-electrode assembly MEA). In a typical fuel cell, gaseous hydrogen reactant H_2 is continuously fed to anode side and a gaseous oxidant (air or oxygen) is fed to the cathode compartment. The electrochemical reactions occur at electrodes and the electrons will be released to the external circuit.

Appreciable progress has been made over past 20 years regarding the development of PEMFC technology. However there are still several technical challenges that need to be addressed in order to promote their commercialization.

Among the metal catalysts for the anode and cathode reactions, platinum (Pt) exhibits the largest electrocatalytic activities for the electro-oxidation of small organic compounds in the fuel from the anode and the reduction of oxygen at the cathode. In order to obtain ideal electrocatalysts for FCs with high catalytic performance and low cost, efforts have been made to develop new structured catalysts.

Recently, several technical issues for the commercialization of PEMFC including water management at the cathode, resistance reduction of the electrolyte membrane, technical realization of electrode assembly (MEA) have been addressed. Thus, in order to improve transport of water generated from electrochemical reaction at the cathode, research has been conducted on developing the mesoporous structures into the electrode [1–9]. Pt nanoparticles based on graphene support have been extensively studied due to their catalytic properties and excellent corrosion and oxidation resistance [10–12]. However, the high cost and limited resources hinder the widespread use of Pt-based catalysts and the widespread commercialization of fuel cells. To reduce the cost of FCs, numerous studies on electrocatalysts as FC electrodes were focused on manufacturing and developing alternatives to non-precious metals [13–18].

One of the major fuel cell limitations is the low rate of oxygen reduction (ORR) at the cathode, which requires a large amount of expensive Pt/C platinum catalyst. Thus, ORR plays a critical role in determining the performance of a fuel cell. ORR is a multi-electron transfer reaction with two possible main pathways: a) a direct path in one step, involving the transfer of four electrons to directly produce H_2O; b) an indirect two-step pathway, involving the transfer of two electrons for the first stage and two second electrons for the second stage to obtain water. Previous studies have shown that, with the exception of metal catalyst degradation due to

the dissolution and aggregation of metal nanoparticles, severe corrosion and oxidation of carbon materials in the actual fuel cell environment could lead to rapid loss of catalyst activity [19–21]. In this context, the unique properties of the graphene meet the basic requirements of an ideal catalyst support. Therefore, a notable effort was devoted to the design of new nanostructured catalysts dispersed on graphene support.

In the carbonaceous family, graphene is a graphite monolayer with a thickness of only 0.34 nm. It consists of carbon atoms in a sp^2 hybridization state, arranged so that each carbon atom is covalently bonded to the other three. Graphene is the two-dimensional graphite variant; is composed of a planar (two-dimensional) arrangement of carbon atoms ensconced in a hexagonal structure. Graphene possesses unique properties such as high mobility of load carriers (up to 10^5 cm^2 V^{-1} s^{-1}) superconductivity, Hall effect at room temperature, high mechanical strength (130 GPa) and high specific surface area. These properties make the material under discussion an excellent support for catalysts used in electrochemical energy systems.

Catalysts based on graphene doped with heteroatoms have proved a stable catalytic activity compared to other ORR composite electrocatalysts. As a catalytic support, compared to other carbonaceous support materials, the graphene combines the advantages of the traditional 2D graphite (high conductivity and high specific surface area) with porous structure and non-agglomerated morphology that can facilitate the deposition and dispersion of the catalyst. Moreover, the interconnected graphene network promotes the rapid transport of electrons between active sites and the electrode and increases the electroactive catalyst surface, all of which increase the catalytic activity and durability of these electrocatalysts for ORR [22–25].

The doped graphene with various heteroatoms removes the disadvantages and limitations described above by improving the catalytic performance of the electrocatalysts due to the high specific surface area and excellent conductivity. Graphene nanosheets (GNS) have exhibited large promising applications as a support for 2-D catalyst because of the following properties: first, the graphene has a large theoretical surface area of more than 2000 m^2/g), which is twice as much as that carbon nanotubes (CNTs); secondly, the graphene has a completely conjugated sp^2 hybrid structure, giving rise to very high electrical conductivity, excellent mechanical properties, and high thermal conductivity. The electronic property of the graphene is very important for its application in electrochemistry. Previous studies have shown that the mobility of electrons in the graphite suspended monolayer can reach around 2 × 105 $cm^2/(V\ s)$ at room temperature, which is higher than that of all other materials, including metals and carbon nanotubes. Doped graphene was noted to show high electrocatalytic activity for the ORR reaction.

Previous studies have found that in the case of non-Pt graphene-based nanocatalysts, there is also a charge transfer process through the graphene-metal interface, which depends on the distance and the Fermi level difference between the graphene and the supported catalysts [22].

However, metal-based electrocatalysts often suffer from some drawbacks, particularly low acidity in the acid medium specific for PEMFC environment. Doping with non-metallic heteroatom is one of the most studied nanocatalysts for the ORR reaction in PEMFC because

it has been shown that heteroatom doping can induce redistribution of graft load. In this regard, heteroatom doped graphene such as N, S, P, B have recently demonstrated that they can effectively improve the ORR catalytic activity [26–30]. It has been suggested that the dopant (whether its electronegativity toward carbon is greater (such as N, S) or lower (such as B) could create electronically loaded sites favorable for O_2 adsorption. To reduce Pt loading and the cost of electrocatalysts in fuel cells, non-Pt catalysts supported on graphene have also been developed in recent years. For N-doped graphene, the ORR catalytic activity is strongly dependent on the nitrogen types and the doping concentration. Nitrogen-doped graphene nanocomposites, have demonstrated an improved electrocatalytic activity of ORR, due to an interpenetration network formed between N and graphene, which can efficiently accelerate the reaction, the transport of ions and electrons and therefore synergistically improves the catalytic activity of ORR. The interaction between graphene support and composites may also affect the stability of electrocatalysts. For example, the strong link between N-doped sites of graphene may result in increased resistance of hybrid catalysts [25].

The main drawbacks of the mentioned catalysts are the preparation methods with multiple operating activities as well as the sophisticated equipment, making the processes less attractive to be transposed on a larger production scale. Other disadvantages are reaction conditions involving high temperatures for thermal decomposition, high vacuum or supercritical conditions.

Calculations using functional density theory (DFT) showed that the electrocatalytic activity of the heteroatom doped graphene is strongly dependent on the electronic spin density and the distribution of the electric charge density on the atoms. Catalytic active sites of doped graphene are typically high density spinning carbon atoms. N, P or B doped graphene introduces unpaired electrons and determines a local high density resulting in a high electrocatalytic ORR performance. Halogens are other important elements that offer new properties for alternative energy devices and technologies due to the effect of the difference in electronegativity between halogen atoms (x = 2.66–3.98) and C atoms (x = 2.55). They have a different electron loss capacity compared to O_2^- (x = 3.44). It is important to note that iodine halide may form partially ionized bonds to promote the transfer of the burden due to its large atomic size (the largest in the halogen group) [31–35]. In addition, it is known that the sides of the halogenated graphite have sufficient possibilities to attract O_2 and to weaken the O—O bond from the adsorbed oxygen, thus facilitating efficient conversion into water after reduction and protonation.

Previous studies have shown that the single layered basal structure of graphene can guarantee its electrochemical durability. In fact, the carbon corrosion starts from graphite defects, and carbonaceous materials with several graphite layers usually exhibit fewer structural defects. Therefore, the intrinsic grafting capacity of the graphene could improve the durability of graphene composite materials. More efforts need to be devoted to scalable and reproducible synthesis, with a compositional and morphological control, as well as investigations into properties and catalytic mechanism. In this area, major efforts have been made to refine these properties, including the adsorption of halogen molecules on the surface of the monolayer graphene as a promising approach due to the diversity of halogen properties and the variety of formed structures. The adsorption of atoms and halogen molecules on the graphene layer has been studied both theoretically and experimentally to adjust the electronic structure of the graphene layer.

Theoretically, adsorption of diatomic halogen molecules on graphene using functional Van der Waals has been studied, which includes nonlocal correlation effects, perfect for geometric optimization. The adsorption of halogen atoms on graphenes was studied using only a semi local function. It is accepted that an iodine atom can accept 0.5 electrons from the carbon substrate. The doping of the graphene through physical adsorption is particularly promising because it can increase the concentration of the carriers without affecting carrier mobility as in the case of chemical adsorbed dopants, where the covalent function can produce crystalline defects and irreversibly alter the electron structure. One of the most promising dopants that could be physically adsorbed on the graphite is iodine. Iodine is also considered to be a stable and practical dopant as compared to other halogen based dopants (Cl, Br and F) and compared to many other physically adsorbed dopants such as alkali metal dopants (K, Li, Na, etc.), acids (hydrochloric acid, HNO_3 and H_2SO_4) and organic compounds (tetracyano quinodimethane, tetrafluorotetracyanoquinodimethane), poly (4-vinylpyridine) and polyethyleneimine). However, the intercalation of iodine in the engraved Bernal multilayer graphite, which is required for potential electrode applications, was considered unlikely due to the strong interaction between the graphene layers and the high molecular size of I_2. In addition, the physicochemical properties of iodine-doped graphite, such as its chemical state, thermal stability, and working function have not been extensively investigated, even if they are critical parameters for successfully achieving graphite-based electrodes in industrial applications. It has been shown that the overlaid monolayer graphite and the double layer of graphite foil can be efficiently doped with iodine.

The request of a chemically stable material and efficient ORR electrocatalyst, directed us to develop a new concept of electrode as alternative cathode catalyst/microporous layer. The recent new application of iodine-doped (I-doped) graphene as electrode in PEMFC has been recently recognized as an improved strategy for effective modification of cathode side efficiency [32–35]. The performed experimental studies revealed that the microporous layer (MPL) placed between catalyst layer (CL) and GDL have many advantages, like: keeping the hydration of the membrane and of the ionomer phase, preventing gas diffusion layer (GDL) flooding, especially at high current densities, forming a more intimate contact between CL and GDL.

The main objective of this work is to improve the ORR performance by including of the nanostructured I-doped graphene and to prove the efficiency of the developed cathode in PEMFC operation conditions. It is important to mention, that only few papers have been reported in respect to the cathode electrocatalyst for PEMFC containing I-doped graphene. In view of these facts, the purpose of this work is to provide valuable information about the recommendation of I-doped graphene as innovative ORR electrode in the PEMFC cathode, based on performances obtained in electrochemical test in FC operation conditions.

2. Experimental

2.1. Materials

Graphite powder, $K_2S_2O_8$, P_2O_5, conc. H_2SO_4, $KMnO_4$, HI were purchased from Sigma-Aldrich., H_2O_2 and HCl were obtained from Oltchim SA Romania. Carbon paper gas diffusion layer

(GDL, SGL), membrane (Nafion-212), ionomer solution (5 wt.% Nafion) were purchased from Ion Power, USA. Commercial catalyst (HISPEC 4000 Pt/C 40 wt.%) was purchased from Alfa Aesar. The purity of reactants (H_2 and O_2) was 99.999%.

2.2. Catalysts preparation

I-doped graphene electrocatalyst was synthesized via a facile process described in detail elsewhere, through nucleophilic substitution of graphene oxide (GrO) by reduction with hydroiodic acid (HI) catalyzed by AlI_3 [24, 25]. Briefly, the graphite oxide (GO) was prepared starting from graphite powder by a modified Hummers method including specific steps, as follows. The pre-oxidation was used to prepare the preoxidized GO, namely the graphite (7.5 g), $K_2S_2O_8$ (6 g), and P_2O_5 (6 g) were introduced into conc. H_2SO_4 (50 ml) and P_2O_5 (50 g), under continuously stirring at 80°C. The product was washed, filtrated, dried at 60°C. The as pre-oxidized GO was mixed into conc. H_2SO_4, and then $KMnO_4$ (45 g) was slowly added during stirring and cooling in water-ice bath. The suspension was stirred at 40°C until it became brown, and then was diluted using de-ionized water. H_2O_2 30 wt.% (50 ml,) solution was slowly introduced. The yellow mixture was centrifuged, washed with a 1:10 HCl aqueous solution in order to remove residual metal ions. The obtained GO solution was dispersed by stirring using an IKA Ultraturrax T 25 (2 h), and ultrasonic bath (ELMA T 490DH model) at 110 W/40 kHz and 35°C (4 h). Graphene oxide (GrO) 4 g L^{-1} was obtained. Taking out a share-part of as-prepared GrO dispersion, the hydroiodic acid HI 55 wt.% (170 g) was added (in 4 h) at 80°C, as reduction agent and precursor iodine dopant. The obtained mixture was washed using de-ionized water for several times, dried to constant weight at 50°C (more than 8 h), and grated to powder. The final step was the elemental iodine removal by repeated extraction in acetone using a Soxhlet extractor.

2.3. Catalysts characterization

The microstructure and morphology of prepared samples were evaluated by using the following equipment: field emission scanning electron microscope (FESEM SU 5000 Hitachi) equipped with EDS-energy dispersive X-ray spectroscopy and WDS-wavelength dispersive; X-ray photoelectron spectroscope (XPS, Quantera SXM equipment), with a base pressure in the analysis chamber of 10^{-9} Torr and X-ray source Al K_α radiation (1486.6 eV, monochromatized) and the overall energy resolution estimated at 0.65 eV by the full width at half maximum (FWHM) of the $Au4f_{7/2}$ line; Fourier transform infrared (FTIR) spectrometer (Nicolet Impact 410, Thermo Fisher, USA); Autosorb IQ (Quantachrome, USA) with adsorption and desorption experiments performed at 77 K after initial pre-treatment of the samples by degassing at 115°C for 4 h; X-ray fluorescence spectrometer (XRF, Rigaku ZSX Primus II), equipped with an X-ray tube with Rh anode, 4.0 kW power, with front Be window of 30 μm thickness.

2.4. Electrode preparation and electrochemical measurements

2.4.1. Electrode preparation and MEA assembling

A detailed description of the electrodes and membrane electrode assembly fabrication procedure was reported in our previous studies. Summarizing, a catalyst ink was prepared by

http://dx.doi.org/10.5772/intechopen.76495

mixing water, 5 wt.% Nafion solution (DuPont), water and isopropyl alcohol (IPA) (Aldrich), ionomer/water/isopropyl alcohol = 6/14/80 (volume), with the Pt/C catalyst (Hispec 4000 Alfa Aesar). The prepared catalyst ink was mixed in an ultrasonic bath (30°C, 2 h) and sprayed using Sono-Tek ultrasonic coating equipment (Exacta Coat, Sono-Tek Corporation, USA), at a flow rate of 0.5 ml min^{-1}, onto the both side of pretreated Nafion 212 membrane in order to fabricate the catalyst coated membrane (CCM). The catalyst loadings were 0.2 mg cm^{-2} at the anode and cathode respectively. Two procedures of operation were used: (i) ultrasonic-spray procedure of catalytic ink containing Pt/C in order to obtain 0.2 mg cm^{-2} Pt at each side and (ii) I-doped graphene 0.2 mg cm^{-2} was integrated into cathode electrode by ultrasonic-spraying on gas diffusion layer GDL (carbon paper Toray TGP-H-120). Thus, the cathode catalyst layer was modified by taking into account the deposition of I-doped graphene supplementary sprayed on GDL (EC-TP1-090T, carbon cloth Toray, USA). The as prepared electrodes were hot-pressed on GDL on each side, for 2 min at 300 kgf and 120°C. Then, the obtained membrane electrode assembly (MEA), together with silicon type gaskets were introduced in a single PEM fuel cell system with an active area of 5 cm^2 (ElectroChem, USA).

2.4.2. Electrochemical measurements

The electrochemical evaluation was performed in a single fuel cell system PEMFC with an active area of 25 cm^2 (ElectroChem, USA). The *home-made* electrochemical test station includes a configured workstation (PARSTAT 2273), fuel cell (ElectroChem, USA), DS electronic load (AMETEK Sorensen SLH 60 V/120 A 600 W), bubble-type humidifier (ARBIN DPHS 10, USA). The PEMFC was operated at 0.3 V for 0.5 h and at 0.5 V for MEA conditioning, until the stable voltage was maintained uniformly. After steady state operating conditions were maintained, the fuel cell polarization plots and ORR performances were recorded. The flow rates of reactants (100 ml min^{-1} and 250 ml min^{-1}) gases (H_2 and air) were adjusted using flow controllers (Alicat Scientific, USA) calibrated before experiments. The cell temperature and pressure were set at 60–65°C and 1 bar pressure. The relative humidity for the anode and the cathode was set to 80 and 90%, respectively. The polarization curves were taken with a scan rate of 1 mV s^{-1}. Polarization curves were taken in a galvanostatic mode with a hold time of 5 min per point. The negative and the positive sweeps were performed and the average values were presented. Cyclic voltammetry measurements were performed in a H_2/N_2 mode cell, while the N2 flow was kept to almost zero, from 1.2 to 0.05 V at a scan rate of 0.05 V/s. The developed control system based on NI c-RIO hardware was used to control the PEMFC system. The electrochemically active Pt surface area (ECSA) was derived by the integration of the inferior hydrogen adsorption peaks. The software used to control and operate the test station with the acquiring of experimental data has been developed in LabVIEW® environment.

3. Results and discussions

3.1. Morphological and structural properties of I-doped graphene

The characterization of the prepared materials was firstly performed in order to validate the structural quality and to confirm the iodine presence.

The morphology and microstructure of as-prepared samples were observed using scanning electron microscopy (SEM). I-doped graphene materials have a typical wrinkled microstructure, fluffy and almost transparent, overlapping layers, forming a cluster composed of many tiny sheets with corrugation and scrolling, building a good porosity (**Figure 1**). These features are highly valuable for PEMFC electrode applications, providing a high surface area and ensuring efficient mass transport and good catalytic sites accessibility. The energy-dispersive X-ray spectroscopy (EDX) used in addition to SEM was used as microanalysis technique for a rough appraisal of chemical composition. The EDX spectrum revealed the microanalysis of doped graphene and confirmed the iodine presence. The spectrum is dominated by peak of C, but additional elements were identified (associated **Table 1**).

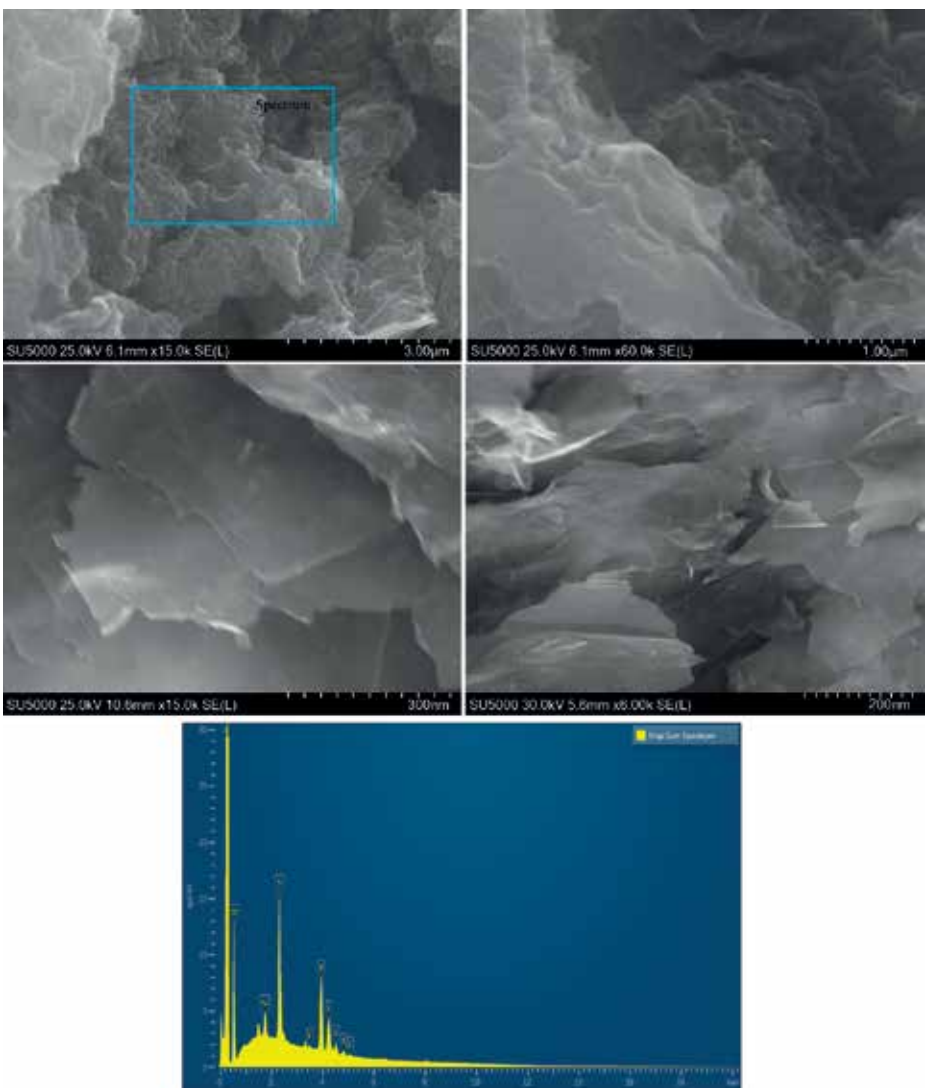

Figure 1. The SEM micrographs and EDX spectrum of prepared I-doped graphene.

http://dx.doi.org/10.5772/intechopen.76495

Element	Line type	Apparent concentration	k ratio	wt.%	wt.% sigma
C	K series	105.92	1.05920	84.39	0.15
O	K series	2.68	0.02346	13.48	0.15
Si	K series	0.30	0.00278	0.13	0.01
S	K series	2.00	0.02121	0.03	0.02
I	L series	4.06	0.05058	2.01	0.04
Total				100.00	

Table 1. Microanalysis of I-doped graphene.

The chemical composition of the I-doped graphene was investigated using X-ray photoelectron spectroscopy (XPS). Surface XPS analysis is an extremely sensitive technique (<10 nm) and was mainly focused on carbon chemistry as well as detection of iodine incorporated in the matrix at the sensitivity limit of the equipment XPS (~ 0.1% atoms). XPS spectra were collected using a monochromatic X-ray (AlK) radiation source (1486.6 eV) after the samples were placed in a 10 to 10 Torr vacuum chamber. Neutralization of the charge loading of the samples was done in dual mode using an electron gun and another argon ion. Thus, the energy calibration with the C1s line (284.8 eV) was made with great accuracy and allowed to be compared with the data from the established databases as well as from the literature [29, 30].

The introduction of chemical bonds was confirmed and high resolution spectra were collected for prominent transitions. The XPS spectra of the most prominent transitions of the chemical elements were obtained: C1s, O1s, I3d5/2, which indicated that iodine had been successfully binded on the surfaces of graphene. As anticipated, on the basis of the composition, in the survey spectra the sample show the predominant presence of carbon (1s, 284.5 eV) along with heteroatoms O (1s, 532 eV) and I (3d, 619.8 eV). High resolution C1s signals from XPS analysis are provided in **Figure 2**. High-resolution XPS spectra were further collected to quantify the doping amounts of the heteroatoms in the carbon framework. The detailed surface compositions of the prepared materials associated numerical values (chemical states rel. conc. wt.%) are systematized in **Table 2**. The C—C peak can be deconvoluted with 2

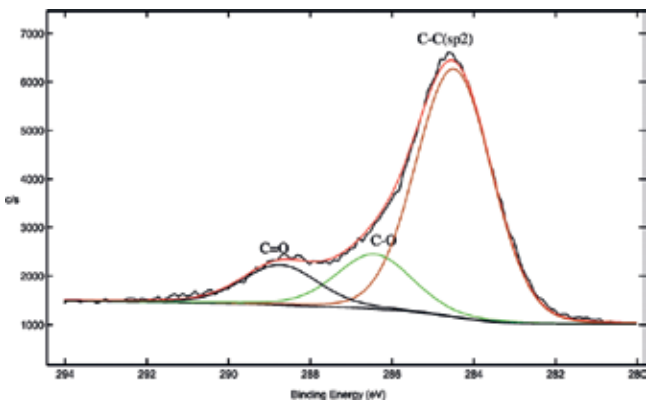

Figure 2. C1s deconvoluted spectra for C1s in I-doped graphene.

Sample	C	O	I	C—C (sp2)	C=C (sp3)	C—O	C=O	C—O=O	OH—C=O
I-doped graphene	86.1	12.4	1.5	71.0	—	16.1	—	12.9	—

Table 2. XPS data: quantification assessment, element relative concentrations (wt.%) and the chemical state relative concentrations (%).

(Gaussian-Lorentzian) curves at 284.5 eV (sp2) and 285.2 eV (sp3) binding energies (BEs). From analysis of the profile, a clear suppression of the C—O species peaks are observed, confirming the successful reduction of oxygen containing species during doping and reduction processes. Moreover, the sp^2 bonded carbon peak is sharp, suggesting an increase in the graphitic carbon configuration. I3d signal was detected as doublet 3d5/2, 3d3/2 with BEs at 619.8 eV and 624 eV.

After examination of **Table 3** it follows:

- Both the standard and ***all*** samples at studied temperatures (60 and 80°C) and different times (4, 8, 24, 28 and 48 h) show *iodine* in their matrix.
- The amount of iodine is at the XPS detection limit (~ 0.1 atom%, ~ 1 wt.%) but still can be detected and quantified
- The samples treated at temperature of 60°C show a higher iodine concentration (~ 0.15 atom%, ~ 1.5 wt.%) than those treated at 80°C (~ 0.11 atom%, ~ 1.15 wt.%).
- Both samples at 28 h (both 60 and 80°C) show a particularity: the 60°C sample shows a diffusion tendency of iodine from the surface in volume, while sample 80°C segregates iodine from the volume to the surface.
- Samples 48 h (both 60 and 80°C) show the highest relative oxygen concentration accompanied by the lowest C concentration. This phenomenon is due to oxygen segregation in volume at the surface of the samples.

The doping of iodine heteroatom into graphene is expected to produce some changes in surface area and pore size of prepared material. Due to the porous appearance of the materials confirmed by SEM analysis and of the need to obtain a high surface area for efficient ORR performance, we subsequently analyzed the surface area. In order to investigate the structure and to characterize the porosity of prepared iodine doped graphene, the nitrogen adsorption–desorption isotherms were studied using Brunauer-Emmett-Teller (BET) and are provided in **Figure 3**. The surface area was determined to be 480 $m^2\ g^{-1}$. The hysteresis study also revealed that hysteresis loops showed parallel adsorption and desorption branches. Such behavior was regarded as Type H1 among the IUPAC classification. This observation allows a better understanding of the porous features of the prepared samples, in the sense to be open at end, but unconnected to each other. As shown, the isotherm curves of adsorption/desorption performance of samples were compatible with isotherm Type IV, with an abrupt increase at high relative pressure, with respect to IUPAC classification. Based on the mentioned classification, a mainly mesoporous structure was estimated for the electrocatalyst samples.

Sample/treatment conditions	Chemical element		
	C1s	O1s	I3d5/2
I-doped graphene fresh material	90.04/86.02	9.81/12.48	0.15/1.50
I-doped grapheme/T = 60°C; t = 8 h	91.56/87.89	8.29/11.69	0.15/1.52
I-doped graphene/T = 60°C; t = 24 h	91.35/87.62	8.50/10.86	0.15/1.52
I-doped graphene/T = 60°C; t = 4 h	90.69/86.87	9.17/11.69	0.14/1.44
I-doped graphene/T = 60°C; t = 28 h	91.44/88.01	8.44/10.82	0.12/1.17
I-doped graphene/T = 60°C; t = 48 h	87.59/83.13	12.27/15.51	0.14/1.36
I-doped graphene/T = 80°C; t = 4 h	90.74/87.10	9.14/11.69	0.12/1.21
I-doped graphene/T = 80°C; t = 8 h	88.22/84.04	11.67/14.81	0.11/1.16
I-doped graphene/T = 80°C; t = 24 h	88.05/83.90	11.85/15.04	0.11/1.06
I-doped graphene/T = 80°C; t = 28 h	90.05/86.14	9.82/12.51	0.13/1.34
I-doped graphene/T = 80°C; t = 48 h	81.28/75.79	18.60/23.11	0.11/1.10

Table 3. XPS experimental data for chemical stability: the studied samples and the atomic concentrations (%) and mass (mass%) at all samples, all temperatures and time intervals.

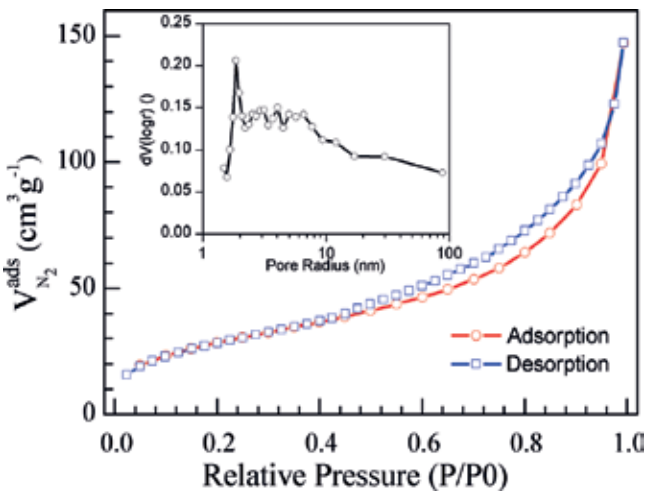

Figure 3. BET isotherm corresponding to I-doped graphene.

Barrett-Joyner-Halenda (BJH) method was utilized to measure the porous texture of prepared iodine doped graphene. A few ultramicropores in the doped graphene material are present, based on the fact that I-doped graphene possess a vertical uptake under $P/P_0 = 0.04$. A hysteresis loop type H1, from $P/P_0 = 0.4$ to $P/P_0 = 1.0$ due to the co-existence of both micropores, mesopores and some macroporous could be observed, the latter possessing a slit-like structure and most likely attributed to the pores between individual graphene sheets. This observation suggests there are good transport properties among the microspores, mesoporous and macroporous channels in I-doped graphene.

A briefly analysis on pore size distribution provided by the desorption branch using the BJH calculation approach was carried out. The pore size distribution curves presented in inserted plot, estimated according to BJH method, confirm that the greater part of the pores in the synthesized materials have size below 4.5 nm. The related curve of pore sizes highlighted a specific mesoporous structure, composed by primary and secondary pores. It is well known that the pores in an ORR catalyst layers must act two complementary roles, namely the primary pores, up to 0.04 μm, work as reaction volume, while secondary pores, from 0.04 to 0.1 μm, play the gas channel role in the porous structure [36]. As pore size distribution for I-doped graphene appears, although the samples possess limited primary structure, a structure of secondary pores is well confirmed, indicating that the transport properties in catalyst volume could be successfully obtained also after doping process.

3.2. Electrochemical characterization of I-doped graphene

Based on the structural information presented above, the prepared iodine doped graphene was evaluated as ORR cathode under practical FC operation conditions. It is easy to anticipate a better performance of cathode including the catalytic system Pt/C and I-doped graphene, mainly based on our recently results [34–36], in comparison to commercial Pt/C. This improvement in performance is likely due to higher electrical conductivity and the durability parameters, essential for the PEMFC commercialization. The fuel cell performance was characterized by measuring current-voltage polarization curves under various experimental conditions.

The testing cell is based on a 5 cm^2 single cell system using 0.2 mg Pt cm^{-2} loading as anode catalyst and the developed cathode (0.2 mg Pt cm^{-2} loading sprayed on the membrane and 0.2 mg I-doped graphene cm^{-2} loading sprayed on the GDL acting the MPL role).

The sensitivity of the fuel cell performance to the cathode side microstructure is analyzed by experimental investigations and numerical simulations, the results being reported in **Figure 4**.

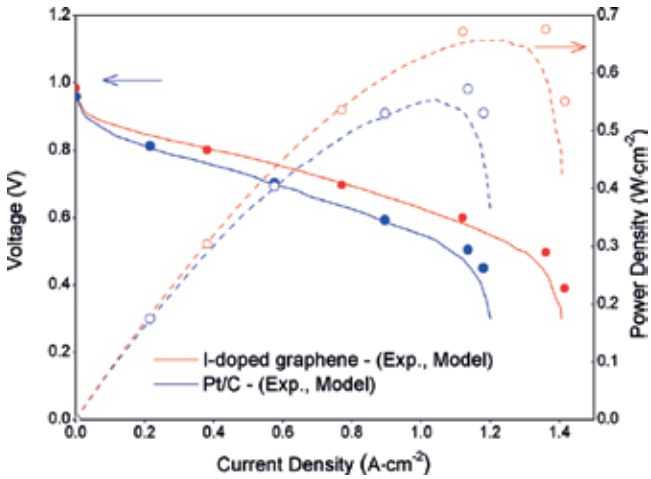

Figure 4. Polarization curves/power density plots (line) and model results (dots) for the PEMFC with cathode: commercial Pt/C (blue), and I-doped graphene (red). Cell runs with H_2/air, 1 bar anode and cathode back pressure; temperature 65C; flow rates H_2/air: 100 ml min^{-1}/250 ml min^{-1}.

One fuel cell with standard cathode configuration based on a commercial Pt catalyst and one fuel cell with an I-doped graphene layer placed between cathode GDL and CL have been considered.

The experimental data are represented as polarization and power density curves, while the numerical simulations are given as points on the curves. The numerical results for the cases investigated are in good agreement with experimental data, imparting the confidence that the computational fluid dynamics (CFD) models can be used as design tool for future improvements, and also to analyze how the fuel cell performs locally. Insightful information on the distribution and uniformity of phenomena that are taking place inside a fuel cell can be obtained by CFD modeling.

In general, the CFD simulation of FC is based on the following phases: development of the geometry; meshing the geometry (splitting into finite volumes) to obtain the computational grid; setting the mathematical model for domains and boundaries (domains for solid and gas-liquid phases, inlet and outlet gas supply system and gas channels, walls, layers combinations and electrode contacts); setting the boundary conditions; running the case for calculating parameters of interest; visualization of calculated results.

In order to compare the performances of the developed cathode versus commercial Pt catalyst with same loading, each FC performance reflected in its polarization curve was carried out. Analyzing the results, it can be seen that I-doped graphene coated GDL can lead to significant improvement in the performance of the fuel cell, up to an average of 20% in terms of both current and power density. The high electrical conductivity of the I-doped graphene layer enhanced the electrical contact between the GDL and CL, leading to an improved performance for all regions of the polarization curve. The microstructure optimization of this microporous layer based on I-doped graphene (high specific surface area, excellent mechanical properties, high thermal and electrical conductivity) promotes the rapid transport of electrons between active sites and the electrode and increases the electroactive catalyst surface, hence the increase of the performance.

3.3. CFD models developed to investigate the PEMFC performance

In addition to the global performance curves, it is important to analyze how the fuel cell performs locally. Namely, the profiles of the key variables within the components of the fuel cell could give information on the uniformity of distributions for these variables. Less uniform distribution of some key variables, e.g., the current density, can lead to the presence of some undesirable phenomena such as hotspots or flooding, thus negatively affecting the lifetime and durability of the fuel cell. In direct connection with the uniformity of key variables it is the microstructure of the fuel cell layers. This complex microstructure (gas pores, carbon particles, Pt catalyst particles, ionomer network) and the possible interactions between fluids (H_2, O_2 and all water phases) are taken into consideration in our study by CFD models developed to investigate the PEM fuel cells performance. The mass transport resistance due to the catalyst microstructure (resistance due to an ionomer film or due to a liquid water film surrounding particles), the liquid water transport through hydrophobic porous layers and the two-phase flow (liquid saturation) in the gas channels are taken into account in our model developed *based on ANSYS Multiphysics software and PEM fuel cell Module.*

Figure 5 shows the distribution of the current density for 0.5 V potential differences between anode and cathode external walls. The plane displayed is at the interface between the cathode catalyst layer and the MPL for both cases investigated. The cathode having I-doped graphene and Pt/C exhibited 85 m^2 Pt g^{-1}, which is about 2.5 times higher than that of commercial Pt/C electrode at the same Pt loading (38 m^2 Pt g^{-1}). These values were taken into consideration in the simulations and the results show clearly the increase of current density value for the FC with higher active area. An average current density of 1.135 A/cm^2 (**Figure 5** left) was obtained for the commercial Pt/C electrode, compared to 1.36 A/cm^2 for the I-doped graphene case (**Figure 5** right). The current density profile is directly linked to the distribution of the water mass fraction at the interface between the cathode catalyst layer and the adjacent MPL, as can be seen in **Figure 6**. A proper water management and a uniform distribution within the fuel cell assist in humidifying the membrane and increasing the performance. It can be concluded that the higher mesoporous and macro porous nanostructures of the I-doped graphene coated

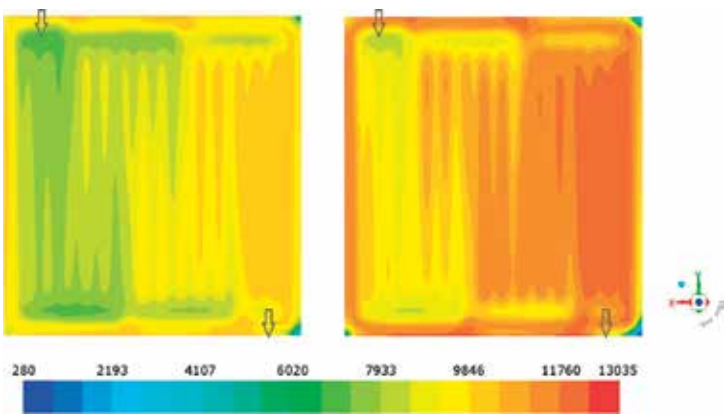

Figure 5. Current density profile for 0.5 V at the interface between the cathode catalyst layer and the MPL for the PEMFC with: commercial Pt/C (left), and I-doped graphene (right).

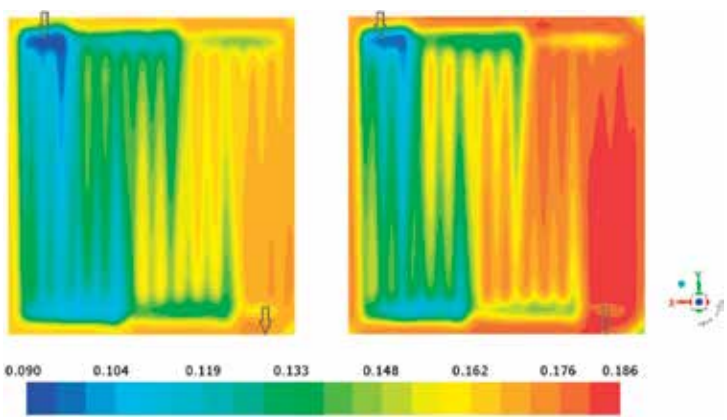

Figure 6. Water mass fraction profile for 0.5 V at the interface between the cathode catalyst layer and the MPL for the PEMFC with: commercial Pt/C (left), and I-doped graphene (right).

http://dx.doi.org/10.5772/intechopen.76495

GDL facilitate the mass transport of oxygen into the catalyst layer, the removal of water molecules from the electrolyte, ensure a conductive paths for the ions and electrons during the global transport process, resulting in a better performance in ohmic and mass transport regions of the polarization curves.

In order to examine the electrochemical stability of I-doped graphene cathode in comparison with Pt/C cathode, the electrodes were tested in the *in-situ* experiment by cyclic voltammetry (CV) measurements, elaborated in Experimental Section. The cyclic voltammetry results are presented in **Figure 7**. The CV curves show three characteristic potential regions: the hydrogen adsorption/desorption region (0.05–0.4 V), double layer plateau region and the formation and reduction of surface Pt oxide. All curves present a well-defined hydrogen adsorption/desorption region.

Operating conditions used are from experiments.

The electrochemical active area of the electrocatalysts were evaluated from the integrated area under the adsorption peaks from CV, representing the total charge associated with H^+ adsorption on metal. Thus, the cathode having Pt/C + I-doped graphene exhibited 85 m^2 Pt g^{-1}, which is about 2.5 times higher than that of commercial Pt/C electrode at the same Pt loading (38 m^2 Pt g^{-1}). This higher active area suggests more platinum sites available for the ORR which leads to the improved FC performances seen in the polarization curves. Generally, the utilization of Pt dispersed on the catalyst support is proportional to the surface area of Pt nanoparticles in contact with the electrolyte, so the ECSA results indicate that interface between catalyst and ionomer increases as effect of I-graphene added into the catalyst layer [29, 33].

Moreover, the open pores and vacancies could serve as active intercalation sites, contributing to the high charge transfer based on the conductive nanosheets with large surface area and a continuous electronic pathway, providing a high electrode-electrolyte contact interface. The mentioned synergistic effects could not only improve the ions and electrons transportation with nanometer-scale diffusion but also limits the ohmic resistance losses with big contribution to electrode stability in PEMFC device.

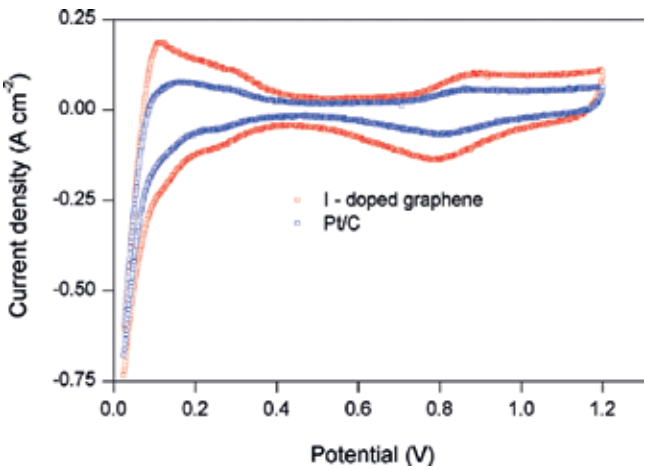

Figure 7. Cyclic voltammetry performed on *in situ* FC measurements in following operation conditions: temperature—60°C; the air in the original FC cathode was replaced with N_2; potential scan rate—50 mV/s.

4. Conclusions

In order to improve the activity and stability of PEMFC catalysts it is necessary to explore more stable catalyst for ORR. Iodine doped graphene was prepared and tested as ORR catalyst. The preparation is seen as overall process as facile, does not require complicated steps and is appropriate for scaling up. The surface compositions of I-doped graphene were analyzed by XPS. The XPS spectra of the most prominent transitions of the chemical elements were obtained: C1s, O1s, I3d 5/2, which indicated that iodine had been successfully binded on the surfaces of graphene. The chemical stability of I-doped graphene was tested in order to assess long-term performance. Insightful information on the distribution and uniformity of phenomena that are taking place inside a fuel cell are obtained from the CFD model used to analyze how this electrochemical device performs locally. The numerical results for two cases investigated (Pt/C with ECSA 35 m^2/g and I-doped graphene with ECSA 85 m^2/g) are validated by experimental data and a good agreement between modeling and experimental data were found. An overall 20% increase in current density was obtained while increasing the electrochemically active surface area (ECSA). The experimental results provide a simple route to synthesize I-doped graphene with potential application for advanced energy storage, as well as useful information to design new graphene base materials. In conclusion, we have designed a novel hybrid structure with enhanced electrochemical performances. The power output can be attributed to synergistic effects from graphene and iodine providing high utilization of Pt and better mass transport in the catalyst layer.

Acknowledgements

This work is supported by the Ministry of Research and Innovation from Romania by the National Plan of R & D, Project PN 18 12 01 02 and PN 18 12 01 04. The authors thank to Dr. Fiz. Catalin Ducu for SEM analysis and to Math. Catalin Capris for experimental study.

Conflict of interest

The authors declare that there is no conflict of interest.

Author details

Adriana Marinoiu[1]*, Elena Carcadea[1], Mircea Raceanu[1,2] and Mihai Varlam[1]

*Address all correspondence to: adriana.marinoiu@icsi.ro

1 RD Institute for Cryogenics and Isotopic Technologies—ICSI, Rm Valcea, Romania

2 University Politehnica of Bucharest, Bucharest, Romania

References

[1] Gasteiger HA, Marković NM. Just a dream—Or future reality? Science. 2009;**324**(5923): 48-49. DOI: 10.1126/science.1172083

[2] Sang MK, Chi-Yeong A, Yong-Hun C, Sungjun K, Wonchan H, Segeun J, Sungsoo S, Gunhee L, Yung-Eun S, Mansoo C. High-performance fuel cell with stretched catalyst-coated membrane: One-step formation of cracked electrode. Scientific Reports. 2016;**6**:26503. DOI: 10.1038/srep26503

[3] Barbir F. PEM Fuel Cells. In: Sammes N, editor. Fuel Cell Technology. Engineering Materials and Processes. London: Springer; DOI: 10.1007/1-84628-207-1_2

[4] Namgee J, Sang MK, Do HK, Dong YC, Yun SK, Young-Hoon C, Yong WC, Changhyun P, Kahp-Yang S, Yung-Eun S. High-performance hybrid catalyst with selectively functionalized carbon by temperature-directed switchable polymer. Chemistry of Materials. 2013;**25**(9):1526-1532. DOI: 10.1021/cm303691e

[5] Sinha PK, Mukherjee PP, Wang CY. Impact of GDL structure and wettability on water management in polymer electrolyte fuel cells. Journal of Materials Chemistry. 2007;**17**:3089-3103. DOI: 10.1039/B703485G

[6] Li H, Tang Y, Wang Z, Shi Z, Wu S, Song D, Zhang J, Fatih K, Zhang J, Wang J, Liu Z, Rami A, Mazza A. A review of water flooding issues in the proton exchange membrane fuel cell. Journal of Power Sources. 2008;**178**(1):103-117. DOI: 10.1016/j.jpowsour.2007.12.068

[7] Tanuma T. Ex situ characterization method for flooding in gas diffusion layers and membrane electrode assemblies with a hydrophilic gas diffusion layer. Journal of Fuel Cell Science and Technology. 2015;**12**(6):061002. DOI: 10.1115/1.4031917

[8] Slade S, Campbell S, Ralph T, Walsh F. Ionic conductivity of an extruded Nafion 1100 EW series of membranes. Journal of the Electrochemical Society. 2002;**149**(12):1556-1564. DOI: 10.1149/1.1517281

[9] Cho H, Kim SM, Kang YS, Kim J, Jang S, Kim M, Park H, Bang JW, Seo S, Suh KY, Sung YE, Choi M. Multiplex lithography for multilevel multiscale architectures and its application to polymer electrolyte membrane fuel cell. Nature Communications. 2015;**6**:8484. DOI: 10.1038/ncomms9484

[10] Kim OH, Cho YH, Kang SH, Park HY, Kim M, Lim JW, Chung DY, Jae Lee MJ, Choe H, Sung YS. Ordered macroporous platinum electrode and enhanced mass transfer in fuel cells using inverse opal structure. Nature Communications. 2013;**4**:2473. DOI: 10.1038/ncomms3473

[11] Hubert AG, Shyam SK, Bhaskar S, Frederick TW. Activity benchmarks and requirements for Pt, Pt-alloy, and non-Pt oxygen reduction catalysts for PEMFCs. Applied Catalysis B: Environmental. 2005;**56**(1-2):9-35. DOI: 10.1016/j.apcatb.2004.06.021

[12] Jiang L, Fan Z. Design of advanced porous graphene materials: From graphene nanomesh to 3D architectures. Nanoscale. 2014;**6**:1922-1945. DOI: 10.1039/C3NR04555B

[13] Liu J, Takeshi D, Sasaki K, Stephen M. Defective graphene foam: A platinum catalyst support for PEMFCs. Journal of the Electrochemical Society. 2014;**161**(9):838-844. DOI: 10.1149/2.0231409jes

[14] Zhu C, Dong S. Recent progress in graphene-based nanomaterials as advanced electrocatalysts towards oxygen reduction reaction. Nanoscale. 2013;**5**:1753-1767. DOI: 10.1039/C2NR33839D

[15] Shao Y, Zhang S, Wang C, Nie Z, Liu J, Wang Y, Lin Y. Highly durable graphene nanoplatelets supported Pt nanocatalysts for oxygen reduction. Journal of Power Sources. 2010;**195**(15):4600-4605. DOI: 10.1016/j.jpowsour.2010.02.044

[16] Reshetenko TV, Kim HT, Kweon HJ. Cathode structure optimization for air-breathing by application of pore-forming agents. Journal of Power Sources. 2007;**171**(2):433-440. DOI: 10.1016/j.jpowsour.2007.05.105

[17] Wang DW, Su D. Heterogeneous nanocarbon materials for oxygen reduction reaction. Energy & Environmental Science. 2014;**7**:576-591. DOI: 10.1039/C3EE43463J

[18] Bing Y, Liu H, Zhang L, Ghosh D, Zhang J. Nanostructured Pt-alloy electrocatalysts for PEM fuel cell oxygen reduction reaction. Chemical Society Reviews. 2010;**39**:2184-2202. DOI: 10.1039/B912552C

[19] Cho YH, Jung N, Kang YS, Chung DY, Lim JW, Choe H, Cho YH, Sung YE. Improved mass transfer using a pore former in cathode catalyst layer in the direct methanol fuel cell. International Journal of Hydrogen Energy. 2012;**37**(16):11969-11974. DOI: 10.1016/j.ijhydene.2012.05.031

[20] Zhao J, He X, Wang L, Tian J, Wan C, Jiang C. Addition of NH_4HCO_3 as pore-former in membrane electrode assembly for PEMFC. International Journal of Hydrogen Energy. 2007;**32**(3):380-384. DOI: 10.1016/j.ijhydene.2006.06.057

[21] Liang J, Du X, Gibson C, Qiao W. N-doped graphene natively grown on hierarchical ordered porous carbon for enhanced oxygen reduction. Advanced Materials. 2013;**25**(43):6226-6231. DOI: 10.1002/adma.201302569

[22] Minmin L, Ruizhong Z, Wei C. Graphene-supported nanoelectrocatalysts for fuel cells: Synthesis, properties, and applications. Chemical Reviews. 2014;**114**(10):5117-5160. DOI: 10.1021/cr400523y

[23] Huimin W, David W, Huakun L. Durability investigation of graphene-supported Pt nanocatalysts for PEM fuel cells. Journal of Solid State Electrochemistry. 2011;**15**(5):1057-1062. DOI: 10.1007/s10008-011-1317-8

[24] Krishna R et al. Facile synthesis of hydrogenated reduced graphene oxide via hydrogen spillover mechanism. Journal of Materials Chemistry. 2012;**22**:10457-10459. DOI: 10.1039/C2JM30945A

[25] Li M, Zhang L, Xu Q, Niu J, Xia Z. N-doped graphene as catalysts for oxygen reduction and oxygen evolution reactions: Theoretical considerations. Journal of Catalysis. 2014;**314**:66-72. DOI: 10.1016/j.jcat.2014.03.011

[26] Shuo D. Molecular doping of graphene as metal-free electrocatalyst for oxygen reduction reaction. Chemical Communications. 2014;**50**:10672-10675

[27] Stefano A, Marco F. Doping graphene with boron: A review of synthesis methods, physicochemical characterization, and emerging applications. Journal of Materials Chemistry A. 2016;**4**:5002-5025. DOI: 10.1039/C5TA10599D

[28] Marinoiu A, Teodorescu C, Carcadea E, Raceanu M, Varlam M, Cobzaru C, Stefanescu I. Graphene-based materials used as the catalyst support for PEMFC applications. Materials Today: Proceedings. 2015;**2**(6):3797-3805. DOI: 10.1016/j.matpr.2015.08.013

[29] Marinoiu A, Raceanu M, Carcadea E, Varlam M, Stefanescu I. Iodinated carbon materials for oxygen reduction reaction in proton exchange membrane fuel cell. Scalable synthesis and electrochemical performances. Arabian Journal of Chemistry. DOI: 10.1016/j.arabjc.2016.12.002 (in press)

[30] Marinoiu A, Raceanu M, Carcadea E, Varlam M, Stefanescu I. Low cost iodine intercalated graphene for fuel cells electrodes. Applied Surface Science. 2017;**424**:93-100. DOI: 10.1016/j.apsusc.2017.01.295

[31] Marinoiu A, Raceanu M, Carcadea E, Varlam M, Stefanescu I. Doped graphene as nonmetallic catalyst for fuel cells. Materials Science. 2017;**23**:108-113. DOI: 10.5755/j01.ms.23.2.16216

[32] Damien T, Pascal P, Iann CG. Theoretical study of graphene doping mechanism by iodine molecules. Journal of Physical Chemistry C. 2015;**119**(21):12071-12078. DOI: 10.1021/acs.jpcc.5b03246

[33] Marinoiu A, Raceanu M, Carcadea E, Varlam M, Stefanescu I, Enachescu M. Iodine-doped graphene for enhanced electrocatalytic oxygen reduction reaction in proton exchange membrane fuel cell applications. Journal of Electrochemical Energy Conversion and Storage. 2017;**14**:31001. DOI: 10.1115/1.4036684

[34] Marinoiu A, Teodorescu C, Carcadea E, Raceanu M, Varlam M, Cobzaru C, Stefanescu I. Convenient graphene based materials as potential candidates for low cost fuel cell catalysts. Reaction Kinetics, Mechanisms and Catalysis. 2016;**118**:281-296. DOI: 10.1007/s11144-016-1016-7

[35] Marinoiu A, Teodorescu C, Carcadea E, Raceanu M, Varlam M, Cobzaru C, Stefanescu I. An experimental approach for finding low cost alternative support material in PEM fuel cells. Revue Roumaine de Chimie. 2016;**61**(4-5):433-440

[36] Lale IS, Vildan B, Ghobad S. Engineered catalyst layer design with graphene-carbon black hybrid supports for enhanced platinum utilization in PEM fuel cell. International Journal of Hydrogen Energy. 2017;**42**(2):1085-1092. DOI: 10.1016/j.ijhydene.2016.08.210

Chapter 6

Concentrated Photovoltaic (CPV): Hydrogen Design Methodology and Optimization

Muhammad Burhan,
Muhammad Wakil Shahzad and Kim Choon Ng

Additional information is available at the end of the chapter

http://dx.doi.org/10.5772/intechopen.78055

Abstract

To compete with the fossil fuel, there is a need for steady power supply from renewable energy systems. Solar energy, being highest potential energy source, is only available during diurnal period. Therefore, for steady power supply, an energy storage system is needed to be coupled with the primary solar energy system. For such application, hydrogen production is proved to provide long term and sustainable energy storage. However, firstly, there is a need to capture solar energy with higher efficiency for minimum energy storage and reduced system size. Concentrated photovoltaic (CPV) system, utilizing multi-junction solar cell (MJC), provides highest energy conversion efficiency among all photovoltaic systems. Despite, there is no model reported in the literature regarding its performance simulation and stand-alone operation optimization. None of the commercial software is capable of handling CPV performance simulation. In this chapter, a detailed performance model and an optimization strategy are proposed for stand-alone operation of CPV with hydrogen production as energy storage. A multi-objective optimization technique is developed using micro-GA for its techno-economic analysis. The performance model of MJC is developed based upon the cell characteristics of InGaP/InGaAs/Ge triple-junction solar cell. The system design is presented for uninterrupted power supply with minimum system cost.

Keywords: optimization, concentrated photovoltaic, genetic algorithm, hydrogen

1. Background

The global warming situations of 1.5°C rise in the average ambient temperature [1] are deemed inevitable due to the excessive emission of greenhouse gases such as carbon dioxide [2]. Today,

renewable energy contributes only about 6.7% of the global energy demand [3]. The reason for the sluggish implementation of renewable energy sources can be attributed to their susceptibility to intermittency, low energy density and localized availability that make these energy sources mediocre as compared to the conventional fossil fuel-based sources. Among all renewable sources, solar energy has the highest potential [4] in meeting a significant portion of the total energy demand of future and for such an energy source to achieve sustainability, its energy quality and supply continuity are to be improved [5].

Current photovoltaic (PV) systems for electricity generation, available hitherto, comprises the stationary single junction silicon-junction-based solar cells such as mono-crystalline, poly-crystalline and thin films [6] with more than 98% share of photovoltaic market. Although such cells have a theoretical limit of 31% efficiency, the actual long-term electricity rating is merely less than 8% [7]. The advent of the third generation multijunction solar cells (MJCs), with the instantaneous cell-efficiency exceeding 46% [8] (but the quantum limit is 86%), has yet to receive widespread acceptance in form of concentrated photovoltaic (CPV) system in the current photovoltaic market. On the other hand, despite high-grade energy production as electricity, it is still intermittent and requires energy storage for steady power supply. Electrochemical storage in the form of battery does not make solar energy as a viable option to replace fossil fuels [9]. Electrolytic production of hydrogen by splitting water using solar electricity not only provides a portable green energy but also acts as high-density energy source, more than just energy storage [10]. The byproduct oxygen has many useful applications ranging from green disinfectant ozone to direct consumption in oxygen-based processes.

So far, in literature, all of the performance simulation models related to solar cells are based upon the single junction-based conventional flat plate PV systems. However, despite having the highest efficiency among all of the solar cells available hitherto [11], there is no performance models available in the literature that can simulate and predict the performance of multijunction solar cells in form of concentrated photovoltaic (CPV) systems. Therefore, as a sustainable energy source with highest solar electricity production efficiency, there is a need to develop a detailed performance optimization and simulation model for the standalone operation of CPV system, utilizing hydrogen as energy storage media. This chapter discusses the comprehensive model and optimization methodology for standalone and long-term operation of concentrated photovoltaic (CPV) with hydrogen production as energy storage and minimum cost. First, a detailed literature review of methodologies and commercial tools is presented. Second, an overall system model is presented, along with the system energy management and optimization methodology. Lastly, the optimized system design and corresponding performance parameters are presented and discussed.

2. Literature review

In order to compete with the conventional fossil fuels, the renewable energy resources must be able to provide uninterrupted power supply for any load demand, during whole day operation.

Such a requirement demands to operate them in standalone mode, without any external input. Therefore, such standalone operation requires the optimized size of each of the system component for uninterrupted power supply and for any load of the system, all the time with lowest overall system cost. Such standalone system design requires extensive system modeling with operational/optimization strategy/algorithm and economical information. In the design of any standalone system, there are three phases which have to be considered. In the first and most important phase, the main requirement is the selection of primary energy conversion system, which can have high efficiency and best performance with high power density. It also requires a detailed system modeling and control strategy of the system to be available to analyze the system performance under different conditions, for optimum design. If the main primary energy source is intermittent in nature, that is, renewable energy sources, the second phase is related to the selection of reliable, long-term and efficient energy storage system. The third and final step deals with the selection of the optimization algorithm which can handle multiple objective functions with less computational power and time to utilize the information received from the first two phases for the sizing of each component of the system.

Regarding the primary energy conversion system, as discussed earlier, concentrated photovoltaic system provides highly efficient solar energy conversion system among all of the photovoltaic units available hitherto. However, due to its intermittent nature and availability during diurnal period, an energy storage system is needed to be coupled for standalone operation and uninterrupted power supply by the system. As compared to the conventional electrochemical energy storage, that is, battery which is only suitable and economical for small-capacity system and short-term storage [12], electrolytic production of hydrogen provides a sustainable and long-term energy storage option, which can be easily converted into electricity when needed. It can also be transported from one place to another like conventional fuels. It can provide the most suitable long-term energy storage option for solar energy systems which a have life span of 20–25 years. Other energy storage methods like compressed air, pumped hydro, thermal storage and super capacitors do not provide either economical or long-term feasible options for such photovoltaic systems [13].

Regarding the third phase, related to optimization strategy and algorithm, there are many techniques available in the literature to do the job. However, the main requirement is to have an efficient and multiobjective solution in less possible time and computational power. The most common algorithm available in the literature is genetic algorithm (GA) which is based upon the concept of nature evolution [14] to optimize a set of design parameters for complex engineering systems. However, there are many new algorithms which have been claimed to be much more efficient than the conventional GA like particle swarm optimization (PSO). As both algorithms have different optimization and searching strategy [15], therefore, there is no benchmark where their performance can be compared. Overall, the PSO is claimed to be efficient as it takes less computational time [16]. Such a lack of performance is due to the large population size requirement of conventional GA. There are some variants of GA discussed in the literature, that is, NSGA-II and micro-genetic-algorithm (micro-GA) which are modified forms of conventional GA but eliminating its limitations for better performance [17]. Among all of the discussed optimization algorithms, micro-GA has been reported to have the best performance due to its small population size, as compared to NSGA-II and PSO [18]. It has

shown better computational power with 8–12 times faster response and better Pareto front than NSGA-II [19]. Therefore, in this study, micro-GA is used as the optimization algorithm to optimize the overall size of standalone CPV-Hydrogen system.

Regarding system models and optimizations strategy, there are many studies in the literature which are related to standalone system size optimization and techno-economic evaluation. However, all of the studies related to photovoltaic system consider conventional flat plate single junction photovoltaic (PV) panels [20]. Even in hybrid renewable energy systems, utilizing wind turbine, battery, hydrogen, and so on, the main solar photovoltaic energy system is conventional PV [21]. All of the studies aim to increase the overall conversion efficiency of the primary energy system by utilizing its full potential, so that the overall size of the system can be reduced. On the other hand, due to many systems involved in hybridization, a complex control and energy management strategy is needed to operate the system. The concentrated photovoltaic (CPV) system provides the most efficient and simple photovoltaic technology for solar energy conversion, without any hybridization. However, there is no study in the literature that discusses the performance model and control strategy related to standalone operation of CPV. In addition, there are many commercial software related to simulation and optimization of renewable energy systems and their hybrids, for example, iHOGA, HYBRIDS2, INSEL, HOMER, TRNSYS + HYDROGEMS, SOMES, ARES, RAPSIM and SOLSIM [22]. But none of the software available hitherto has the capability to simulate and optimize the performance of concentrated photovoltaic (CPV) system. Therefore, the main objective of this chapter is to introduce and discusses the comprehensive model and optimization methodology for standalone and long-term operation of concentrated photovoltaic (CPV) with hydrogen production as energy storage.

3. Introduction to standalone CPV-hydrogen system

The simple schematic of concentrated photovoltaic (CPV) system with hydrogen as energy storage is shown in **Figure 1** for steady power supply and standalone operation. The concentrated photovoltaic (CPV) system, acting as primary energy supply unit, consists of multijunction solar cells (MJC)-based CPV modules, mounted onto two-axis solar trackers. As the solar concentrators require beam radiation for their operation, therefore, accurate two axis solar tracking is of prime importance for CPV operation. The arrangement of concentrating assembly of CPV system can be either a reflective type, that is, Cassegrain arrangement of reflectors or refractive type, that is, Fresnel lens. The developed performance model will be able to handle any type of concentrating assembly as it is based upon the final concentration ratio required by the MJC. For efficient CPV performance, maximum power point tracking (MPPT) device is attached to its output. The produced electricity after passing through MPPT device and DC/DC converter is supplied to the main DC line. The power consuming devices, such as solar trackers, take the power from main DC line for their operation.

The objective of targeted standalone CPV-hydrogen system is to provide an uninterrupted power supply to external consumer load, at any time and at level load level, by taking into account its own operational energy requirements. The consumer load is connected to the main

http://dx.doi.org/10.5772/intechopen.78055

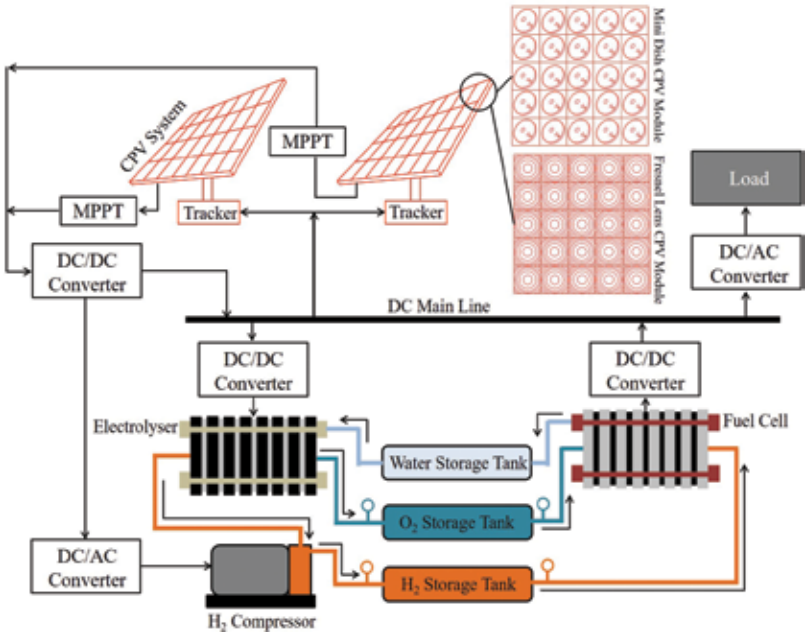

Figure 1. CPV-hydrogen system schematic for steady power supply and standalone operation [17].

DC line through DC/AC converter. The power supply to the consumer load is the first priority of the system, followed by the system operational needs. However, any excess power available is then supplied to the electrolyzer to produce hydrogen and oxygen by electrolytic splitting of water. The produced hydrogen is compressed and sent to tanks for storage and future use. However, the oxygen is stored at produced pressure as it can also be taken from environment in case of shortage. The power requirement of hydrogen compressor also comes from main DC line through DC/AC converter. In case of power deficit by the CPV system, the stored hydrogen is supplied to the fuel cell, with oxygen, to produce electricity and water. The produced electricity is then supplied to the main DC line through DC/DC converter. However, the produced water goes to storage tank, to be used as a loop in electrolyzer.

4. Performance model development for CPV-hydrogen system

In this section, detailed performance model of CPV-hydrogen system is discussed which is based upon the performance model of individual components which are linked together as a complete system through energy management strategy as shown in **Figure 2**. The main power input of the system is the solar energy in form of beam radiations or direct normal irradiance (DNI) as CPV cannot accept diffuse radiations. The weather data in the form of direct normal irradiance (DNI) are provided to the CPV performance model as input solar energy. The received solar energy is then used to calculate the concentration at the MJC area, according to the optical efficiency of the solar concentrators. By knowing the temperature characteristics of

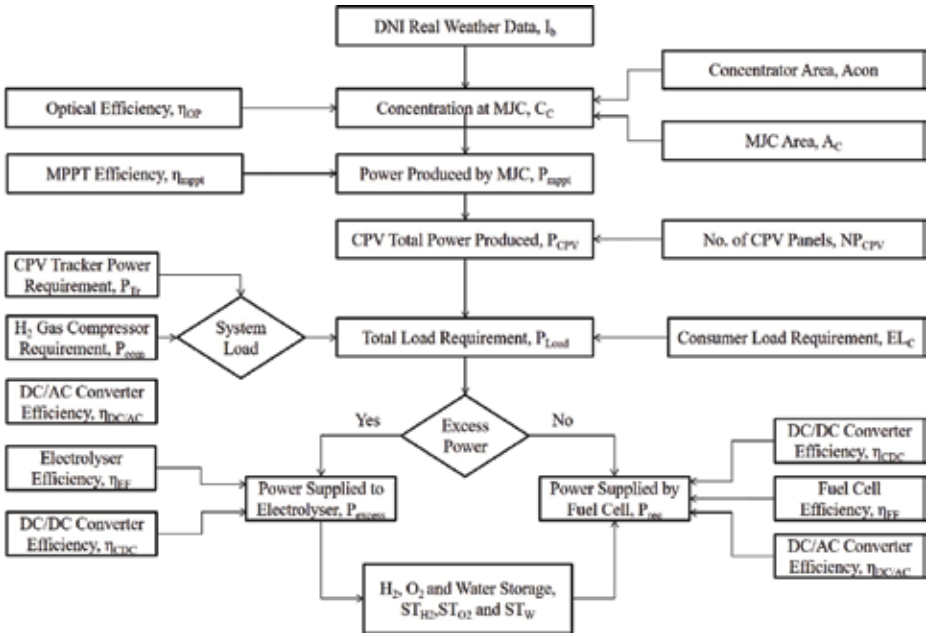

Figure 2. Energy management strategy for performance model of CPV-hydrogen system [17].

MJC and the total number of MJC units, the total power output from CPV can be calculated. Another input to the system performance model is the consumer electrical load requirements which is then combined with the system operational power requirements to calculated overall load of the system needed to be powered. The performance models for each individual components of the system are discussed later.

4.1. Concentrated photovoltaic system

The performance model of concentrated photovoltaic (CPV) system is based upon the single diode model, representing solar cell characteristic curves but considering concentration factor, is given by Eq. (1) [23].

$$P_C = I_C V_C = V_C \left[I_o \left\{ \exp\left(\frac{qV_C}{nkT_C}\right) - 1 \right\} - I_{SC} \right] \tag{1}$$

It must be noted that the values of all of the parameters appearing in the model of any component of the system are given in **Table 1**. For open circuit voltage, the diode saturation current factor "I_o" can be found by using $V = V_{OC}$ and $I = 0$ in Eq. (1).

$$I_o = \frac{I_{SC}}{\left[\exp\left(\frac{qV_{OC}}{nkT_C}\right) - 1 \right]} \tag{2}$$

As the multijunction solar cells (MJC) can operate at higher concentrations, therefore, their performance characteristics are depending upon both temperature and concentration at cell area.

Parameter	Value	Parameter	Value
q (Coulomb) [24]	$1.6021765 \times 10^{-19}$	a1 [25]	0.995
k ($m^2kgs^{-2}\,K^{-1}$) [24]	$1.3806488 \times 10^{-23}$	a2 ($m^2\,A^{-1}$) [25]	−9.5788
n_C [24]	2	a3 ($m^2\,A^{-1}\,°C^{-1}$) [25]	−0.0555
η_{mppt} [26]	85%	a4 [25]	0
$\eta_{DC/AC}$ [27, 28]	90%	F ($As\,mol^{-1}$) [25]	96,485
η_{CDC} [29, 30]	95%	a5 ($m^4\,A^{-1}$) [25]	1502.7083
U_{rev} (V) [25]	1.229	a6 ($m^4\,A^{-1}\,°C^{-1}$) [25]	−70.8005
r_1 (Ωm^2) [25]	7.331×10^{-5}	a7 [25]	0
r_2 ($\Omega m^2\,°C^{-1}$) [25]	-1.107×10^{-7}	n [25]	2
S_1 (V) [25]	1.586×10^{-1}	U_o (mV) [25]	1065
S_2 ($V\,°C^{-1}$) [25]	1.378×10^{-3}	b ($mV\,dec^{-1}$) [25]	80
A_E (m^2) [25]	0.25	R (Ωcm^{-2}) [25]	0.438
S_3 ($V\,°C^{-2}$) [25]	-1.606×10^{-5}	M_{H2} (g/mol)	2.0159
t_1 ($m^2\,A^{-1}$) [25]	1.599×10^{-2}	CP_H (J/kg K)	14,304
t_2 ($m^2\,A^{-1}\,°C^{-1}$) [25]	−1.302	T_{com} (K)	306
t_3 ($m^2\,A^{-1}\,°C^{-2}$) [25]	4.213×10^2	$\eta_{DC/AC}$ (%)	90
r	1.4	η_{com} (%) [31]	70

Table 1. Information regarding constant factors appearing in CPV-hydrogen performance model.

The cell under consideration is a triple junction InGaP/InGaAs/Ge cell, for which the characteristics curves are shown in **Figure 3**. The short circuit current is proportional to the concentration ratio. However, open circuit voltage is following logarithmic variation against concentration ratio. In order to find out cell voltage and current, there is a need for "V_{OC}" and "I_{SC}" of cell to be known at that operating condition. If the trends of "V_{OC}" and "I_{SC}" are known at 25°C, then

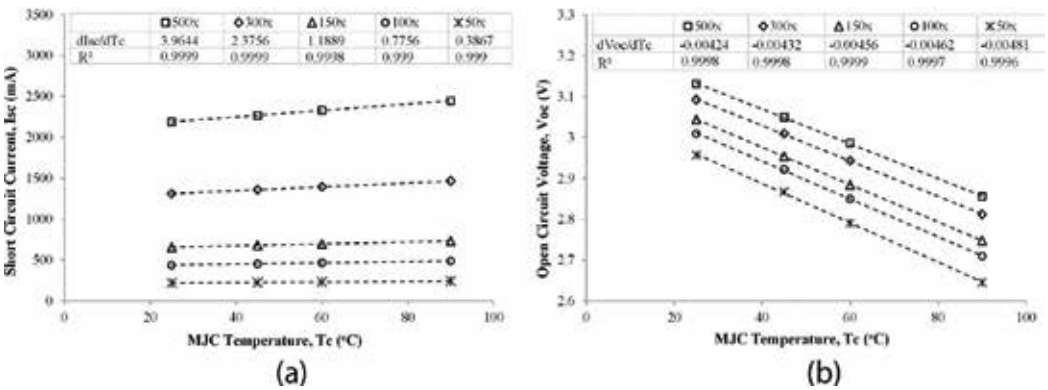

Figure 3. Variation in (a) short circuit current and (b) open circuit voltage of InGaP/InGaAs/Ge triple-junction solar cell with temperature and concentration [17].

their corresponding values at different temperature and concentration can be found using Eqs. (3) and (4).

$$V_{OC}(T_C, C_C) = [V_{OC}(at\ \ 25^oC)]_C + (T_C - 25)\left[\frac{dV_{OC}}{dT_C}\right]_C \tag{3}$$

$$I_{SC}(T_C, C_C) = [I_{SC}(at\ \ 25^oC)]_C + (T_C - 25)\left[\frac{dI_{SC}}{dT_C}\right]_C \tag{4}$$

Another required parameter is the cell temperature, which is assumed to be 40°C higher than the then ambient temperature, with 10°C temperature difference between cell surface and back plate temperature [32]. However, remaining temperature drop is between ambient and the heat sink/back plate. The concentration at cell area is given by Eq. (5).

$$C_C = I_b \times \frac{A_{con}}{A_C} \times \eta_{OP} \tag{5}$$

In order to model maximum power point tracking (MPPT) device, the derivative of cell power output equation can be equated to zero, as:

$$\frac{dP_C}{dV_C} = 0 \tag{6}$$

$$\frac{d}{dV_C}\left[V_C I_o\left\{\exp\left(\frac{qV_C}{nkT_C}\right) - 1\right\} - V_C I_{SC}\right] = 0 \tag{7}$$

After simplification, we can have the expression for power output of MJC as:

$$V_{mppt} = V_{OC} - \frac{nkT_C}{q}\ln\left[1 + \frac{qV_{mppt}}{nkT_C}\right] \tag{8}$$

$$\mathrm{I_{mppt}} = \mathrm{I_o}\left\{\exp\left(\frac{qV_{mppt}}{nkT_C}\right) - 1\right\} - I_{SC} \tag{9}$$

$$P_{mppt} = \eta_{mppt} \times I_{mppt} \times V_{mppt} \tag{10}$$

The simulated and experimental efficiencies of MJC are shown in **Figure 4**. By incorporating the efficiencies of voltage converters and the tracker power requirement, the net power output of CPV units is given by Eq. (11).

$$P_{CPV} = \eta_{DC/AC} \times \eta_{CDC} \times \eta_{Tr} \times P_{mppt} \times N_{CM} \times NP_{CPV} \tag{11}$$

For the current study, a CPV panel is assumed to be made of 25 MJCs, arranged into a 5 × 5 array. In addition, the power consumption of solar tracker is considered only during diurnal period, that is, from sunrise to sunset as calculated from solar geometry model [33].

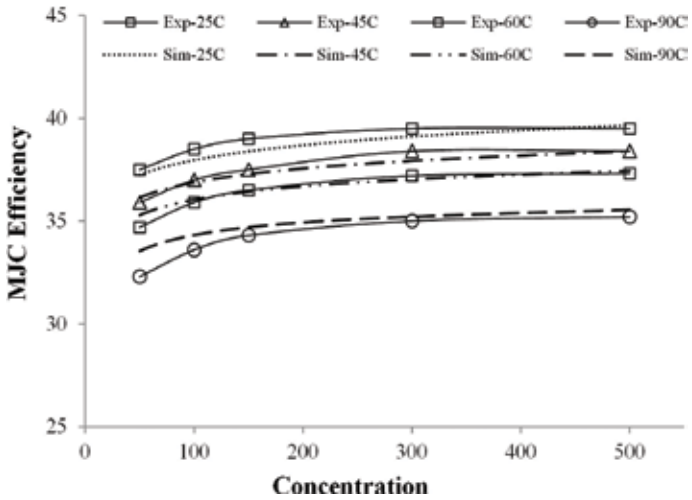

Figure 4. Comparison of experimentally measured and simulated efficiency of MJC at different concentrations and temperatures [19].

4.2. Electrolyzer

For the electrolyzer unit, the considered theoretical model is based upon the characteristics of an alkaline electrolyzer available in the literature [25]. The operating temperature of unit is assumed to be fixed at 80°C. The performance model for the operating voltage of single electrolyzer cell, under consideration, is given by Eq. (12).

$$U_E = U_{rev} + \frac{r_1 + r_2 T_E}{A_E} I_E + \left(S_1 + S_2 T_E + S_3 {T_E}^2\right).\log\left(\frac{t_1 + \frac{t_2}{T_E} + \frac{t_3}{{T_E}^2}}{A_E} I_E + 1\right) \tag{12}$$

It must be noted that the values of all required constant parameters are given in **Table 1**. The amount of hydrogen and oxygen production is based upon the amount of current passing through the electrolyzer and the Faraday efficiency, as given by Eqs. (13) and (14).

$$\dot{n}_{E,H2} = \eta_{EF} \frac{N_{EC} I_E}{nF} = 2\dot{n}_{E,O2} \tag{13}$$

$$\eta_{EF} = a_1.\exp\left(\frac{a_2 + a_3 T_E + a_4 {T_E}^2}{\frac{I_E}{A_E}} + \frac{a_5 + a_6 T_E + a_7 {T_E}^2}{\left(\frac{I_E}{A_E}\right)^2}\right) \tag{14}$$

In the design of the electrolyzer, the important parameter is the total number of cells needed. The number of electrolyzer cells depend upon the maximum amount of excess power that can be expected throughout the operational cycle of the system. By assuming the maximum rated current of 750 A and single cell voltage of 1.8 V [25], and the maximum MJC power output of 5 W, the required number of electrolyzer cells can be calculated as:

$$N_{EC} = \frac{\left(P_{MJC,\max} \times N_{CM} \times NP_{CPV}\right) - L_{\min}}{V_{EC,\max} \times I_{EC,\max}} \tag{15}$$

If the electrolyzer cells are assumed to be connected in series, then the current flow through the electrolyzer is given by Eq. (16). It must be noted that the excess power available must be calculated after fulfilling the total load requirements, that is, consumer load plus the system operational power requirement.

$$I_E = \frac{\eta_{CDC} \times P_{excess}}{N_{EC} \times U_E} \tag{16}$$

4.3. Fuel cell

For the current study, the proton exchange membrane (PEM) type of fuel cell is considered for which the performance characteristics are given in literature [25] and the performance model is given by Eq. (17).

$$U_F = U_o - b.\log\left(\frac{I_F}{A_F}\right) - R\left(\frac{I_F}{A_F}\right) \tag{17}$$

Like the electrolyzer, the gas consumption by fuel cell depends upon its total current flow, as per required power, which is given by Eq. (18). The amount of current flow through the fuel cell is given by Eq. (19), which is the same for each cell as they are connected in series. It must be noted that the fuel cell is assumed to be operated with a Faraday efficiency of 70% and the surface area for a single cell is taken as 300 cm^2.

$$\dot{n}_{F,H2} = \eta_{FF}\frac{N_{FC}I_F}{nF} = 2\dot{n}_{F,O2} \tag{18}$$

$$I_F = \frac{P_{req}}{\eta_{CDC} \times \eta_{DC/AC} \times N_{FC} \times U_F} \tag{19}$$

Like CPV and electrolyzer design, the fuel cell design is also based upon the maximum possible number of cells needed to meet the total load demand. As per the considered fuel cell characteristics [25], the maximum power per cell is 114.6 W. Therefore, for maximum load requirement of the customer, the total number of cells required in the design of a fuel cell is given by Eq. (19).

$$N_{FC} = \frac{L_{\max}}{\eta_{CDC} \times \eta_{DC/AC} \times P_{FC,\max}} \tag{20}$$

4.4. Hydrogen compressor

As mentioned earlier, the produced hydrogen is compressor by a mechanical compressor to be stored in the storage tank as the mechanical compression system provides a most compact and reliable storage solution. The performance model for mechanical compressor, for its power

requirements, is based upon the thermodynamic equation depending upon the pressure ratio, that is, pressure at inlet and outlet of compressor, which is given by Eq. (21) [31].

$$P_{com} = \left(\dot{n}_{E,H2} \times \frac{M_{H2}}{1000}\right) \times CP_H \times \frac{T_{com}}{\eta_{DC/AC} \times \eta_{com}} \left\{ \left(\frac{P_{ta}}{P_E}\right)^{\left(\frac{r-1}{r}\right)} - 1 \right\} \tag{21}$$

It must be noted that the hydrogen produced by the electrolyzer goes to the compressor as they are connected in series. Therefore, the flow of hydrogen through compressor is the same as the rate of hydrogen production in electrolyzer. In addition, the compressor operating pressure is also assumed to be the same as the electrolyzer operating pressure as hydrogen directly goes to the compressor after production. The pressure at inlet of compressor is the same as the operating pressure of electrolyzer "P_E" and the pressure at the outlet of compressor is the same as the pressure inside storage tank "P_{ta}."

4.5. Hydrogen storage tank

In order to model the hydrogen storage tank, ideal gas equation is considered with compressibility factor "Z," as given by Eq. (22), to find out the tank pressure according to the stored amount of hydrogen.

$$P_{ta} = \frac{n_{ta} R T_{ta}}{V_{ta}} \times Z_H \tag{22}$$

$$Z_H = 3.5 \times 10^{-11} {n_H}^2 + 4.3 \times 10^{-5} n_H + 1 \tag{23}$$

A cylindrical tank of 3.34 m^3 capacity is considered and the Eq. (23) for compressibility factor for hydrogen storage tank is obtained from the actual gas pressure data obtained at 33°C from REFPROP (Reference Fluid Thermodynamic and Transport Properties), provided by NIST (National Institute of Standards and Technology) standard reference database Version 8.0 [34]. Eq. (22) for tank pressure, after putting the compressibility factor "Z," takes the final form as Eq. (24).

$$P_H = 2.666 \times 10^{-8} {n_H}^3 + 0.0032872 {n_H}^2 + 761.7476 n_H \tag{24}$$

5. Multiobjective optimization criteria

It has been mentioned that the main motivation of this study is to optimize the individual component of the CPV-Hydrogen system for uninterrupted power supply to consumer load, while meeting the system operational power requirements. However, for such system design problem, there can be many system size configurations that can fulfill the condition of steady power supply to the consumer. The main purpose of this optimization is to define a set of objective functions to look for system configuration which will not only provide uninterrupted power supply but at minimum cost and optimum system performance. Therefore, to achieve

such a target, three objective functions are defined to be met as per proposed optimization strategy to find optimum system size configuration.

First, the main objective function defined is the power supply failure time (PSFT) which defines the number of seconds for which the system was unable to meet the total load requirements, that is, consumer load plus system operational power requirements. Such PSFT factor must be zero for any selected configurations, as given by Eq. (25). This objective function is of prime importance and has main priorities, before proceeding to the second objective function.

$$PSFT = \sum_{year} t_{PF} = 0 \tag{25}$$

In order to start the optimization simulation cycle, it is assumed that the gas storage tanks are filled with a certain amount of gases so that the optimization cycle can be started. Otherwise, in case of empty tanks, the simulation cycle will be stuck in achieving the first objective function if the input weather data value is poor at the start. However, at the end of the simulation cycle, such initial amounts of stored gases must be stored so that it can be assured that the system is self-sustaining and it was not operating because of the initial stored energy. Therefore, the second objective function for such a study is defined by Eq. (26).

$$L1 < ST_{H2(f)} - ST_{H2(i)} < L2 \tag{26}$$

where $ST_{H2(f)}$ and $ST_{H2(i)}$ define the state of the hydrogen storage tanks after and before the simulation cycle, respectively. On the other hand, L1 and L2 define the upper and lower limit of the difference between state of hydrogen tank before and after simulation cycle. The current simulation cycle is operated in a yearly manner. Therefore, the second objective function is computed at the end of each year. The value of L1 and L2 are selected as "−10" and "35," respectively, for the current study. The lower value L1 is kept minimum because it is desired that the system recovers to initial state at the end of the simulation cycle. However, the upper limit is kept a bit high so that system is well prepared for the simulation cycle and it can handle the load requirements with enough available storage, in case of poor weather conditions.

The last and the most important objective function is the overall system cost, including investment cost, operational cost and replacement cost. The overall system cost function is given by Eq. (27). The cost functions associated with individual components of the system are given by Eqs. (28)–(33). The system is operated for a lifetime of 20 years. Therefore, the cost parameters associated with each component of the system are given in **Table 2** [35]. In addition, the CRF (capital recovery factor) and the SPPW (single payment present worth) factor are also given by Eqs. (34) and (35). The interest rate considered in the current analysis is 6% [36].

$$C_{AT} = C_{CPV} + C_{EL} + C_{FC} + C_{STH2} + C_{STO2} + C_{com} \tag{27}$$

$$C_{CPV} = \left(NP_{CPV} \times N_{CM} \times P_{MJC,\max}\right) \times [CC_{CPV} + (OMC_{CPV} \times CRF)] \tag{28}$$

$$C_{EL} = (N_{EC} \times P_{EL,\max}) \times [CC_{EL} + (RC_{EL} \times SPPW) + (OMC_{EL} \times CRF)] \tag{29}$$

$$C_{FC} = (N_{FC} \times P_{FC,\max}) \times [CC_{FC} + (RC_{FC} \times SPPW) + (OMC_{FC} \times CRF)] \tag{30}$$

$$C_{STH2} = STM_{H2} \times [CC_{STH2} + (OMC_{STH2} \times CRF)] \tag{31}$$

$$C_{STO2} = STM_{O2} \times [CC_{STO2} + (OMC_{STO2} \times CRF)] \tag{32}$$

$$C_{com} = P_{com} \times [CC_{com} + (OMC_{com} \times CRF)] \tag{33}$$

$$CRF = \left[\frac{i \times (1+i)^L}{(1+i)^L - 1}\right] \tag{34}$$

$$SPPW = \frac{1}{(1+i)^y} \tag{35}$$

It must be noted that the cost associated with the voltage converters is assumed to be included in the cost of the primary component of the system. The solar trackers cost is included in the cost of the CPV system. However, cost for water storage is not considered due to its negligible effect on the overall system cost.

Component	CC	OMC	RC	Replacement
Hydrogen storage	666 $/kg	2% of CC	N.A.	N.A.
Oxygen storage	44.4 $/kg	2% of CC	N.A.	N.A.
Electrolyzer	3.774 $/W	2% of CC	0.777 $/W	10 years
Hydrogen compressor	3000 $/kW	20% of CC	N.A.	N.A.
Fuel cell	2.997 $/W	2% of CC	0.888 $/W	10 years
Concentrated photovoltaic (CPV)	2.62 $/$W_P$	2.125% of CC	N.A.	N.A.

Table 2. Costing parameters considered for techno-economic evaluation of CPV-hydrogen system [17].

6. System optimization algorithm and strategy with micro-GA

As mentioned earlier, the micro-genetic-algorithm (micro-GA) is considered as the main optimization algorithm to search for the optimum system configuration, as per defined objective functions. Based upon the defined performance model of CPV-Hydrogen system, the simulation and optimization program was developed in FORTRAN as per strategy shown in **Figure 5**. The program consists of two parts. The first part is associated with the performance simulation of CPV-Hydrogen system, based upon the developed model. The second part is associated with the system optimization, based upon the defined objective function, to find the optimum system size configuration using micro-GA. There are only two sizing parameters which are given as input to the program to be optimized, that is, the total number of CPV modules needed and the amount of initial hydrogen needed at the start of simulation and optimization cycle. However, the remaining parameters are calculated from these input parameters. The micro-GA is run with a population size of 5 and maximum 300 generations. The results of the study are presented in the next section.

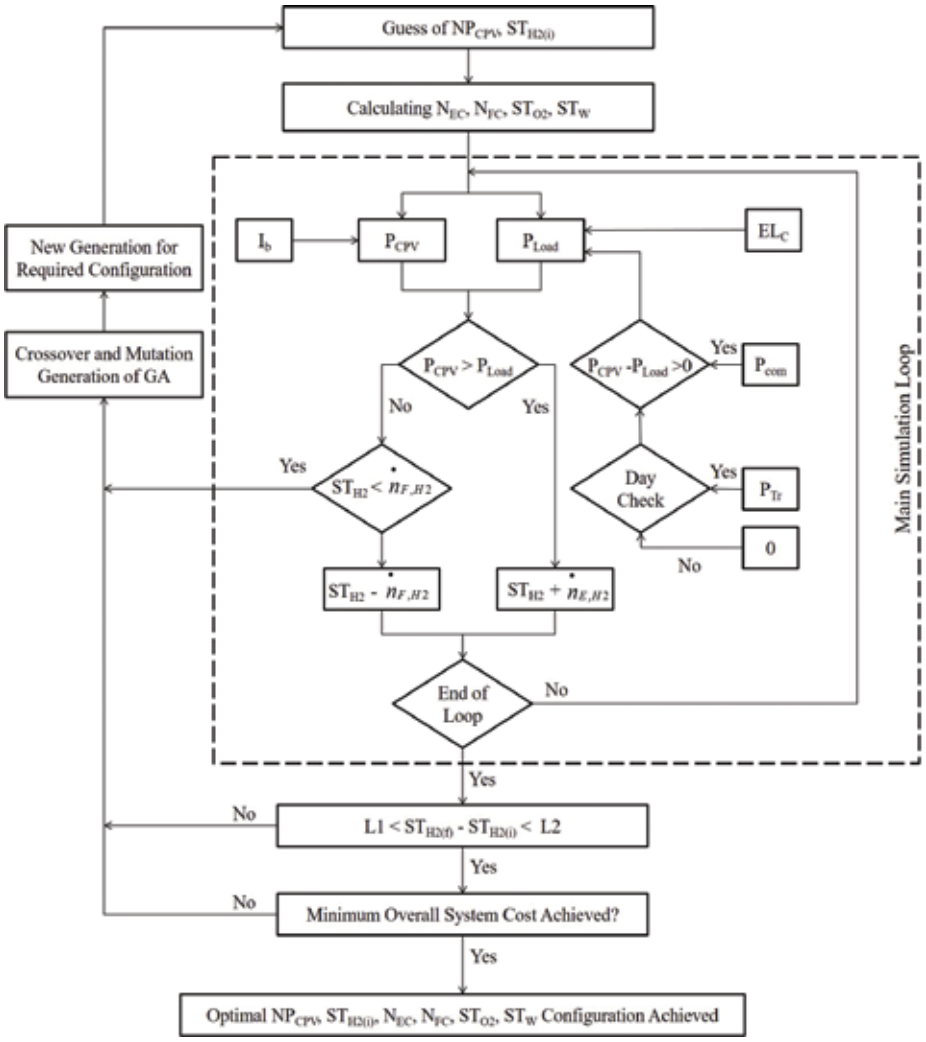

Figure 5. System size optimization strategy for standalone operation of CPV-hydrogen system [17].

7. Results and discussion

In order to simulate the system performance, the direct normal irradiance (DNI) data, obtained under tropical conditions of Singapore, at the rooftop of EA building of National University of Singapore, are shown in **Figure 6**. The DNI data were collected for a 1-year period from September 2014 to August 2015, at an interval of 1 s. To capture the DNI data, the pyrheliometer from Eppley Laboratory was mounted onto a two-axis solar tracker with tracking accuracy of 0.1°. **Figure 6** also shows the electrical load data, obtained from EMA (energy market authority) Singapore at an interval of 30 min. This acts as the input to the simulation cycle for

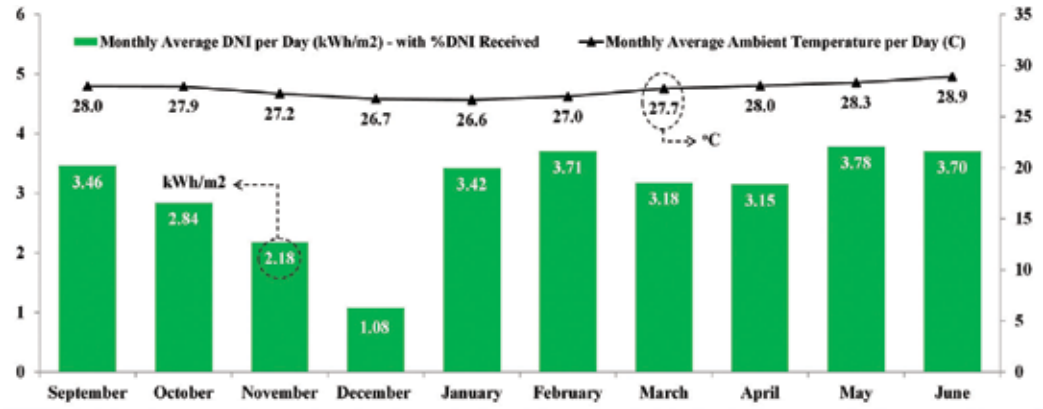

Electrical Load Profile																		
	Time	12:00am	12:30am	01:00am	01:30am	02:00am	02:30am	03:00am	03:30am	04:00am	04:30am	05:00am	05:30am	06:00am	06:30am	07:00am	07:30am
	Load(W)	5009.80	4774.90	4670.60	4586.50	4530.60	4472.30	4426.30	4413.70	4384.90	4385.90	4402.80	4467.50	4622.30	4827.30	5008.00	5171.50
	Time	08:00am	08:30am	09:00am	09:30am	10:00am	10:30am	11:00am	11:30am	12:00pm	12:30pm	01:00pm	01:30pm	02:00pm	02:30pm	03:00pm	03:30pm
	Load(W)	5366.90	5656.70	5864.10	6023.30	6089.60	6162.50	6221.10	6221.60	6206.10	6127.40	6131.70	6163.30	6209.00	6242.30	6224.20	6193.50
	Time	04:00pm	04:30pm	05:00pm	05:30pm	06:00pm	06:30pm	07:00pm	07:30pm	08:00pm	08:30pm	09:00pm	09:30pm	10:00pm	10:30pm	11:00pm	11:30pm
	Load(W)	6203.40	6203.80	6185.50	6152.90	6059.60	5921.20	5913.50	5942.40	5937.30	5904.60	5838.00	5781.70	5680.50	5493.50	5320.10	5169.70

Figure 6. DNI weather data and consumer electric load for Singapore [19].

consumer load demand. The actual load data were in megawatt units, which are scaled down to watts. The shown ambient temperature data were obtained from NEA (national environment agency) Singapore. The weather data shown in **Figure 6** act as the primary input for which the system performance is calculated and the optimum configuration of CPV-Hydrogen system is proposed.

As per the proposed system performance model, presented weather and load input data, energy management and optimization strategies and objective functions, the system optimization was performed by the developed program in FORTRAN using micro-GA. The optimization results are shown in **Figure 7**. From these results, it can be seen that the optimization calculations converge after 52 generations, with minimum overall system cost. It can also be seen that for all generations, the PSFT factor is zero and the difference between states of stored hydrogen, before and after the simulation cycle, is within the defined limits of L1 and L2. However, the stored hydrogen difference is closer to L1 limit, which shows that the system has successfully restored its state to initial conditions and it is ready for the next-year performance cycle. If the overall system cost is broken down, then the details are shown in **Figure 7**. It can be seen that the electrolyzer has the major cost proportion as 51%, followed by the CPV with 35%. In total, these two sub-systems account for 86% of the total system cost. It is important to mention here that the higher cost for electrolyzer is due to its replacement cost as the system has a lifetime period of 10 years and the overall CPV-Hydrogen system is targeted for a 20-year lifetime period.

In order to see the variations in the stored hydrogen energy against the operational period, the state of hydrogen and oxygen storage tanks is shown in **Figure 8**. It can be seen that the state of stored gases is decreasing during initial months of operation. This is because of the fact that for

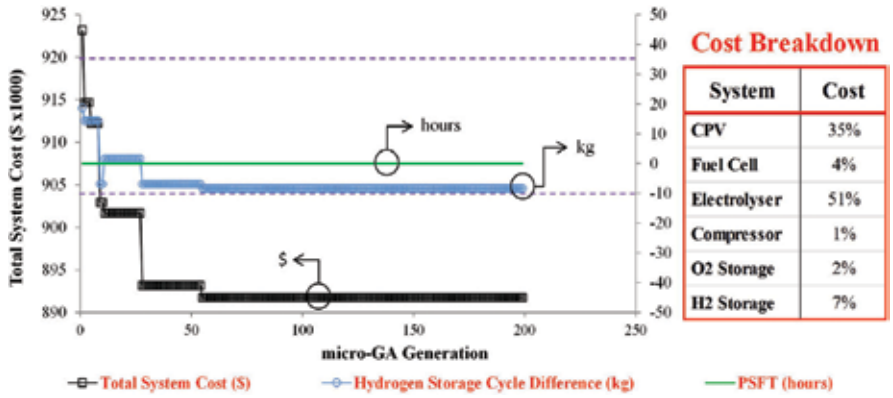

Figure 7. Optimization curve and cost breakdown of the system [19].

these months, the received DNI is also decreasing, which can be seen in **Figure 6**. These months represent the rainy season of Singapore and that is why the received DNI is lower for these months. The share of fuel cell, to meet the load demand during diurnal period, is also shown in **Figure 8**. It can be seen that the fuel cell share is also increasing for these months and for December, it hits about 60%. However, after this rainy season period, the state of energy storage tanks starts to recover and the received DNI as well as the fuel cell share also stabilize. But there is still about 25% fuel cell load share for each month. This is because of the tropical weather conditions as one cannot get clear sky for the whole day. However, the good thing is the stabilized weather conditions with less variations, which is good for the reliable operation of the designed system.

In order to further analyze the performance of CPV-Hydrogen system from its power production point of view, **Figure 9** shows the monthly average values of CPV electrical output and the Hydrogen output of CPV-Hydrogen system for the period of 1 year. The presented data are

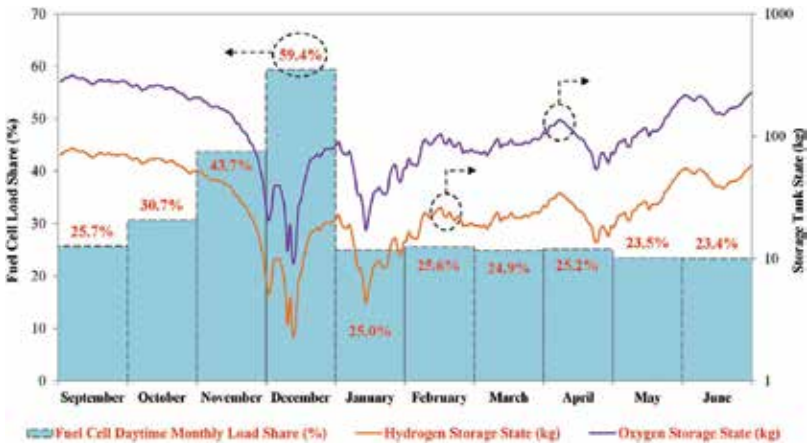

Figure 8. State of energy storage tanks and fuel cell share on monthly basis [19].

http://dx.doi.org/10.5772/intechopen.78055

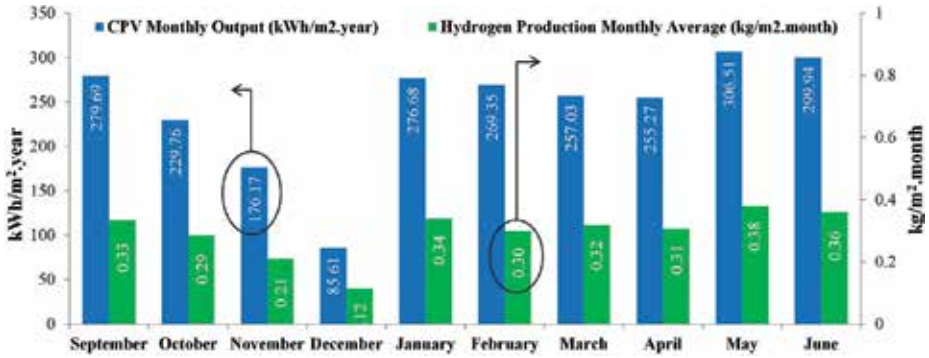

Figure 9. Summary of CPV-hydrogen system performance for electricity and hydrogen production [19].

normalized for per m^2 area. The trend of system output for both parameters is similar to the received monthly DNI, except for rainy season. The electrical output of the system dropped about three times in December than the usual operating month. That is why, a sharp decrease in the state of stored hydrogen was observed during this period. As the presented data are in per m^2 format, therefore, if the main objective of the system is to produce electricity or hydrogen, instead of standalone operation, then the system can be designed based upon the presented performance data.

Table 3 shows the overall summary of optimized CPV-Hydrogen system for standalone operation for defined objective functions and with minimum system cost. The interesting thing to be observed is that the power rating of electrolyzer is same as CPV. This is because of the fact that the design of electrolyzer is depending upon the maximum excess power available, which is proportional to the size of CPV. That is why a higher portion of cost was associated with the electrolyzer, even higher than the CPV. That was due to the replacement cost. It can also be seen that the power rating of CPV system is very large as compared to the consumer load. First, this is because of the fact that the system is designed to be operated in standalone mode while also meeting the system operational power needs, and at night, there is only stored hydrogen which can supply power to the load. Therefore, enough excess power is generated

Parameter description	Units	Value
No. of CPV modules		758
Rated power of CPV system	kW	94.75
Electrolyzer rated power	kW	91
No. of electrolyzer cells connected in series		67
Total hydrogen production	kg	622.22
Total oxygen production	kg	2469.23
Total water consumption	kg	2780.28
Fuel cell rated power	kW	7.33
No. of cells of fuel cell connected in series		64

Parameter description	Units	Value
Total hydrogen consumption	kg	630.55
Total oxygen consumption	kg	2502.28
Total water production	kg	2817.49
Hydrogen storage maximum	kg	81
Oxygen storage maximum	kg	319
Hydrogen storage maximum pressure	bar	200
No. of hydrogen storage cylinders	—	2
Maximum water storage tank	kg	358
Hydrogen compressor rated power	kW	1.13

Table 3. Summary of optimized CPV-hydrogen system design for standalone operation [17].

during the daytime to have enough storage for night operation. Second, as the weather input data were based upon tropical climate conditions, therefore, the system is oversized to have enough hydrogen generated to sustain during rainy period. This design summary is only for the mentioned location and the consumer load data. However, the main objective of proposing design methodology for standalone operation of CPV-Hydrogen system is achieved which can be easily implemented for any load requirement and weather conditions.

8. Summary of chapter

In order for the renewable energy sources to replace conventional fossil fuel-based energy sources, there is need for them to provide steady power supply for any load demand. Due to the intermittent nature of renewable energy sources, energy storage system is needed for steady power supply. Among all renewable energy sources, solar energy has the highest energy potential. But it is only available during diurnal period, with unsteady intensity. In order for such a system to compete with conventional fossil fuel-based system, there is a need for it to operate in standalone mode with sustainable and long-term energy storage system. For such standalone operations, it is very important to capture solar energy with high efficiency.

Photovoltaic system provides a most simple mean to convert sunlight into electricity and concentrated photovoltaic (CPV) technology provides the highest solar energy conversion efficiency among all photovoltaic systems. However, the entire photovoltaic market is dominated with conventional flat plate PV panels. In addition, the literature also focuses on the performance model and optimization strategy of conventional PV system, for its standalone operation. There is not even a single commercial software available which can handle CPV for the system performance analysis. Therefore, a detailed performance model and optimization strategy is proposed for standalone operation of CPV. For energy storage purpose, hydrogen is considered to provide a sustainable and long-term energy storage option than the conventional battery-based electrochemical storage.

http://dx.doi.org/10.5772/intechopen.78055

A detailed energy management technique, performance model and optimization strategy is proposed for standalone operation of CPV-Hydrogen system. The proposed model and strategy is successfully developed and implemented using micro-GA in FORTRAN programming. The overall system size is optimized for uninterrupted power supply to the consumer load with minimum cost. The proposed dynamic strategy is not based upon hourly performance of the system but it also restores the system to its initial state and prepares it for varying weather conditions. The system is not only designed to handle hourly weather variations but it also efficiently performs during seasonal weather variations. Such tech-economic optimization and analysis can be performed for any load demand and at any condition. Moreover, the proposed methodology can be integrated into commercial simulation tools so that they can become capable of handling CPV in their analysis.

Nomenclature

I_b	direct normal irradiance (DNI), (W/m^2)
A_{con}	area of solar concentrator (m^2)
A_C	solar cell area (m^2)
C_C	solar concentration at solar cell area (Suns)
I_C	solar cell current (A)
N_{CM}	number of solar cells in one panel
V_C	solar cell voltage (V)
NP_{CPV}	number of CPV panels
I_{SC}	solar cell short circuit current (A)
EL_C	electrical load demand of consumer (W)
V_{OC}	solar cell open circuit voltage (V)
ST_{H2}	state of hydrogen storage (kg)
T_C	solar cell temperature (°C)
ST_{O2}	state of oxygen storage (kg)
I_{mppt}	solar cell maximum power point current (A)
ST_W	state of water storage (kg)
V_{mppt}	solar cell maximum power point voltage (V)
STM_{H2}	maximum hydrogen storage capacity (kg)
P_C	solar cell power (W)

STM_{O2}	maximum oxygen storage capacity (kg)
P_{mppt}	solar cell maximum power point power (W)
η_{OP}	optical efficiency of concentrating assembly (%)
P_{CPV}	CPV power output (W)
η_{mppt}	Efficiency of Maximum Power Point Tracking Device (%)
P_{Load}	total load demand (W)
$\eta_{DC/AC}$	efficiency of DC to AC converter (%)
P_{excess}	excess available power from CPV (W)
η_{EF}	Faraday efficiency of electrolyzer (%)
P_{Tr}	solar tracker power requirement (W)
η_{CDC}	efficiency of DC to DC converter (%)
P_{com}	hydrogen compressor power (W)
η_{FF}	Faraday efficiency of fuel cell (%)
$P_{MJC,max}$	MJC maximum rated power (W)
η_{com}	efficiency of compressor (%)
$n^{\bullet}_{E,H2}$	hydrogen production flow rate from Electrolyzer (mol/s)
$n^{\bullet}_{F,H2}$	hydrogen consumption flow rate from fuel cell (mol/s)
$n^{\bullet}_{E,O2}$	oxygen production flow rate from electrolyzer (mol/s)
$n^{\bullet}_{F,O2}$	oxygen consumption flow rate from fuel cell (mol/s)
T_E	electrolyzer temperature (°C)
I_F	fuel cell current (mA)
I_E	electrolyzer current (A)
A_F	cell area of fuel cell (cm^2)
A_E	electrolyzer cell area (m^2)
U_F	cell voltage of fuel cell (mV)
U_E	electrolyzer cell voltage (V)
N_{FC}	number of cells of fuel cell
N_{EC}	number of cells of electrolyzer
$P_{FC,max}$	cell maximum power of fuel cell (W)
$V_{EC,max}$	electrolyzer cell maximum voltage (V)

L_{max}	maximum electrical load requirement (W)
$I_{EC,max}$	electrolyzer cell maximum current (A)
P_{req}	electrical power deficiency not supplied by the CPV (W)
$P_{EL,max}$	electrolyzer cell maximum power (W)
U_o	reversible voltage of fuel cell (mV)
L_{min}	Minimum Electrical Load Requirement (W)
F	Faraday constant (A.s/mol)
U_{rev}	reversible voltage of electrolysis (V)
n	electrons requirement for water splitting
M_{H2}	molar mass of hydrogen (g/mol)
P_{ta}	instantaneous pressure of hydrogen tank (Pa)
CP_H	specific heat capacity of hydrogen (J/kg.K)
P_E	pressure of hydrogen production from electrolyzer (Pa)
T_{com}	hydrogen compressor temperature (K)
n_{ta}	instantaneous number of moles of hydrogen gas in storage tank (mol)
r	isentropic exponent of hydrogen
R	universal gas constant (J/mol.K)
Z_H	compressibility factor of hydrogen
T_{ta}	temperature of hydrogen storage tank (K)
V	volume of storage tank of hydrogen (m^3)
n_H	number of hydrogen stage tank
P_H	pressure of hydrogen storage tank (Pa)
t_{PF}	time for power failure (sec)
PSFT	power supply failure time factor (sec)
L2	maximum limit for cyclic hydrogen storage (kg)
L1	minimum limit for cyclic hydrogen storage (kg)
CC	capital cost ($)
C_{AT}	total annual system cost ($)
OMC	operation and maintenance cost ($)
C_{CPV}	CPV total cost ($)

RC	replacement cost ($)
C_{EL}	electrolyzer total cost ($)
CRF	capital recovery factor
C_{FC}	fuel cell total cost ($)
SPPW	single payment present worth
C_{STH2}	hydrogen storage total cost ($)
y	payment duration (years)
C_{STO2}	oxygen storage total cost ($)
i	compound interest rate (%)
C_{com}	hydrogen compressor total cost ($)
L	lifetime period of system (years)

Author details

Muhammad Burhan*, Muhammad Wakil Shahzad and Kim Choon Ng

*Address all correspondence to: muhammad.burhan@kaust.edu.sa

Biological and Environmental Science and Engineering Division, Water Desalination and Reuse Centre, King Abdullah University of Science and Technology, Saudi Arabia

References

[1] Trop P, Goricanec D. Comparisons between energy carriers' productions for exploiting renewable energy sources. Energy. 2016;**108**:155-161

[2] Ng KC, Burhan M, Shahzad MW, Ismail AB. A universal isotherm model to capture adsorption uptake and energy distribution of porous heterogeneous surface. Scientific Reports. 2017;**7**(1):10634

[3] Burhan M, Chua KJE, Ng KC. Electrical rating of concentrated photovoltaic (CPV) systems: Long-term performance analysis and comparison to conventional PV systems. International Journal of Technology. 2016;**7**(2):189-196. DOI: 10.14716/ijtech.v7i2.2983

[4] Burhan M, Oh SJ, Chua KJE, Ng KC. Double lens collimator solar feedback sensor and master slave configuration: Development of compact and low cost two axis solar tracking system for CPV applications. Solar Energy. 2016;**137**:352-363

[5] Burhan M, Shahzad MW, Choon NK. Hydrogen at the rooftop: Compact CPV-hydrogen system to convert sunlight to hydrogen. Applied Thermal Engineering. 2018;**132**:154-164

[6] Burhan M, Chua KJE, Ng KC. Simulation and development of a multi-leg homogeniser concentrating assembly for concentrated photovoltaic (CPV) system with electrical rating analysis. Energy Conversion and Management. 2016;**116**:58-71

[7] Burhan M, Shahzad MW, Ng KC. Long-term performance potential of concentrated photovoltaic (CPV) systems. Energy Conversion and Management. 2017;**148**:90-99

[8] Burhan M, Shahzad MW, Oh SJ, Ng KC. A pathway for sustainable conversion of sunlight to hydrogen using proposed compact CPV system. Energy Conversion and Management. 2018;**165**:102-112

[9] Burhan M, Oh SJ, Chua KJ, Ng KC. Solar to hydrogen: Compact and cost effective CPV field for rooftop operation and hydrogen production. Applied Energy. 2017;**194**:255-266

[10] Burhan M, Shahzad MW, Ng KC. Sustainable cooling with hybrid concentrated photovoltaic thermal (CPVT) system and hydrogen energy storage. International Journal of Computational Physics Series. 2018;**1**(2):40-51

[11] Muhammad B, Seung JO, Ng KC, Chun W. Experimental investigation of multijunction solar cell using two Axis solar tracker. Applied Mechanics and Materials. 2016;**819**:536-540. Trans Tech Publications

[12] Agbossou K, Kolhe M, Hamelin J, Bose TK. Performance of a stand-alone renewable energy system based on energy storage as hydrogen. IEEE Transactions on Energy Conversion. 2004;**19**(3):633-640

[13] Burhan M. Theoretical and experimental study of concentrated photovoltaic (CPV) system with hydrogen production as energy storage [Doctoral dissertation]; 2015

[14] Deb K. Genetic algorithm in search and optimization: the technique and applications. In: Proceedings of International Workshop on Soft Computing and Intelligent Systems, (ISI, Calcutta, India); 1998. pp. 58-87

[15] Bai Q. Analysis of particle swarm optimization algorithm. Computer and Information Science. 2010;**3**(1):180

[16] Shukla M, Dhaliwal BS. Review of Multi-objective Optimization using Genetic Algorithm and Particle Swarm Optimization. IP Multimedia Communications, A Special Issue from IJCA. pp. 72-74

[17] Burhan M, Chua KJE, Ng KC. Sunlight to hydrogen conversion: Design optimization and energy management of concentrated photovoltaic (CPV-hydrogen) system using micro genetic algorithm. Energy. 2016;**99**:115-128

[18] Choi S. Speedups for efficient genetic algorithms: Design optimization of low-boom supersonic jet using parallel GA and micro-GA with external memory. In: Genetic

Algorithms and Genetic Programming at Stanford. 2003. pp. 21-30. http://www.genetic-programming.org/sp2003/Choi.pdf

[19] Burhan M, Shahzad MW, Ng KC. Development of performance model and optimization strategy for standalone operation of CPV-hydrogen system utilizing multi-junction solar cell. International Journal of Hydrogen Energy. 2017;**42**(43):26789-26803

[20] Avril S, Arnaud G, Florentin A, Vinard M. Multi-objective optimization of batteries and hydrogen storage technologies for remote photovoltaic systems. Energy. 2010;**35**(12):5300-5308

[21] Dufo-López R, Bernal-Agustín JL, Contreras J. Optimization of control strategies for stand-alone renewable energy systems with hydrogen storage. Renewable Energy. 2007; **32**(7):1102-1126

[22] Bernal-Agustin JL, Dufo-Lopez R. Simulation and optimization of stand-alone hybrid renewable energy systems. Renewable and Sustainable Energy Reviews. 2009;**13**:2111-2118

[23] Nishioka K, Takamoto T, Agui T, Kaneiwa M, Uraoka Y, Fuyuki T. Annual output estimation of concentrator photovoltaic systems using high-efficiency InGaP/InGaAs/Ge triple-junction solar cells based on experimental solar cell's characteristics and field-test meteorological data. Solar Energy Materials & Solar Cells. 2006;**90**:57-67

[24] Cotal H, Sherif R. Temperature dependence of the IV parameters from triple junction GaInP/InGaAs/Ge concentrator solar cells. In: IEEE 4th World Conference on Photovoltaic Energy Conversion; Vol.1; 2006. pp. 845-848

[25] Ulleberg Ø. Stand-alone power systems for the future: optimal design, operation & control of solar-hydrogen energy systems [PhD Thesis]. Trondheim, Norway: Department of Thermal Energy and Hydropower, Norwegian University of Science and Technology; 1998

[26] Pan CT, Juan YL. A novel sensorless MPPT controller for a high-efficiency microscale wind power generation system. IEEE Transactions on Energy Conversion. 2010;**25**(1):207-216

[27] Chiu HJ, Lin LW. A high-efficiency soft-switched AC/DC converter with current-doubler synchronous rectification. IEEE Transactions on Industrial Electronics. 2005;**52**(3):709-718

[28] Ki SK, Lu DDC. Implementation of an efficient transformerless single-stage single-switch AC/DC converter. IEEE Transactions on Industrial Electronics. 2010;**57**(12):4095-4105

[29] Wang K, Lin CY, Zhu L, Qu D, Lee FC, Lai JS. Bi-directional DC to DC converters for fuel cell systems. In: Power Electronics in Transportation. IEEE; 1998. pp. 47-51. https://ieeexplore.ieee.org/abstract/document/731056/

[30] Nymand M, Andersen MA. High-efficiency isolated boost DC–DC converter for high-power low-voltage fuel-cell applications. IEEE Transactions on Industrial Electronics. 2010;**57**(2):505-514

[31] Li CH, Zhu XJ, Cao GY, Sui S, Hu MR. Dynamic modeling and sizing optimization of stand-alone photovoltaic power systems using hybrid energy storage technology. Renewable Energy. 2009;**34**(3):815-826

[32] Yu X, Gen M. Introduction to Evolutionary Algorithms. London: Springer Science & Business Media; 2010

[33] Oh SJ, Burhan M, Ng KC, Kim Y, Chun W. Development and performance analysis of a two-axis solar tracker for concentrated photovoltaics. International Journal of Energy Research. 2015;**39**(7):965-976

[34] REFPROP Reference Fluid Thermodynamic and Transport Properties. National Institute of Standards and Technology (NIST) Standard Reference Database 23, Version 8.0. http://www.nist.gov

[35] Simbeck D, Supply CEH. Cost Estimate for Hydrogen Pathways—Scoping Analysis. Mountain View, California: SFA Pacific, Inc.; 2002. NREL

[36] Rehman S, Al-Hadhrami LM. Study of a solar PV–diesel–battery hybrid power system for a remotely located population near Rafha, Saudi Arabia. Energy. 2010;**35**(12):4986-4995

Edited by Murat Eyvaz

Among energy sources, hydrogen gas is clean and renewable and has the potential to solve the growing energy crisis in today's society because of its high-energy density and noncarbon fuel properties. It is also used for many potential applications in nonpolluting vehicles, fuel cells, home heating systems, and aircraft. In addition, using hydrogen as an energy carrier is a long-term option to reduce carbon dioxide emissions worldwide by obtaining high-value hydrocarbons through the hydrogenation of carbon dioxide. This book presents the recent progresses and developments in water-splitting processes as well as other hydrogen generation technologies with challenges and future perspectives from the point of energy sustainability.

I would like to record my sincere thanks to all the authors for their contributions.

Published in London, UK

IntechOpen

ISBN 978-1-83881-629-2